

Trade-off between Gradient Measurement Efficiency and Expressivity in Deep Quantum Neural Networks

Koki Chinzei,^{1, *} Shinichiro Yamano,^{1, 2, †} Quoc Hoan Tran,¹ Yasuhiro Endo,¹ and Hiroataka Oshima¹

¹*Quantum Laboratory, Fujitsu Research, Fujitsu Limited, 4-1-1 Kawasaki, Kanagawa 211-8588, Japan*

²*Department of Applied Physics, Graduate School of Engineering,
The University of Tokyo, 7-3-1 Hongo Bunkyo-ku, Tokyo 113-8656, Japan*

(Dated: June 27, 2024)

Quantum neural networks (QNNs) require an efficient training algorithm to achieve practical quantum advantages. A promising approach is the use of gradient-based optimization algorithms, where gradients are estimated through quantum measurements. However, it is generally difficult to efficiently measure gradients in QNNs because the quantum state collapses upon measurement. In this work, we prove a general trade-off between gradient measurement efficiency and expressivity in a wide class of deep QNNs, elucidating the theoretical limits and possibilities of efficient gradient estimation. This trade-off implies that a more expressive QNN requires a higher measurement cost in gradient estimation, whereas we can increase gradient measurement efficiency by reducing the QNN expressivity to suit a given task. We further propose a general QNN ansatz called the stabilizer-logical product ansatz (SLPA), which can reach the upper limit of the trade-off inequality by leveraging the symmetric structure of the quantum circuit. In learning an unknown symmetric function, the SLPA drastically reduces the quantum resources required for training while maintaining accuracy and trainability compared to a well-designed symmetric circuit based on the parameter-shift method. Our results not only reveal a theoretical understanding of efficient training in QNNs but also provide a standard and broadly applicable efficient QNN design.

I. INTRODUCTION

Deep learning is a breakthrough technology that has a significant impact on a variety of fields, including computational and natural sciences [1]. In deep learning, neural networks are trained to approximate unknown target functions to represent input-output relationships in various tasks such as image recognition [2], natural language processing [3], predictions of protein structure [4], and quantum state approximation [5]. Behind the great success of deep learning lies an efficient training algorithm equipped with backpropagation [6, 7]. Backpropagation allows us to efficiently evaluate the gradient of an objective function at approximately the same computational cost as a single model evaluation and to optimize the neural network’s training parameters based on the evaluated gradient. This technique is essential for training large neural networks with enormous parameters.

In analogy with deep learning, variational quantum algorithms (VQAs) have emerged as a promising technology for solving classically intractable problems in quantum chemistry and physics [8], optimization [9], machine learning [10–14], and so on [15–18]. In VQAs, a parameterized quantum circuit, called a quantum neural network (QNN) in the context of quantum machine learning (QML) [19–22], is optimized by minimizing an objective function with quantum and classical computers [23]. As in classical neural networks, gradient-based optimization

algorithms are promising for training QNNs, where gradients are estimated by quantum measurements [Fig. 1 (a)]. However, unlike classical models, an efficient gradient estimation is challenging in QNNs because quantum states collapse upon measurement. In fact, it is known that QNNs lack a general and efficient gradient measurement algorithm that achieves the same computational cost scaling as classical backpropagation when only one copy of the quantum data is accessible at a time [24]. Instead, the gradient is usually estimated using the parameter-shift method [12, 25], where each gradient component is measured independently. This method leads to a high measurement cost that is proportional to the number of parameters, which prevents QNNs from scaling up in near-term quantum devices without sufficient computational resources.

Despite the lack of general algorithms to achieve backpropagation scaling, a commuting block circuit (CBC) has recently been proposed as a well-structured QNN for efficient gradient estimation [26]. The CBC consists of B blocks containing multiple variational rotation gates, and the generators of rotation gates in two blocks are either all commutative or all anti-commutative. Because of its specific structure, the CBC allows us to estimate the gradient using only $2B - 1$ types of quantum measurements, which is independent of the number of variational rotation gates in each block. Therefore, the CBC can be trained more efficiently than conventional QNNs based on the parameter-shift method [27]. However, there are several remaining questions on the CBC. First, it remains unclear how the specific structure of the CBC affects the QNN capability, particularly the expressivity, which is related to the accuracy of solving a problem. Second, although the basic framework of the CBC has been pro-

* chinzei.koki@fujitsu.com

† yamano@qi.t.u-tokyo.ac.jp

These authors contributed equally to this work.

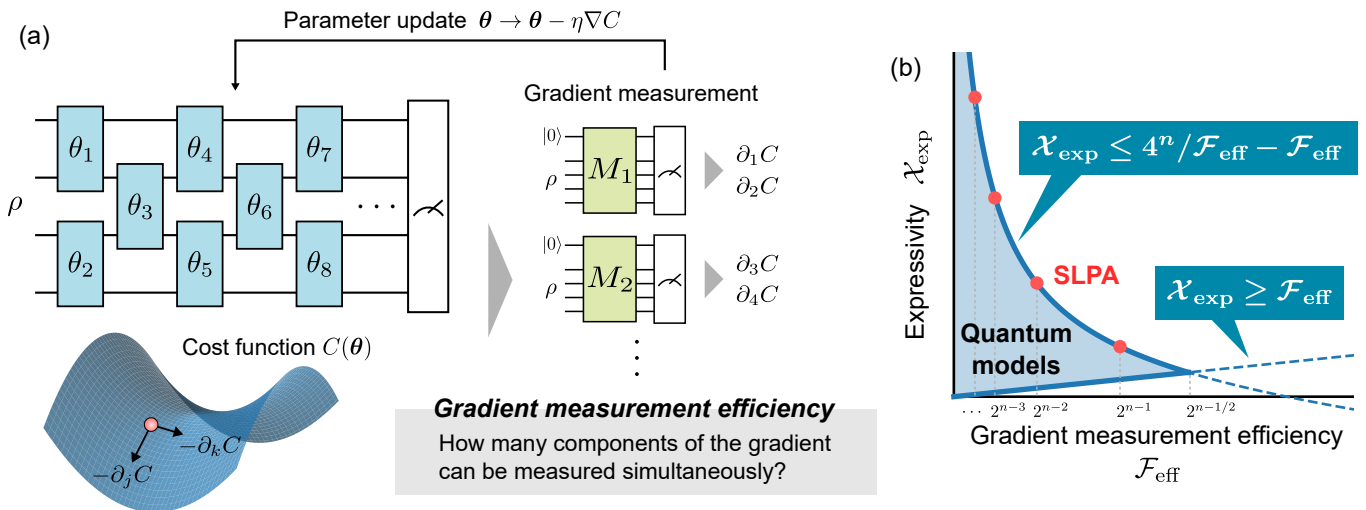


FIG. 1. (a) Illustration of VQAs. The parameterized quantum circuit is optimized based on the gradient of the cost function estimated by quantum measurements. (b) Trade-off relation between gradient measurement efficiency and expressivity. Any quantum model can only exist in the blue region. Gradient measurement efficiency, \mathcal{F}_{eff} , is defined as the number of simultaneously measurable components in the gradient, and expressivity χ_{exp} is the dimension of the dynamical Lie algebra of the parameterized quantum circuit. The red circles denote the stabilizer-logical product ansatz (SLPA), where 2^s gradient components can be measured simultaneously (i.e., $\mathcal{F}_{\text{eff}} = 2^s$, s is an integer), reaching the upper limit of the trade-off inequality.

posed, the general method of circuit construction has not yet been established. Answering these questions is crucial not only for the theoretical understanding of efficient training in QNNs but also for the realization of practical QML.

This work answers these questions for more general QNNs, including the CBC. We first define gradient measurement efficiency in terms of the simultaneous measurability of gradient components, proving a general trade-off between gradient measurement efficiency and expressivity in a wide class of deep QNNs [Fig. 1 (b)]. This trade-off implies that a more expressive QNN requires a higher measurement cost in gradient estimation, whereas the gradient measurement efficiency can be increased by reducing the QNN expressivity to suit a given task. Based on this trade-off, we further propose a general ansatz of CBC, the stabilizer-logical product ansatz (SLPA). This ansatz can reach the upper limit of the trade-off inequality, i.e., it allows us to measure the gradient with theoretically the fewest types of quantum measurements for a given expressivity [Fig. 1 (b)]. The SLPA leverages the symmetric structure of the quantum circuit to enhance the gradient measurement efficiency, where the generators of the ansatz are constructed by taking the products of stabilizers and logical operators (Fig. 2). Owing to this symmetric structure, the SLPA can be applied to various problems involving symmetry, which are common in quantum chemistry, physics, and machine learning. As a demonstration, we consider the task of learning an unknown symmetric function and show that the SLPA drastically reduces the quantum resources needed for training while maintaining accuracy and trainability compared to several QNNs based on the parameter-shift

method. These results reveal the theoretical limits and possibilities of efficient training in QNNs, paving the way for realizing practical advantages in QML.

The remainder of this paper is organized as follows. Section II introduces the variational quantum model of interest and defines gradient measurement efficiency and expressivity. Section III shows the main theorem of this work and describes the trade-off relation between gradient measurement efficiency and expressivity and its consequences. Section IV proves the main theorem by introducing a graph representation of dynamical Lie algebra. Section V proposes the SLPA as a general ansatz of CBC that can reach the upper limit of the trade-off inequality. Section VI verifies the practical effectiveness of the SLPA in the specific task of learning an unknown symmetric function. Finally, Sec. VII summarizes this paper and discusses potential future research directions.

II. MODEL, EFFICIENCY, AND EXPRESSIVITY

This section introduces variational quantum models of interest and defines their gradient measurement efficiency and expressivity.

A. Model

We consider the following QNN on an n -qubits system:

$$U(\boldsymbol{\theta}) = \prod_{j=1}^L \exp(i\theta_j G_j), \quad (1)$$

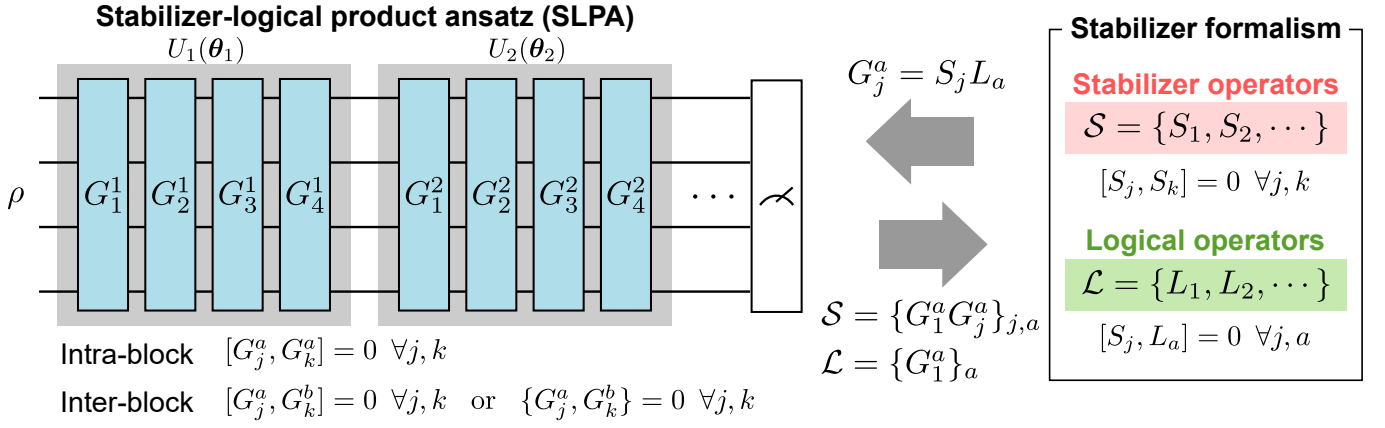


FIG. 2. Stabilizer-logical product ansatz (SLPA) of commuting block circuit (CBC). The generators of SLPA are constructed by taking the products of stabilizers and logical operators.

where $G_j \in \{I, X, Y, Z\}^{\otimes n}$ is an n -qubits Pauli operator, $\theta = (\theta_1, \theta_2, \dots)$ is variational rotation angles, and L is the number of rotation gates. Let $\mathcal{G} = \{G_j\}_{j=1}^L$ be the set of generators. We consider a cost function defined as the expectation value of a Pauli observable O :

$$C(\theta) = \text{Tr}[U(\theta)\rho U^\dagger(\theta)O], \quad (2)$$

where ρ is an input quantum state. This type of cost function is often used to solve QML tasks. Note that even if the circuit has non-variational Clifford gates (e.g., CZ and CNOT gates), we can transform the circuit into the form of Eq. (1) by swapping the Clifford gates and the Pauli rotation gates (see Appendix A for details). Hence, Eq. (1) includes a wide class of parameterized quantum circuits.

To remove redundant and irrelevant quantum gates, we assume the following conditions on the quantum circuit $U(\theta)$ (throughout this paper, we use the commutation and anti-commutation relations, $[A, B] = AB - BA$ and $\{A, B\} = AB + BA$):

Condition 1 (No redundant quantum gates). For any $j < k$, if $G_j = G_k$, there exists ℓ ($j < \ell < k$) such that $\{G_j, G_\ell\} = 0$.

Condition 2 (No irrelevant quantum gates). For any $G_j \in \mathcal{G}$ commuting with O (i.e., $[G_j, O] = 0$), there exist $Q_1, \dots, Q_m \in \mathcal{G}$ such that $\{G_j, Q_1\} = \{Q_1, Q_2\} = \dots = \{Q_{m-1}, Q_m\} = \{Q_m, O\} = 0$.

The first condition removes the redundancy of quantum gates. If there is no ℓ satisfying the condition, the two rotation gates, $e^{i\theta_j G_j}$ and $e^{i\theta_k G_k}$, can be merged into one rotation gate, $e^{i(\theta_j + \theta_k)G_j}$, by swapping the positions of gates. This means that one of the two rotation gates is redundant. The second condition removes irrelevant quantum gates. If there is a quantum gate that violates the condition, the circuit is decomposed into two mutually commuting unitaries as $U = U_1 U_2$, where U_2 commutes with the observable O (i.e., $[U_1, U_2] = [U_2, O] = 0$). Then, the cost function is written as $C = \text{Tr}[\rho U^\dagger O U] =$

$\text{Tr}[\rho U_1^\dagger O U_1]$, which implies that U_2 is irrelevant in this QNN (see Sec. IV B for details). Therefore, we impose these two conditions on the quantum circuit to remove the redundant and irrelevant quantum gates.

B. Gradient measurement efficiency

In QNNs, the circuit parameters θ are optimized to solve a given problem. One of the most promising approaches is the use of gradient-based optimization algorithms, which update the parameters based on the gradient of the cost function as $\theta \rightarrow \theta - \eta \nabla C$ (η is a learning rate). In classical neural networks, gradient-based optimization algorithms are highly successful thanks to backpropagation, which allows us to compute the gradient at approximately the same cost as a single model evaluation [6, 7]. Even in QNNs, gradient-based optimization is a powerful method, but there are no general algorithms for measuring gradients as efficiently as classical backpropagation [24]. Instead, in many VQAs, each gradient component is measured independently using the parameter-shift method [12, 25], where the derivative of the cost function is estimated by shifting the parameter: $\partial_j C(\theta) = C(\theta + \pi e_j/4) - C(\theta - \pi e_j/4)$ ($\partial_j \equiv \partial/\partial\theta_j$ and e_j is the j th unit vector). This method is easy to implement but leads to a high measurement cost proportional to the number of training parameters.

To reveal the theoretical limit of efficient gradient estimation, let us first define the simultaneous measurability of two different components in the gradient. By straightforward calculations, we have the derivative of the cost function by θ_j (see Appendix B for derivation):

$$\partial_j C(\theta) = \text{Tr}[\rho \Gamma_j(\theta)], \quad (3)$$

where Γ_j is a *gradient operator* defined as

$$\Gamma_j(\theta) = -i[\tilde{G}_j(\theta), \tilde{O}(\theta)] \quad (4)$$

with $\tilde{O}(\boldsymbol{\theta}) = U^\dagger(\boldsymbol{\theta})OU(\boldsymbol{\theta})$ and $\tilde{G}_j(\boldsymbol{\theta}) = U_{j+}^\dagger(\boldsymbol{\theta})G_jU_{j+}(\boldsymbol{\theta})$ ($U_{j+}(\boldsymbol{\theta}) = \prod_{k=1}^{j-1} e^{i\theta_k G_k}$ is the unitary circuit before the j th gate). In other words, $\partial_j C$ is identical to the expectation value of the gradient operator Γ_j for the input state ρ . In quantum mechanics, two observables A and B can be simultaneously measured for any input quantum state ρ if and only if $[A, B] = 0$. Therefore, we define the simultaneous measurability in the gradient as follows:

Definition 1 (Simultaneous measurability in gradient). We say that $\partial_j C(\boldsymbol{\theta})$ and $\partial_k C(\boldsymbol{\theta})$ can be simultaneously measured when

$$[\Gamma_j(\boldsymbol{\theta}), \Gamma_k(\boldsymbol{\theta})] = 0 \quad \forall \boldsymbol{\theta}. \quad (5)$$

This definition assumes that the commutation relation holds for any $\boldsymbol{\theta}$. Thus, even if $\partial_j C(\boldsymbol{\theta})$ and $\partial_k C(\boldsymbol{\theta})$ cannot be simultaneously measured in the sense of this definition, they may be simultaneously measurable for certain $\boldsymbol{\theta}$. Note that this definition implicitly considers situations where only a single copy of ρ is available at a time. This is because if multiple copies are available at the same time, we can measure any two observables simultaneously by measuring each observable for each copy. In multi-copy settings, an efficient algorithm is known to estimate the gradient, where $\mathcal{O}(\text{polylog}(L))$ copies of ρ are coherently manipulated to be measured by shadow tomography [24, 28]. However, such an algorithm is hard to implement in near-term quantum devices due to the requirements of many qubits and long execution times. This work focuses only on single-copy settings and does not consider multi-copy ones.

Based on Definition 1, we divide the gradient operators into N_{sim} simultaneously measurable groups as

$$\{\Gamma_j(\boldsymbol{\theta})\}_{j=1}^L = M_1 \sqcup \cdots \sqcup M_{N_{\text{sim}}}, \quad (6)$$

where \sqcup is the disjoint union. In this grouping, all the operators in the same group are simultaneously measurable in the sense of Definition 1, i.e., the following commutation relation holds for a group M_m :

$$[\Gamma_j(\boldsymbol{\theta}), \Gamma_k(\boldsymbol{\theta})] = 0 \quad \forall \Gamma_j(\boldsymbol{\theta}), \Gamma_k(\boldsymbol{\theta}) \in M_m, \forall \boldsymbol{\theta}. \quad (7)$$

This grouping enables us to estimate all the gradient components using N_{sim} types of quantum measurements in principle. Thereby, we define gradient measurement efficiency for finite-depth QNNs:

Definition 2 (Gradient measurement efficiency of finite-depth QNNs). The gradient measurement efficiency of finite-depth QNNs is defined as

$$\mathcal{F}_{\text{eff}}^{(L)} = \frac{L}{\min(N_{\text{sim}})}, \quad (8)$$

where $\min(N_{\text{sim}})$ is the minimum number of groups among all possible groupings.

In this definition, $\mathcal{F}_{\text{eff}}^{(L)}$ indicates the mean number of simultaneously measurable components in the gradient.

Therefore, the larger $\mathcal{F}_{\text{eff}}^{(L)}$ is, the more efficiently the gradient can be measured. We also define the gradient measurement efficiency in the deep circuit limit:

Definition 3 (Gradient measurement efficiency of deep QNNs). The gradient measurement efficiency of deep QNNs is defined as

$$\mathcal{F}_{\text{eff}} = \lim_{L \rightarrow \infty} \mathcal{F}_{\text{eff}}^{(L)}. \quad (9)$$

This work mainly focuses on \mathcal{F}_{eff} rather than $\mathcal{F}_{\text{eff}}^{(L)}$ and investigates its theoretical upper limit. Nevertheless, our results also have implications for efficient gradient measurement in finite-depth QNNs as shown in Sec. VI B.

C. Expressivity

Expressivity is related to the capacity of QNNs. Typically, QNNs can express more types of unitaries as expressivity increases, potentially improving accuracy for a given problem. This work quantifies the QNN expressivity using the dynamical Lie algebra (DLA) [29–31]. To this end, we consider the following Lie closure:

$$i\mathcal{G}_{\text{Lie}} = \langle i\mathcal{G} \rangle_{\text{Lie}}, \quad (10)$$

where the Lie closure $\langle i\mathcal{G} \rangle_{\text{Lie}}$ is defined as the set of Pauli operators obtained by repeatedly taking the nested commutator between the circuit generators in $i\mathcal{G} = \{iG_j\}_{j=1}^L$, i.e., $[\cdots [iG_j, iG_k], iG_\ell], \cdots] \in i\mathcal{G}_{\text{Lie}}$ for $G_j, G_k, G_\ell, \cdots \in \mathcal{G}$. Letting $\mathcal{P}_n = \{I, X, Y, Z\}^{\otimes n}$ be the set of n -qubits Pauli operators, $\mathcal{G} \subseteq \mathcal{G}_{\text{Lie}} \subseteq \mathcal{P}_n$ holds by definition, where we ignore the coefficients of Pauli operators in \mathcal{G}_{Lie} . The DLA is defined by \mathcal{G}_{Lie} as

$$\mathfrak{g} = \text{span}(\mathcal{G}_{\text{Lie}}), \quad (11)$$

which is the subspace of $\mathfrak{su}(2^n)$ spanned by the Pauli operators in \mathcal{G}_{Lie} . The DLA characterizes the types of unitaries that the QNN can express in the overparameterized regime of $L \gtrsim \dim(\mathfrak{g})$: that is, $U(\boldsymbol{\theta}) \in e^{\mathfrak{g}}$ for all $\boldsymbol{\theta}$ [32]. For example, a hardware-efficient ansatz with $\mathcal{G} = \{X_j, Y_j, Z_j Z_{j+1}\}_{j=1}^n$ has the DLA of $\dim(\mathfrak{g}) = 4^n - 1$ [33], indicating that it can express all unitaries in the deep circuit limit [note that $\dim(\mathfrak{g}) \leq 4^n - 1$ since \mathfrak{g} is a subset of $\mathfrak{su}(2^n)$]. Therefore, we define the expressivity of the QNN in the deep circuit limit as the dimension of the DLA:

Definition 4 (Expressivity of deep QNNs). The expressivity of deep QNNs is defined as

$$\mathcal{X}_{\text{exp}} = \dim(\mathfrak{g}). \quad (12)$$

Here, we assume another condition on the quantum circuit in relation to expressivity:

Condition 3. Let U_{fin} be the final part of the circuit with depth L_{fin} :

$$U_{\text{fin}} = \prod_{j=L-L_{\text{fin}}+1}^L e^{i\theta_j G_j}. \quad (13)$$

Then, there exists a constant L_{fin} (independent of L) such that U_{fin} can express $e^{i\phi_1 Q_1} e^{i\phi_2 Q_2}$ for any $Q_1, Q_2 \in \mathcal{G}_{\text{Lie}}$ and any $\phi_1, \phi_2 \in \mathbb{R}$.

This condition is easily satisfied in the limit of $L \rightarrow \infty$ when all generators in \mathcal{G} appear uniformly in the circuit. We use this condition to prove the main theorem. Note that the contribution from U_{fin} with depth $L_{\text{fin}} = \mathcal{O}(1)$ to the gradient measurement efficiency \mathcal{F}_{eff} vanishes in the deep circuit limit $L \rightarrow \infty$. Thus, for evaluating \mathcal{F}_{eff} , it suffices to consider only the contribution from the initial part of the circuit with depth $L_{\text{ini}} = L - L_{\text{fin}} = \mathcal{O}(L)$.

III. MAIN THEOREM

Remarkably, the upper limit of gradient measurement efficiency depends on expressivity. Here, we present the main theorem on the relationship between gradient measurement efficiency and expressivity:

Theorem 1. *In deep QNNs satisfying Conditions 1–3, gradient measurement efficiency and expressivity obey the following inequalities:*

$$\mathcal{X}_{\text{exp}} \leq \frac{4^n}{\mathcal{F}_{\text{eff}}} - \mathcal{F}_{\text{eff}}, \quad (14)$$

and

$$\mathcal{X}_{\text{exp}} \geq \mathcal{F}_{\text{eff}}, \quad (15)$$

where n is the number of qubits.

The inequality (14) represents a trade-off relation between gradient measurement efficiency and expressivity as shown in Fig. 1 (b). This trade-off indicates that a more expressive QNN requires a higher measurement cost for gradient estimation. For example, when a QNN has maximum expressivity $\mathcal{X}_{\text{exp}} = 4^n - 1$ (e.g., a hardware-efficient ansatz with $\mathcal{G} = \{X_j, Y_j, Z_j Z_{j+1}\}_{j=1}^n$), the gradient measurement efficiency must be $\mathcal{F}_{\text{eff}} = 1$, which implies that we cannot measure two or more gradient components simultaneously in such models. The inequality (15) shows that gradient measurement efficiency is bounded by expressivity. Therefore, in the highly overparametrized regime of $L \gg \mathcal{X}_{\text{exp}}$, we need $L/\mathcal{F}_{\text{eff}} (\gg \mathcal{X}_{\text{exp}}/\mathcal{F}_{\text{eff}} \geq 1)$ types of quantum measurements to estimate the gradient, leading to a high measurement cost for training such QNNs. Also, combining the two inequalities (14) and (15), we have $\mathcal{F}_{\text{eff}} \leq 2^{n-1/2}$, which is the upper bound of gradient measurement efficiency in QNNs.

The trade-off inequality (14) suggests that we can increase gradient measurement efficiency by reducing the expressivity to fit a given problem, i.e., by encoding prior knowledge of the problem into the QNN as an inductive bias. In the context of QML, such a problem-tailored model is considered crucial to achieving quantum advantages [34]. For instance, an equivariant QNN, where the symmetry of a problem is encoded into the QNN structure, is one of the promising problem-tailored quantum models and exhibits high trainability and generalization by reducing the parameter space to be searched [35–45]. In Sec. V, we will introduce a general QNN ansatz called the stabilizer-logical product ansatz (SLPA) that leverages prior knowledge of a problem’s symmetry to reach the upper limit of the trade-off inequality (14).

We remark on the relationship between gradient measurement efficiency and trainability. In deep QNNs, it is known that the variance of the cost function in the parameter space decays inversely proportional to $\dim(\mathfrak{g})$: $\text{Var}_{\theta}[C(\theta)] \sim 1/\dim(\mathfrak{g}) = 1/\mathcal{X}_{\text{exp}}$ [33, 46, 47]. Thus, exponentially high expressivity results in an exponentially flat landscape of the cost function (so-called the barren plateaus [48]), which makes efficient training of QNNs impossible. In other words, expressivity has a trade-off with trainability. On the other hand, high gradient measurement efficiency and high trainability are compatible. By the trade-off inequality (14) and $\text{Var}_{\theta}[C(\theta)] \sim 1/\mathcal{X}_{\text{exp}}$, we have

$$\mathcal{F}_{\text{eff}} \lesssim 4^n \text{Var}_{\theta}[C(\theta)], \quad (16)$$

where we have used $4^n/\mathcal{F}_{\text{eff}} - \mathcal{F}_{\text{eff}} \leq 4^n/\mathcal{F}_{\text{eff}}$. This inequality means that we can increase \mathcal{F}_{eff} and $\text{Var}_{\theta}[C(\theta)]$ simultaneously, indicating the compatibility of high gradient measurement efficiency and trainability. In Sec. VI, we will numerically show that the SLPA can exhibit high gradient measurement efficiency and trainability at the same time, verifying their compatibility.

IV. PROOF OF MAIN THEOREM

This section gives the proof of Theorem 1. Beginning with the sketch of the proof, we present some lemmas on the simultaneous measurability of gradient components and then prove Theorem 1 using the lemmas.

A. Sketch of proof

This subsection gives the sketch of the proof. A more detailed and exact proof can be found in the following subsections and Appendix C.

In this proof, we introduce a graph representation of the DLA called a DLA graph to clarify the relationship between gradient measurement efficiency and expressivity. The DLA graph consists of nodes and edges. Each node P corresponds to the Pauli basis of the DLA \mathcal{G}_{Lie}

(i.e., $P \in \mathcal{G}_{\text{Lie}}$), and two nodes $P \in \mathcal{G}_{\text{Lie}}$ and $Q \in \mathcal{G}_{\text{Lie}}$ are connected by an edge if they anti-commute, $\{P, Q\} = 0$. As shown below, the (anti-)commutation relations between the Pauli bases of the DLA are closely related to the simultaneous measurability of gradient components. Therefore, the DLA graph visualizes the (anti-)commutation relations of the DLA, allowing us to clearly understand the relationship between the gradient measurement efficiency and the DLA structure.

The proof of Theorem 1 requires understanding the gradient measurement efficiency \mathcal{F}_{eff} and the expressivity \mathcal{X}_{exp} in terms of the DLA graph. By definition, the expressivity \mathcal{X}_{exp} corresponds to the total number of nodes in the DLA graph. On the other hand, the relationship between the gradient measurement efficiency \mathcal{F}_{eff} and the DLA graph is nontrivial. The first step to obtaining the gradient measurement efficiency is to consider whether given two gradient operators Γ_j and Γ_k are simultaneously measurable (i.e., whether $[\Gamma_j, \Gamma_k] = 0$). The gradient operator Γ_j is defined from the generator of the quantum circuit $G_j \in \mathcal{G}$, which corresponds to a node of the DLA graph. In Sec. IV B, we will present Lemmas 1–5 to show that the simultaneous measurability of Γ_j and Γ_k are determined by some structural relations between the nodes G_j, G_k , and the observable O in the DLA graph. Hence, how many gradient components can be simultaneously measured, namely \mathcal{F}_{eff} , is also determined by the structure of the DLA graph.

Based on Lemmas 1–5, we decompose the DLA graph into several subgraphs, where nodes belonging to different subgraphs cannot be measured simultaneously. Therefore, the number of nodes in each subgraph bounds the number of simultaneously measurable gradient components, i.e., the gradient measurement efficiency. Using this idea, we can map the problem on \mathcal{F}_{eff} and \mathcal{X}_{exp} to the problem on the DLA graph, or specifically on the relation between the total number of nodes and the size of subgraphs in the DLA graph. In Sec. IV C, by considering constraints on the number of nodes derived from the DLA decomposition, we prove the inequalities between \mathcal{F}_{eff} and \mathcal{X}_{exp} .

For later convenience, we introduce an abbreviation for operator sets $\mathcal{A} = \{A_1, A_2, \dots\}$ and $\mathcal{B} = \{B_1, B_2, \dots\}$ as

$$[\mathcal{A}, \mathcal{B}] = 0 \stackrel{\text{def}}{\iff} [A_j, B_k] = 0 \quad \forall A_j \in \mathcal{A}, \forall B_k \in \mathcal{B},$$

$$\{\mathcal{A}, \mathcal{B}\} = 0 \stackrel{\text{def}}{\iff} \{A_j, B_k\} = 0 \quad \forall A_j \in \mathcal{A}, \forall B_k \in \mathcal{B}.$$

Similarly, we define an abbreviation for an operator set $\mathcal{A} = \{A_1, A_2, \dots\}$ and an operator B_k as

$$[\mathcal{A}, B_k] = 0 \stackrel{\text{def}}{\iff} [A_j, B_k] = 0 \quad \forall A_j \in \mathcal{A},$$

$$\{\mathcal{A}, B_k\} = 0 \stackrel{\text{def}}{\iff} \{A_j, B_k\} = 0 \quad \forall A_j \in \mathcal{A}.$$

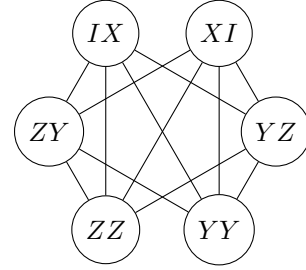
In this section and Appendix C, we ignore the coefficients of Pauli operators as we only consider the commutation and anti-commutation relations for the proof.

B. DLA graph and simultaneous measurability

The proof of Theorem 1 requires understanding the relationship between the simultaneous measurability of gradient components and the DLA structure. Here, we introduce a graph representation associated with the DLA, a DLA graph, to visualize the DLA. In the DLA graph, each node P corresponds to the Pauli basis of the DLA \mathcal{G}_{Lie} , and two nodes $P \in \mathcal{G}_{\text{Lie}}$ and $Q \in \mathcal{G}_{\text{Lie}}$ are connected by an edge if and only if $\{P, Q\} = 0$:

$$[P, Q] = 0: \quad \begin{array}{c} \textcircled{P} \quad \quad \textcircled{Q} \\ \\ \textcircled{P} \text{---} \textcircled{Q} \end{array}$$

For example, the following figure is the DLA graph with $\mathcal{G}_{\text{Lie}} = \{IX, XI, ZY, YZ, ZZ, YY\}$ for a two-qubits system:



Here, we define the connectivity on the DLA graph:

Definition 5 (DLA-connectivity). We say that $P, Q \in \mathcal{P}_n$ ($P \neq Q$) are \mathfrak{g} -connected and denote $P \xleftrightarrow{\mathfrak{g}} Q$ when $\{P, Q\} = 0$ or there exist $R_1, R_2, \dots, R_{d-1} \in \mathcal{G}_{\text{Lie}}$ such that $\{P, R_1\} = \{R_1, R_2\} = \dots = \{R_{d-1}, Q\} = 0$.

In terms of the DLA graph, $P, Q \in \mathcal{P}_n$ are \mathfrak{g} -connected when there exists a path connecting P and Q on the DLA graph. This connectivity satisfies a transitive relation that $P \xleftrightarrow{\mathfrak{g}} Q$ and $Q \xleftrightarrow{\mathfrak{g}} R$ lead to $P \xleftrightarrow{\mathfrak{g}} R$ for $P, R \in \mathcal{P}_n$ and $Q \in \mathcal{G}_{\text{Lie}}$. Below, we represent the \mathfrak{g} -connectivity as

$$P \text{ and } Q \text{ are } \mathfrak{g}\text{-connected:} \quad \textcircled{P} \xleftrightarrow{\mathfrak{g}} \textcircled{Q}$$

$$P \text{ and } Q \text{ are not } \mathfrak{g}\text{-connected:} \quad \textcircled{P} \not\xleftrightarrow{\mathfrak{g}} \textcircled{Q}$$

Note that the \mathfrak{g} -connectivity are defined for $P, Q \in \mathcal{P}_n = \{I, X, Y, Z\}^{\otimes n}$ not only for $P, Q \in \mathcal{G}_{\text{Lie}}$. We also define the separability of the DLA graph as follows:

Definition 6 (Separability). We say that a DLA subgraph $\mathcal{G}_{\text{Lie}1} \subset \mathcal{G}_{\text{Lie}}$ is separated when $[\mathcal{G}_{\text{Lie}1}, \mathcal{G}_{\text{Lie}2}] = 0$,

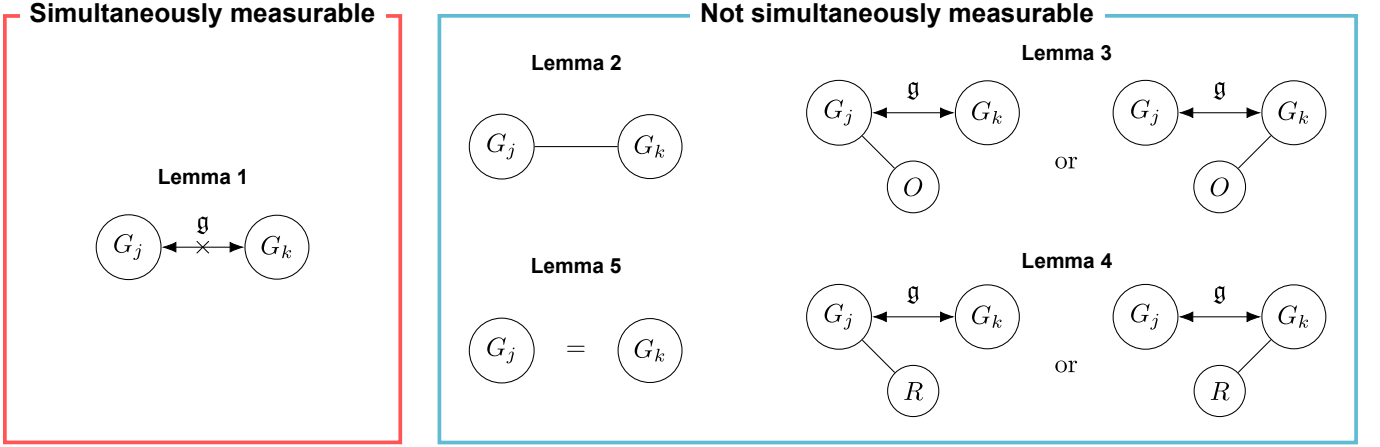


FIG. 3. Summary of Lemmas 1–5. Whether two gradient operators Γ_j and Γ_k are simultaneously measurable is determined by the structural relations between the corresponding nodes $G_j, G_k \in \mathcal{G}$ and the observable O in the DLA graph.

where $\mathcal{G}_{\text{Lie}2} = \mathcal{G}_{\text{Lie}} \setminus \mathcal{G}_{\text{Lie}1}$ is the complement of $\mathcal{G}_{\text{Lie}1}$ in \mathcal{G}_{Lie} . We also say that the DLA graph is separable when it consists of two or more separated subgraphs.

From a graph perspective, this separability means that a subgraph $\mathcal{G}_{\text{Lie}1}$ is not connected to the rest of the DLA graph $\mathcal{G}_{\text{Lie}2}$ by edges, i.e., $\forall P \in \mathcal{G}_{\text{Lie}1}$ and $\forall Q \in \mathcal{G}_{\text{Lie}2}$ are not \mathfrak{g} -connected. Conversely, if the DLA graph is not separable, any two nodes are \mathfrak{g} -connected.

Let us revisit Condition 2 in terms of the DLA graph. This condition states that, for any $G \in \mathcal{G}$, there exist $Q_1, \dots, Q_m \in \mathcal{G}$ such that $\{G, Q_1\} = \dots = \{Q_m, O\} = 0$. That is, the observable O is \mathfrak{g} -connected to $\forall G \in \mathcal{G}$ and thus $\forall G \in \mathcal{G}_{\text{Lie}}$. Otherwise, the DLA graph can be decomposed into separated subgraphs as $\mathcal{G}_{\text{Lie}} = \mathcal{G}_{\text{Lie}1} \sqcup \mathcal{G}_{\text{Lie}2}$, where $\mathcal{G}_{\text{Lie}1}$ ($\mathcal{G}_{\text{Lie}2}$) is (not) \mathfrak{g} -connected to O (i.e., $[\mathcal{G}_{\text{Lie}1}, \mathcal{G}_{\text{Lie}2}] = [\mathcal{G}_{\text{Lie}2}, O] = 0$). Then, the unitary circuit is also decomposed as $U = U_1 U_2$ with $U_1 \in e^{\mathfrak{g}_1}$ and $U_2 \in e^{\mathfrak{g}_2}$, where we have defined $\mathfrak{g}_1 = \text{span}(\mathcal{G}_{\text{Lie}1})$ and $\mathfrak{g}_2 = \text{span}(\mathcal{G}_{\text{Lie}2})$. From $[U_1, U_2] = [U_2, O] = 0$ (which is derived from $[\mathcal{G}_{\text{Lie}1}, \mathcal{G}_{\text{Lie}2}] = [\mathcal{G}_{\text{Lie}2}, O] = 0$), we have $C = \text{Tr}[\rho U^\dagger O U] = \text{Tr}[\rho U_1^\dagger O U_1]$, indicating that U_2 does not affect the result. Therefore, we assume that such irrelevant gates are absent in the circuit.

In this proof, we map the problem on \mathcal{F}_{eff} and \mathcal{X}_{exp} to the problem on the DLA graph. To this end, we need to interpret \mathcal{F}_{eff} and \mathcal{X}_{exp} in terms of the DLA graph. By definition, the expressivity \mathcal{X}_{exp} corresponds to the total number of nodes in the DLA graph. On the other hand, identifying the gradient measurement efficiency \mathcal{F}_{eff} from the DLA graph is not straightforward. The first step in evaluating \mathcal{F}_{eff} is to understand when two gradient operators Γ_j and Γ_k (namely $\partial_j C$ and $\partial_k C$) are simultaneously measurable. The gradient operator Γ_j is defined from the generator of the circuit $G_j \in \mathcal{G}$, which corresponds to a node of the DLA graph \mathcal{G}_{Lie} . Remarkably, whether Γ_j and Γ_k are simultaneously measurable is determined from the structural relations between the corresponding nodes G_j, G_k and the observable O on the DLA graph.

The following lemmas show the relationship between the simultaneous measurability of gradient components and the DLA structure (see Appendix C 2 for their proofs):

Lemma 1. *If $G_j, G_k \in \mathcal{G}$ are not \mathfrak{g} -connected, $\partial_j C$ and $\partial_k C$ can be simultaneously measured.*

Lemma 2. *For $j, k \leq L_{\text{ini}}$, if $G_j, G_k \in \mathcal{G}$ anti-commute, $\partial_j C$ and $\partial_k C$ cannot be simultaneously measured.*

Lemma 3. *Consider \mathfrak{g} -connected $G_j, G_k \in \mathcal{G}$ for $j, k \leq L_{\text{ini}}$. If $\{G_j, O\} = [G_k, O] = 0$ or $[G_j, O] = \{G_k, O\} = 0$, $\partial_j C$ and $\partial_k C$ cannot be simultaneously measured.*

Lemma 4. *Consider \mathfrak{g} -connected $G_j, G_k \in \mathcal{G}$ for $j, k \leq L_{\text{ini}}$. If there exists $R \in \mathcal{G}_{\text{Lie}}$ such that $\{G_j, R\} = [G_k, R] = 0$ or $[G_j, R] = \{G_k, R\} = 0$, $\partial_j C$ and $\partial_k C$ cannot be simultaneously measured.*

Lemma 5. *For $j < k \leq L_{\text{ini}}$, if $G_j = G_k$, $\partial_j C$ and $\partial_k C$ cannot be simultaneously measured.*

Lemma 1 (Lemmas 2–5) gives the sufficient (necessary) condition of the DLA structure for measuring multiple gradient components simultaneously. Figure 3 illustrates the DLA graph representation of these lemmas. We note that although Lemmas 2–5 assume $j, k \leq L_{\text{ini}} = \mathcal{O}(L)$, the contribution from the final part of the circuit with constant depth $L_{\text{fin}} = \mathcal{O}(1)$ to the gradient measurement efficiency is negligible in the deep circuit limit (see Definition 3). Thus, in the following subsection, we only consider the gradient components for $j, k \leq L_{\text{ini}}$.

C. Trade-off between \mathcal{F}_{eff} and \mathcal{X}_{exp}

Here, we prove Theorem 1 using Lemmas 1–5. Let us begin with showing Eq. (15). By Lemma 5, $\partial_j C$ and $\partial_k C$ are not simultaneously measurable if $G_j = G_k$, which indicates that the maximum number of simultaneously measurable gradient components is bounded by the total

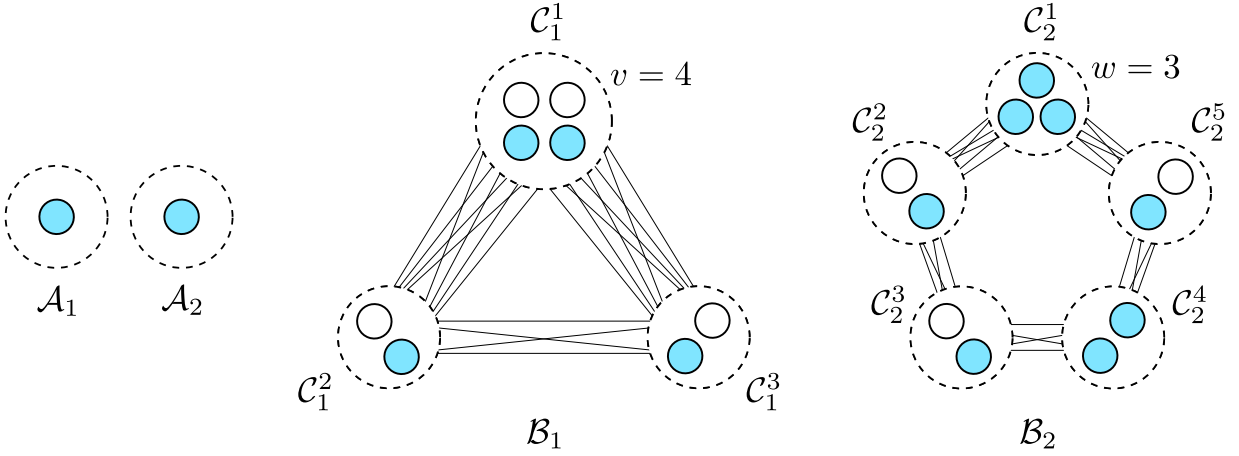


FIG. 4. Example of DLA decomposition. The white (blue) circles denote Pauli operators in \mathcal{G}_{Lie} that (anti-)commute with the observable O . This DLA graph is decomposed as $\mathcal{G}_{\text{Lie}} = \mathcal{A}_1 \sqcup \mathcal{A}_2 \sqcup \mathcal{B}_1 \sqcup \mathcal{B}_2$ with $\mathcal{B}_1 = \bigsqcup_{a=1}^3 \mathcal{C}_1^a$ and $\mathcal{B}_2 = \bigsqcup_{a=1}^5 \mathcal{C}_2^a$, where $p = 2, q = 2, r_1 = 3$, and $r_2 = 5$. As defined in Eqs. (27)–(30), we have $v = 4, w = 3, \mathcal{C}_v = \mathcal{C}_1^1, \mathcal{C}_w = \mathcal{C}_2^1$, and $\mathcal{S} = \{A_1, A_2, F_1 F_1, F_1 F_2, F_1 F_3\}$ with $\mathcal{A}_1 = \{A_1\}, \mathcal{A}_2 = \{A_2\}$, and $\mathcal{C}_w = \{F_1, F_2, F_3\}$.

number of nodes in the DLA graph, namely the expressivity \mathcal{X}_{exp} . Since the gradient measurement efficiency \mathcal{F}_{eff} is defined as the mean number of simultaneously measurable components in the gradient, we obtain $\mathcal{X}_{\text{exp}} \geq \mathcal{F}_{\text{eff}}$.

To prove Eq. (14), we identify the gradient measurement efficiency \mathcal{F}_{eff} in the DLA graph. Lemmas 1–5 give the conditions for measuring two gradient components simultaneously. Based on these lemmas, we decompose the DLA graph into several subgraphs that consist of (potentially) simultaneously measurable nodes, deriving the upper limit of the gradient measurement efficiency. To this end, let us first decompose the DLA graph as

$$\mathcal{G}_{\text{Lie}} = (\mathcal{A}_1 \sqcup \dots \sqcup \mathcal{A}_p) \sqcup (\mathcal{B}_1 \sqcup \dots \sqcup \mathcal{B}_q), \quad (17)$$

where \mathcal{A}_x 's and \mathcal{B}_x 's are separated subgraphs that have one and multiple nodes, respectively (i.e., $|\mathcal{A}_x| = 1$ and $|\mathcal{B}_x| \geq 2$, see Fig. 4). Here, p and q are the numbers of subgraphs \mathcal{A}_x 's and \mathcal{B}_x 's. Since \mathcal{A}_x and \mathcal{B}_x are separated, they satisfy

$$[\mathcal{A}_x, \mathcal{A}_y] = [\mathcal{B}_x, \mathcal{B}_y] = 0 \quad \forall x \neq y, \quad (18)$$

$$[\mathcal{A}_x, \mathcal{B}_y] = 0 \quad \forall x, y. \quad (19)$$

According to Lemma 1, the gradient components for not \mathfrak{g} -connected $G_j, G_k \in \mathcal{G}$ can be measured simultaneously. Therefore, when G_j and G_k are nodes in different subgraphs in the decomposition of Eq. (17), $\partial_j C$ and $\partial_k C$ are simultaneously measurable. We note that the element $A_x \in \mathcal{A}_x$ anti-commutes with the observable O , $\{A_x, O\} = 0$, because all the Pauli operators in \mathcal{G}_{Lie} must be \mathfrak{g} -connected to O by Condition 2. Also, $A_x \in \mathcal{A}_x$ can appear in the quantum circuit just once due to Condition 1 since it commutes with all the other generators in the circuit.

To examine the simultaneous measurability in each \mathcal{B}_x , we further decompose it into r_x subgraphs, based

on Lemmas 2 and 4:

$$\mathcal{B}_x = \mathcal{C}_x^1 \sqcup \dots \sqcup \mathcal{C}_x^{r_x}, \quad (20)$$

where \mathcal{C}_x^a 's satisfy

$$[\mathcal{C}_x^a, \mathcal{C}_x^b] = 0 \quad \text{or} \quad \{\mathcal{C}_x^a, \mathcal{C}_x^b\} = 0 \quad (21)$$

and

$\forall a \neq b, \exists c$, s.t.

$$\begin{cases} [\mathcal{C}_x^a, \mathcal{C}_x^c] = 0 \\ [\mathcal{C}_x^b, \mathcal{C}_x^c] = 0 \end{cases} \quad \text{or} \quad \begin{cases} \{\mathcal{C}_x^a, \mathcal{C}_x^c\} = 0 \\ \{\mathcal{C}_x^b, \mathcal{C}_x^c\} = 0 \end{cases} \quad (22)$$

Equation (21) means that all the nodes in a subgraph \mathcal{C}_x^a share the same (anti-)commutation relations with all the nodes in a subgraph \mathcal{C}_x^b : $[P, Q] = 0 \forall P \in \mathcal{C}_x^a, \forall Q \in \mathcal{C}_x^b$ or $\{P, Q\} = 0 \forall P \in \mathcal{C}_x^a, \forall Q \in \mathcal{C}_x^b$ (see Fig. 4). Considering $a = b$, this condition naturally leads to the commutation relation within each \mathcal{C}_x^a : $[P, Q] = 0 \forall P, Q \in \mathcal{C}_x^a$. Thus, Lemma 2 does not exclude the simultaneous measurability for $P, Q \in \mathcal{C}_x^a$. Also, because of Eq. (22), it is impossible to merge several \mathcal{C}_x^a 's into a larger subgraph satisfying Eq. (21). That is, when $P, Q \in \mathcal{B}_x$ are nodes in different \mathcal{C}_x^a 's, there always exists $R \in \mathcal{B}_x$ such that $[P, R] = \{Q, R\} = 0$ or $\{P, R\} = [Q, R] = 0$. Therefore, for circuit generators $G_j, G_k \in \mathcal{G}$ belonging to different subgraphs \mathcal{C}_x^a 's, their corresponding gradient components $\partial_j C$ and $\partial_k C$ are not simultaneously measurable by Lemma 4.

Finally, we decompose \mathcal{C}_x^a into the commuting and anti-commuting parts with the observable O , based on Lemma 3:

$$\mathcal{C}_x^a = \mathcal{C}_x^{a+} \sqcup \mathcal{C}_x^{a-}, \quad (23)$$

where $\mathcal{C}_x^{a\pm}$ commute and anti-commute with the observable O , respectively:

$$[\mathcal{C}_x^{a+}, O] = 0, \quad \{\mathcal{C}_x^{a-}, O\} = 0. \quad (24)$$

By Lemma 3, for $G_j \in \mathcal{C}_x^{a+}$ and $G_k \in \mathcal{C}_x^{a-}$, their corresponding gradient components $\partial_j C$ and $\partial_k C$ are not simultaneously measurable.

In summary, when $G_j, G_k \in \mathcal{G}$ are nodes in different separated subgraphs \mathcal{A}_x or \mathcal{B}_x , $\partial_j C$ and $\partial_k C$ are simultaneously measurable. Meanwhile, within each \mathcal{B}_x , the necessary condition for simultaneously measuring $\partial_j C$ and $\partial_k C$ for $G_j, G_k \in \mathcal{B}_x$ is that G_j and G_k are nodes in the same $\mathcal{C}_x^{a\pm}$. Therefore, the maximum size of $\mathcal{C}_x^{a\pm}$ bounds the maximum number of simultaneously measurable gradient components in each \mathcal{B}_x .

Using this decomposition, we first show the trade-off inequality for $q = 0$, where q is the number of \mathcal{B}_x . This case corresponds to the commuting generator circuit in Ref. [26], where all the circuit generators $A_x \in \mathcal{A}_x$ are mutually commuting. Then, the number of gates L is finite by Condition 1. In this case, the total number of nodes is p , and they can all be measured simultaneously by Lemma 1. Therefore, the gradient measurement efficiency and the expressivity are

$$\mathcal{F}_{\text{eff}} = \mathcal{X}_{\text{exp}} = p. \quad (25)$$

Meanwhile, A_1, \dots, A_p and $A_1 A_1, \dots, A_1 A_p$ are Pauli operators that differ and commute with each other [49]. Because the maximum number of mutually commuting Pauli operators is 2^n , we have

$$2p \leq 2^n. \quad (26)$$

From Eqs. (25) and (26), we obtain $\mathcal{X}_{\text{exp}} \leq 4^n / \mathcal{F}_{\text{eff}} - \mathcal{F}_{\text{eff}}$.

Next, to prove the case of $q \neq 0$, we define

$$v = \max_{\mathcal{C}_x^a} (|\mathcal{C}_x^a|), \quad (27)$$

$$w = \max_{\mathcal{C}_x^{a\pm}} (|\mathcal{C}_x^{a\pm}|), \quad (28)$$

$$\mathcal{C}_v = \operatorname{argmax}_{\mathcal{C}_x^a} (|\mathcal{C}_x^a|), \quad (29)$$

$$\mathcal{C}_w = \operatorname{argmax}_{\mathcal{C}_x^{a\pm}} (|\mathcal{C}_x^{a\pm}|). \quad (30)$$

Then, by Lemmas 1–5, the gradient measurement efficiency \mathcal{F}_{eff} and the expressivity \mathcal{X}_{exp} (i.e., the total number of nodes) are bounded as

$$\mathcal{F}_{\text{eff}} \leq qw, \quad (31)$$

$$\mathcal{X}_{\text{exp}} \leq p + v(r_1 + \dots + r_q). \quad (32)$$

Note that there are no contributions from \mathcal{A}_x to the right-hand side of Eq. (31). This is because, since the generator $A_x \in \mathcal{A}_x$ commutes with all the other generators, it cannot appear more than once in the circuit due to Condition 1 and thus does not contribute to the gradient measurement efficiency in the deep circuit limit.

Besides Eq. (32), the DLA decomposition uncovers another constraint on the expressivity \mathcal{X}_{exp} . To see that, let us define a set of Pauli operators \mathcal{S} as follows. If $v \geq w + p$, we define

$$\mathcal{S} = \{E_1 E_1, E_1 E_2, \dots, E_1 E_v\} \quad (33)$$

with $\mathcal{C}_v = \{E_1, \dots, E_v\}$. Otherwise, we define

$$\mathcal{S} = \{F_1 F_1, F_1 F_2, \dots, F_1 F_w\} \sqcup \{A_1, \dots, A_p\} \quad (34)$$

with $\mathcal{C}_w = \{F_1, \dots, F_w\}$ and $\mathcal{A}_x = \{A_x\}$. From Eq. (21), all the operators in \mathcal{S} commute with themselves and with \mathcal{G}_{Lie} : $[\mathcal{S}, \mathcal{S}] = [\mathcal{G}_{\text{Lie}}, \mathcal{S}] = 0$. Thus, \mathcal{S} is the stabilizer (or symmetry) of the quantum circuit $U(\theta)$, limiting the degrees of freedom in the DLA, i.e., the expressivity \mathcal{X}_{exp} .

We can derive the inequality (14) by counting the remaining degrees of freedom within the subspace stabilized by \mathcal{S} . For instance, let us consider the simplest case of $p = 0, q = 1$, and $[\mathcal{C}_v, O] = 0$ or $\{\mathcal{C}_v, O\} = 0$ (i.e., $\mathcal{C}_v = \mathcal{C}_w$). In this case, $v = w = |\mathcal{S}|$ and $[O, \mathcal{S}] = 0$ hold. Then the gradient measurement efficiency is bounded as $\mathcal{F}_{\text{eff}} \leq w = |\mathcal{S}|$ from Eq. (31). As for the expressivity, on the other hand, the stabilizers \mathcal{S} constrain the dimension of the DLA as $4^n / |\mathcal{S}|$ (see Lemma 11 in Appendix C3a). Furthermore, since $[\mathcal{G}_{\text{Lie}}, \mathcal{S}] = [O, \mathcal{S}] = 0$, the stabilizers \mathcal{S} are not included in the generators \mathcal{G} and thus the DLA \mathcal{G}_{Lie} because of Condition 2. Hence, we have $\mathcal{X}_{\text{exp}} \leq 4^n / |\mathcal{S}| - |\mathcal{S}|$. These results lead to the inequality $\mathcal{X}_{\text{exp}} \leq 4^n / \mathcal{F}_{\text{eff}} - \mathcal{F}_{\text{eff}}$. In Appendix C3, this trade-off inequality is proved in general cases, where we use the following nontrivial constraints derived from the DLA decomposition, the stabilizers \mathcal{S} , and Eq. (32):

$$\mathcal{X}_{\text{exp}} \leq \frac{4^n v}{4^{q-1} |\mathcal{S}|^2} + (3q - 4)v + p \quad (35)$$

and

$$\frac{4^n v}{4^{q-1} |\mathcal{S}|^2} + (3q - 4)v + p \leq \frac{4^n}{qw} - qw. \quad (36)$$

Combining Eqs. (31), (35), and (36), we finally obtain the trade-off inequality $\mathcal{X}_{\text{exp}} \leq 4^n / \mathcal{F}_{\text{eff}} - \mathcal{F}_{\text{eff}}$, as required.

V. STABILIZER-LOGICAL PRODUCT ANSATZ

While Theorem 1 reveals the general trade-off relation between gradient measurement efficiency and expressivity, designing efficient quantum models that reach the upper limit of the trade-off inequality is a separate issue for realizing practical QML. Here, we propose a general ansatz of the commuting block circuit (CBC) called the stabilizer-logical product ansatz (SLPA), which is constructed from stabilizers and logical operators to reach the upper limit of the trade-off inequality. This ansatz is also insightful in understanding the trade-off relation from a symmetry perspective.

A. Commuting block circuits

This subsection briefly reviews the CBC proposed in Ref. [26] as a variational quantum circuit allowing for efficient gradient estimation. The CBC consists of B block

unitaries:

$$U(\boldsymbol{\theta}) = \prod_{a=1}^B U_a(\boldsymbol{\theta}_a), \quad (37)$$

where each block contains multiple variational rotation gates as

$$U_a(\boldsymbol{\theta}_a) = \prod_j \exp(i\theta_j^a G_j^a). \quad (38)$$

Here, G_j^a is the Pauli generator of the j th rotation gate in the a th block, and $\boldsymbol{\theta}_a = (\theta_1^a, \theta_2^a, \dots)$ is the variational rotation angles. The generators of CBC must satisfy the following two conditions. First, generators within the same block are commutative:

$$[G_j^a, G_k^a] = 0 \quad \forall j, k. \quad (39)$$

Second, generators in any two distinct blocks are either all commutative or all anti-commutative:

$$[G_j^a, G_k^b] = 0 \quad \forall j, k \quad \text{or} \quad \{G_j^a, G_k^b\} = 0 \quad \forall j, k. \quad (40)$$

The structure of CBC is shown in Fig. 2.

This specific structure of CBC allows us to measure the gradient components of the cost function $C(\boldsymbol{\theta}) = \text{Tr}[U(\boldsymbol{\theta})\rho U^\dagger(\boldsymbol{\theta})O]$ (O is a Pauli operator) with only two different quantum circuits for each block. To measure the gradient components for the a th block, we divide the generators of the rotation gates $\mathcal{G}_a = \{G_j^a\}_j$ into the commuting and anti-commuting parts with the observable O : $\mathcal{G}_a = \mathcal{G}_a^{\text{com}} \sqcup \mathcal{G}_a^{\text{ant}}$, where $[\mathcal{G}_a^{\text{com}}, O] = \{\mathcal{G}_a^{\text{ant}}, O\} = 0$. Then the gradient components in $\mathcal{G}_a^{\text{com}}$ ($\mathcal{G}_a^{\text{ant}}$) can be measured simultaneously using the linear combination of unitaries with an ancilla qubit (see Appendix D or Ref. [26] for details). Therefore, the full gradient of $U(\boldsymbol{\theta})$ can be estimated with only $2B$ types of quantum measurements, which is independent of the number of rotation gates in each block (to be precise, $2B - 1$ quantum measurements are sufficient because the commuting part of the final block does not contribute to the gradient). This allows us to measure the gradient more efficiently than conventional variational models based on the parameter-shift method, where the measurement cost is proportional to the number of parameters.

The basic framework of the CBC has been proposed, but there are still several unresolved issues. First, it remains unclear how the specific structure of the commuting block circuit affects the QNN expressivity. Second, a general method to construct the CBC or find the generators G_j^a that satisfy the commutation relations of Eqs. (39) and (40) has not yet been established. Below, we propose the SLPA as a general ansatz of CBC that can reach the upper limit of the trade-off inequality (14). This ansatz also provides a clear understanding of the trade-off relation between gradient measurement efficiency and expressivity from a symmetry perspective.

Before introducing the SLPA, we clarify the relationship between the CBC structure and Lemmas 2–4. First,

Lemma 2 states that measuring two gradient components $\partial_j C$ and $\partial_k C$ simultaneously requires that the corresponding generators G_j and G_k are commutative. This requirement is satisfied in the CBC since the generators in the same block are all commutative as Eq. (39). Second, by Lemma 3, two gradient components $\partial_j C$ and $\partial_k C$ are not simultaneously measurable if the corresponding generators G_j and G_k have different (anti-)commutation relations with the observable O , $\{G_j, O\} = [G_k, O] = 0$ or $[G_j, O] = \{G_k, O\} = 0$. This corresponds to the fact that the gradient of CBC must be measured separately for the commuting and anti-commuting parts $\mathcal{G}_a^{\text{com}}$ and $\mathcal{G}_a^{\text{ant}}$ in each block. Finally, by Lemma 4, two gradient components $\partial_j C$ and $\partial_k C$ are not simultaneously measurable if there exists another generator $R \in \mathcal{G}$ such that $\{G_j, R\} = [G_k, R] = 0$ or $[G_j, R] = \{G_k, R\} = 0$. In the CBC, from Eq. (40), there does not exist such R for generators in the same block, and thus the simultaneous gradient measurement is possible.

B. Stabilizer-logical product ansatz

1. Stabilizer formalism

Here, we propose a general ansatz of CBC, the SLPA, which leverages the symmetric structure of the quantum circuit to enhance the gradient measurement efficiency. To this end, let us begin with defining a stabilizer group $\mathcal{S} = \{S_1, S_2, \dots\} \subset \mathcal{P}_n$, which satisfies

$$[S_j, S_k] = 0 \quad \forall j, k, \quad (41)$$

where $S_j \in \mathcal{S}$ is a Pauli operator (note that the following circuit construction is valid for any stabilizer group). Given that s is the number of independent stabilizers in \mathcal{S} , the order of \mathcal{S} is given by $|\mathcal{S}| = 2^s$, where an arbitrary element of \mathcal{S} is written as a product of the s independent stabilizers. For this stabilizer group, we consider logical operators $\mathcal{L} = \{L_1, L_2, \dots\} \subset \mathcal{P}_n$, which commute with the stabilizers:

$$[S_j, L_a] = 0 \quad \forall j, a, \quad (42)$$

where $L_a \in \mathcal{L}$ is a Pauli operator. The terms stabilizer and logical operators are named after their commutation relations in the field of quantum error correction. Then, by taking the product of the stabilizer S_j and the logical operator L_a , we construct the j th generator of the a th block as (Fig. 2)

$$G_j^a = S_j L_a. \quad (43)$$

Using these generators, we obtain the SLPA

$$U_{\text{SL}}(\boldsymbol{\theta}) = \prod_a U_a(\boldsymbol{\theta}_a) \quad (44)$$

with block unitaries

$$U_a(\boldsymbol{\theta}_a) = \prod_j \exp(i\theta_j^a G_j^a), \quad (45)$$

where each block can contain at most $|\mathcal{S}| = 2^s$ rotation gates. The generators of this ansatz always satisfy the commutation relations of the CBC in Eqs. (39) and (40) as

$$[G_j^a, G_k^a] = [S_j L_a, S_k L_a] = 0 \quad \forall j, k$$

and

$$\begin{aligned} [G_j^a, G_k^b] &= [S_j L_a, S_k L_b] = 0 \quad \forall j, k \quad \text{if } [L_a, L_b] = 0, \\ \{G_j^a, G_k^b\} &= \{S_j L_a, S_k L_b\} = 0 \quad \forall j, k \quad \text{if } \{L_a, L_b\} = 0, \end{aligned}$$

where we have used Eqs. (41) and (42). Therefore, the SLPA is an ansatz of CBC. Remarkably, the SLPA has symmetry \mathcal{S} :

$$[U_{\text{SL}}(\boldsymbol{\theta}), \mathcal{S}] = 0, \quad (46)$$

which is derived from $[G_j^a, \mathcal{S}] = [S_j L_a, \mathcal{S}] = 0$. Furthermore, when the stabilizers \mathcal{S} commute with the observable O (i.e., $[O, \mathcal{S}] = 0$), we can measure all gradient components within a block simultaneously because the generators of the block are either all commutative or all anti-commutative with O : $[G_j^a, O] = 0$ for $\forall j$ or $\{G_j^a, O\} = 0$ for $\forall j$.

Conversely, any CBC can be formulated as an SLPA. To show this, we consider a CBC with generators $\mathcal{G} = \{G_j^a\}$ that satisfy the commutation relations of Eqs. (39) and (40). For these generators, we can define stabilizers $\mathcal{S} = \{G_1^a G_j^a\}_{j,a} = \{S_{ja}\}_{j,a}$ and logical operators $\mathcal{L} = \{G_1^a\}_a = \{L_a\}_a$ with $S_{ja} = G_1^a G_j^a$ and $L_a = G_1^a$. These operator sets \mathcal{S} and \mathcal{L} not only satisfy the requirements of stabilizers and logical operators in Eqs. (41) and (42) but also reproduce the original CBC through Eq. (43). That is, the CBC with generators $\mathcal{G} = \{G_j^a\}$ is equivalent to the SLPA constructed from the stabilizers $\mathcal{S} = \{G_1^a G_j^a\}_{j,a}$ and the logical operators $\mathcal{L} = \{G_1^a\}_a$. In fact, \mathcal{S} and \mathcal{L} obey the commutation relations of stabilizers and logical operators as $[S_{ja}, S_{kb}] = [G_1^a G_j^a, G_1^b G_k^b] = 0$ and $[S_{ja}, L_b] = [G_1^a G_j^a, G_1^b] = 0$, where we have used Eqs. (39) and (40). Besides, the CBC can be constructed from \mathcal{S} and \mathcal{L} by taking their product as $G_j^a = (G_1^a G_j^a) G_1^a = S_{ja} L_a$. Therefore, any CBC can be formulated with stabilizers and logical operators, which implies that the SLPA is a general ansatz of CBC.

2. Enhancing gradient measurement efficiency of symmetric circuits

Using the SLPA, we can enhance the gradient measurement efficiency of a symmetric circuit. Suppose that we have an \mathcal{S} -symmetric circuit $U_{\text{SC}}(\boldsymbol{\theta})$, whose unitary is given by

$$U_{\text{SC}}(\boldsymbol{\theta}) = \prod_{a=1}^B \exp(i\theta_a L_a). \quad (47)$$

Here, L_a is a Pauli operator satisfying $[L_a, \mathcal{S}] = 0$. Typically, L_a is a local Pauli operator, and such symmetric circuits are often used in various applications. We can construct the SLPA from this symmetric circuit via Eqs. (43)–(45) by regarding the generator of the symmetric circuit L_a as the logical operator. In other words, we construct each block of the SLPA from each rotation gate of the symmetric circuit by taking the product of the generator L_a and the stabilizers \mathcal{S} . Whereas the original symmetric circuit has low gradient measurement efficiency in general, the SLPA constructed in this way has high gradient measurement efficiency, where at most $|\mathcal{S}| = 2^s$ gradient components of each block can be measured simultaneously. In addition, symmetry \mathcal{S} retains even in the SLPA (i.e., $[U_{\text{SL}}(\boldsymbol{\theta}), \mathcal{S}] = 0$). Therefore, this SLPA enhances the gradient measurement efficiency of the symmetric circuit while maintaining the symmetric property.

We note that the generator of the SLPA, $G_j^a = S_j L_a$, is generally global, which may make it challenging to implement the SLPA in noisy intermediate-scale quantum devices [50]. Nevertheless, some (early) fault-tolerant quantum computing architectures, such as the surface code with lattice surgery, can easily perform global rotations [51, 52]. Thus, the SLPA is a variational ansatz that is particularly suitable for the (early) fault-tolerant quantum computing era.

3. Backpropagation scaling

The stabilizer formalism also clarifies when the CBC achieves the backpropagation scaling, which specifies the scalability of learning models with respect to the number of training parameters [24, 26]. The backpropagation scaling is defined as

$$\frac{\text{Time}(\nabla C)}{\text{Time}(C)} \leq \mathcal{O}(\log L), \quad (48)$$

where $\text{Time}(C)$ and $\text{Time}(\nabla C)$ are the time complexity of estimating the cost function C and its gradient ∇C with a certain accuracy. Although Ref. [26] proved that the backpropagation scaling is achievable for $B = 1$, whether it is possible even for $B \neq 1$ remains unclear.

In the CBC, the cost function can be estimated with one quantum circuit, whereas $2B - 1$ quantum circuits are needed to estimate the gradient. Therefore, when ignoring the difference between the single circuit execution times for estimating C and ∇C , we have $\text{Time}(\nabla C)/\text{Time}(C) \sim B$. Also, in the stabilizer formalism, the CBC has at most $L = 2^s B$ training parameters. Therefore, the backpropagation scaling is written as

$$B \leq \mathcal{O}(\log B + s \log 2). \quad (49)$$

This indicates that s must increase proportionally to or faster than B to achieve the backpropagation scaling. We note that this discussion ignores the circuit execution time, thus requiring a more thorough analysis to

understand the precise condition for the backpropagation scaling.

C. Trade-off in stabilizer-logical product ansatz

Here, we show that the SLPA can reach the upper limit of the trade-off inequality (14) when the stabilizers \mathcal{S} commute with the observable O . This discussion also offers a clear understanding of the trade-off relation between gradient measurement efficiency and expressivity.

Let us first consider the gradient measurement efficiency of SLPA. When the stabilizers \mathcal{S} commute with the observable O , the generators of each block, $G_j^a = S_j L_a$, are either all commutative or all anti-commutative with the observable O : $[G_j^a, O] = 0$ for $\forall j$ or $\{G_j^a, O\} = 0$ for $\forall j$. Then, we can simultaneously measure all gradient components of each block in the SLPA. Therefore, given that each block can contain at most $|\mathcal{S}| = 2^s$ rotation gates, the gradient measurement efficiency, which is the mean number of simultaneously measurable components in the gradient, obeys

$$\mathcal{F}_{\text{eff}} \leq 2^s. \quad (50)$$

The equality holds if all the blocks of the SLPA have 2^s rotation gates.

While the stabilizers lead to high gradient measurement efficiency, they also limit the expressivity of the quantum circuit. Since all the generators of the SLPA commute with the stabilizers (i.e., $[\mathcal{G}, \mathcal{S}] = 0$), the DLA generated by them commute with the stabilizers as well (i.e., $[\mathcal{G}_{\text{Lie}}, \mathcal{S}] = 0$). Then, the dimension of the subspace in $\mathfrak{su}(2^n)$ stabilized by (commuting with) \mathcal{S} is $4^n/|\mathcal{S}| = 4^n/2^s$ (see Lemma 11 in Appendix C 3a). Furthermore, given that $[\mathcal{G}_{\text{Lie}}, \mathcal{S}] = [O, \mathcal{S}] = 0$, the stabilizers \mathcal{S} are not included in the generators \mathcal{G} and thus the DLA \mathcal{G}_{Lie} due to Condition 2. This consideration provides the upper limit of the DLA dimension, namely the expressivity:

$$\mathcal{X}_{\text{exp}} \leq \frac{4^n}{2^s} - 2^s, \quad (51)$$

where the equality holds if the DLA covers the entire subspace stabilized by \mathcal{S} , except for \mathcal{S} . Combining inequalities (50) and (51), we obtain the trade-off inequality (14) for the SLPA, $\mathcal{X}_{\text{exp}} \leq 4^n/\mathcal{F}_{\text{eff}} - \mathcal{F}_{\text{eff}}$. Then, the upper limit of the inequality is attained when the numbers of rotation gates in all blocks are $|\mathcal{S}| = 2^s$ and the DLA covers the entire subspace stabilized by \mathcal{S} , except for \mathcal{S} [Fig. 1 (b)].

These results intuitively describe the trade-off relation between gradient measurement efficiency and expressivity from a symmetry point of view: we can measure several gradient components simultaneously by leveraging the symmetric structure of the quantum circuit, which instead constrains the expressivity.

VI. NUMERICAL DEMONSTRATION: LEARNING A SYMMETRIC FUNCTION

In this section, we numerically verify the trade-off relation between gradient measurement efficiency and expressivity and demonstrate the high performance of the SLPA in a specific learning problem.

A. Problem and models

Due to its symmetric structure, the SLPA is particularly effective in problems involving symmetry. Such problems are common in quantum chemistry, physics, and machine learning, which are the main targets of quantum computing. In these problems, symmetry provides a guiding principle for designing efficient quantum algorithms or circuits. In VQAs, for instance, the accuracy, trainability, generalization, and feasibility of QNNs can be improved by designing quantum circuits based on the symmetry of quantum states and dynamics of interest [23]. In addition to these improvements, the SLPA increases the gradient measurement efficiency up to the theoretical limit by leveraging the symmetry of problems.

For demonstration, we consider the task of learning an unknown symmetric real scalar function $f(\rho)$, where ρ is an input quantum state. Suppose that we know in advance that $f(\rho)$ satisfies $f(\rho) = f(S_j \rho S_j^\dagger)$ for $\forall S_j \in \mathcal{S}$. To learn this function, we employ a quantum model $h_\theta(\rho) = \text{Tr}[U(\theta)\rho U^\dagger(\theta)O]$ to approximate $f(\rho)$. Then the design of the parameterized quantum circuit $U(\theta)$ is crucial to approximate the target function with high accuracy. In learning this type of symmetric function, an equivariant QNN is effective [35–45]. The equivariant QNN is represented by an \mathcal{S} -symmetric circuit $U(\theta)$ with an \mathcal{S} -symmetric observable O , $[U(\theta), \mathcal{S}] = [O, \mathcal{S}] = 0$, to automatically satisfy the same invariance as the target function $h_\theta(\rho) = h_\theta(S_j \rho S_j^\dagger)$, which improves the trainability and generalization of the learning model. Here, we show that the SLPA can enhance the gradient measurement efficiency of the equivariant QNN while maintaining high trainability and generalization.

For concreteness, we define the target symmetric function as $f(\rho) = \text{Tr}[U_{\text{tag}}\rho U_{\text{tag}}^\dagger O]$ with an \mathcal{S} -symmetric target unitary U_{tag} and the \mathcal{S} -symmetric observable O (i.e., $[U_{\text{tag}}, \mathcal{S}] = [O, \mathcal{S}] = 0$). Assume that \mathcal{S} is given by

$$\mathcal{S} = \{I, \prod_{j=1}^n X_j, \prod_{j=1}^n Y_j, \prod_{j=1}^n Z_j\} \quad (52)$$

with even n . Here, the number of independent operators in \mathcal{S} is $s = 2$. To satisfy this symmetry, the target unitary is set as $U_{\text{tag}} = U_{++} \oplus U_{+-} \oplus U_{-+} \oplus U_{--}$, where $U_{\pm\pm}$ is a 2^{n-2} -dimensional Haar-random unitary acting on the eigenspace of $\prod_{j=1}^n X_j = \pm 1$ and $\prod_{j=1}^n Z_j = \pm 1$. We also assume the symmetric observable $O = X_1 X_2$. To learn this function, we use N_t training data $\{|x_i\rangle, y_i\}_{i=1}^{N_t}$,

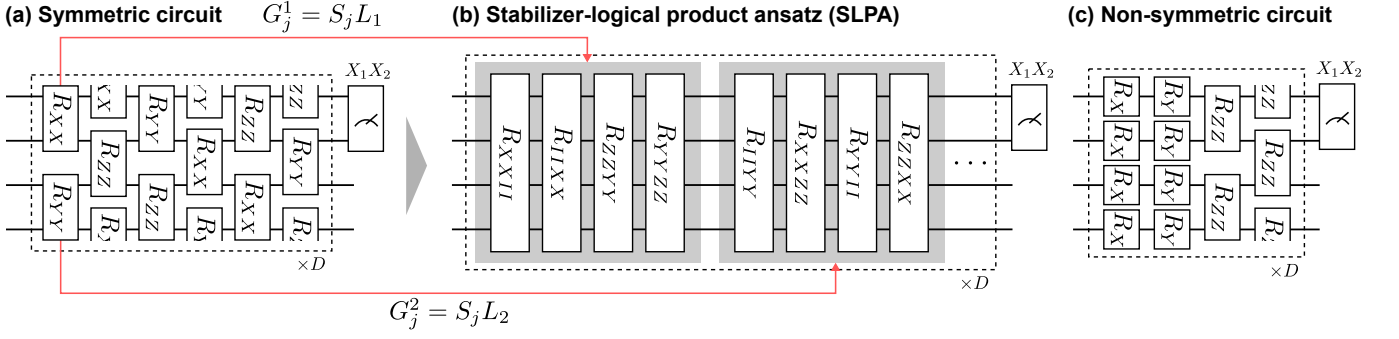


FIG. 5. Illustrations of (a) symmetric circuit, (b) stabilizer-logical product ansatz, and (c) non-symmetric circuit for $n = 4$.

where $|x_i\rangle = \bigotimes_{j=1}^n |s_i^j\rangle$ and $y_i = f(|x_i\rangle)$ are the product state of single qubit Haar-random states and its label, respectively. The model is optimized by minimizing a loss function

$$\text{Loss} = \frac{1}{N_t} \sum_{i=1}^{N_t} [y_i - h_{\theta}(|x_i\rangle)]^2. \quad (53)$$

We also prepare N_t test data for validation, which are sampled independently of training data. Below, we set $N_t = 50$.

To solve this problem, we first consider a local symmetric circuit commuting with \mathcal{S} as follows [Fig. 5 (a)]:

$$U_{\text{SC}}(\theta) = \prod_{d=1}^D \prod_{k=1}^{3n} \exp(i\theta_k^d L_k). \quad (54)$$

Here, a local Pauli operator L_k is defined as

$$L_k = \begin{cases} P_{2k-1}^{\mu_k} P_{2k}^{\mu_k} & \text{for } k = an + b, \\ P_{2k}^{\nu_k} P_{2k+1}^{\nu_k} & \text{for } k = \left(a + \frac{1}{2}\right)n + b \end{cases} \quad (55)$$

with

$$P_j^{\mu} = \begin{cases} X_j & \text{for } \mu = 3\ell + 1 \\ Y_j & \text{for } \mu = 3\ell + 2, \\ Z_j & \text{for } \mu = 3\ell \end{cases} \quad (56)$$

where $a \in \{0, 1, 2\}$, $b \in \{1, \dots, n/2\}$, $\mu_k = a + b$, $\nu_{jk} = a + b + n/2$, $\ell \in \mathbb{Z}$, and $P_j^{\mu} = P_{j+n}^{\mu}$. The number of parameters in this model is $L = 3nD$. The set of generators is given by $\mathcal{G}_{\text{SC}} = \{L_k\} = \{X_j X_{j+1}, Y_j Y_{j+1}, Z_j Z_{j+1}\}_{j=1}^n$, which commutes with the stabilizers \mathcal{S} . In Appendix E, we show that the DLA generated by \mathcal{G}_{SC} covers the entire subspace stabilized by \mathcal{S} , except for \mathcal{S} , which leads to $\mathcal{X}_{\text{exp}} = 4^n/4 - 4$. Then, although the upper limit of the gradient measurement efficiency is $\mathcal{F}_{\text{eff}} = 4$ by Theorem 1, this symmetric circuit cannot reach the upper limit but instead exhibits $\mathcal{F}_{\text{eff}} = 1$ as shown later.

The SLPA is constructed by taking the products of the stabilizers \mathcal{S} and the generators of $U_{\text{SC}}(\theta)$ as [Fig. 5 (b)]

$$U_{\text{SL}}(\theta) = \prod_{d=1}^D \prod_{k=1}^{3n} U_k(\theta_k^d), \quad (57)$$

where $U_k(\theta_k^d)$ is the block unitary defined as

$$U_k(\theta_k^d) = \prod_{j=1}^4 \exp(i\theta_{kj}^d S_j L_k). \quad (58)$$

The number of parameters is $L = 12nD$. Here, the set of the generators is given by $\mathcal{G}_{\text{SL}} = \mathcal{G}_{\text{SC}} \times \mathcal{S}$. The dimension of the DLA, or the expressivity, is the same as the symmetric circuit, $\mathcal{X}_{\text{exp}} = 4^n/4 - 4$. Meanwhile, given that the generators of each block are either all commutative or all anti-commutative with the observable O (which is derived by $[O, \mathcal{S}] = 0$), we can measure four gradient components of each block simultaneously. Therefore, in contrast to the symmetric circuit $U_{\text{SC}}(\theta)$, this SLPA can reach the upper limit of the gradient measurement efficiency $\mathcal{F}_{\text{eff}} = 4$.

For comparison, we also consider the following local non-symmetric circuit [Fig. 5 (c)]:

$$U_{\text{NSC}}(\theta) = \prod_{d=1}^D V_{\text{ent}}(\theta_3^d) V_{\text{rot}}(\theta_1^d, \theta_2^d) \quad (59)$$

with

$$V_{\text{rot}}(\theta_1^d, \theta_2^d) = \prod_{j=1}^n \exp(i\theta_{2j}^d Y_j) \exp(i\theta_{1j}^d X_j), \quad (60)$$

$$V_{\text{ent}}(\theta_3^d) = \prod_{j=1}^n \exp(i\theta_{3j}^d Z_j Z_{j+1}), \quad (61)$$

where the number of parameters is $L = 3nD$. The generators $\mathcal{G}_{\text{NSC}} = \{X_j, Y_j, Z_j Z_{j+1}\}_{j=1}^n$ do not commute with the stabilizers \mathcal{S} and lead to the maximum expressivity in the full Hilbert space $\mathcal{X}_{\text{exp}} = 4^n - 1$ [33]. Hence, the gradient measurement efficiency of this model must be $\mathcal{F}_{\text{eff}} = 1$ by Theorem 1.

In gradient estimation, we employ the parameter-shift method for the symmetric and non-symmetric circuits and the direct measurement with an ancilla qubit for the SLPA (see Appendix D or Ref. [26] for details), where N_{shot} measurement shots are used per circuit. We minimize the loss function using the Adam algorithm [53] based on the estimated gradient. The hyper-parameter

values used in this work are initial learning rate = 10^{-3} , $\beta_1 = 0.9$, $\beta_2 = 0.999$, and $\epsilon = 10^{-8}$. We also adopt the stochastic gradient descent [54], where only one training data is used to estimate the gradient at each iteration.

B. Gradient measurement efficiency

First, we investigate the gradient measurement efficiency for the SLPA and symmetric and non-symmetric circuits. In Figs. 6 (a)–(c), we numerically compute the commutation relations between all the pairs of the gradient operators for random θ , where the black and yellow regions indicate $[\Gamma_j(\theta), \Gamma_k(\theta)] = 0$ and $[\Gamma_j(\theta), \Gamma_k(\theta)] \neq 0$, respectively. In the symmetric and non-symmetric circuits, most pairs of gradient operators are not commutative, which implies that we cannot measure two or more gradient components simultaneously, with a few exceptions. In other words, the gradient measurement efficiency is almost one. In the SLPA, on the other hand, we observe a 4×4 block structure in Fig. 6 (b). This means that four gradient operators can be measured simultaneously, indicating that the gradient measurement efficiency of the SLPA is almost four. Note that the gradient components for the final parts of the circuits [the lower right parts of Figs. 6 (a)–(c)] are simultaneously measurable because the generators in the final part are effectively not \mathfrak{g} -connected by assuming that the initial part of the circuit is already applied to the input state ρ and not included in \mathcal{G} (use Lemma 1).

Figure 6 (d) shows the gradient measurement efficiency for finite-depth circuits, $\mathcal{F}_{\text{eff}}^{(L)}$, with varying the number of parameters L . In the symmetric and non-symmetric circuits, $\mathcal{F}_{\text{eff}}^{(L)}$ has a relatively large value for small L but decreases to one as the circuit becomes deeper. In particular, since the non-symmetric circuit has $\mathcal{N}_{\text{exp}} = 4^n - 1$, $\mathcal{F}_{\text{eff}} = 1$ is the theoretical upper limit in $L \rightarrow \infty$ according to Theorem 1. The SLPA shows a similar behavior, but $\mathcal{F}_{\text{eff}}^{(L)}$ of the SLPA is larger than those of the other two models for the entire region of L , eventually approaching the theoretical upper limit $\mathcal{F}_{\text{eff}} = 4$ in the deep circuit limit. These results support the validity of our trade-off relation and show the high gradient measurement efficiency of the SLPA in both shallow and deep circuit regions.

C. Reduction in training cost

The SLPA can decrease the measurement cost required for training due to its high gradient measurement efficiency. We demonstrate this advantage in learning the symmetric function $f(\rho)$. In this demonstration, we use $N_{\text{shot}} = 1000$ measurement shots per circuit for gradient estimation and set the number of parameters to $L = 96$ for all the models.

Figure 7 illustrates that the SLPA shows significantly

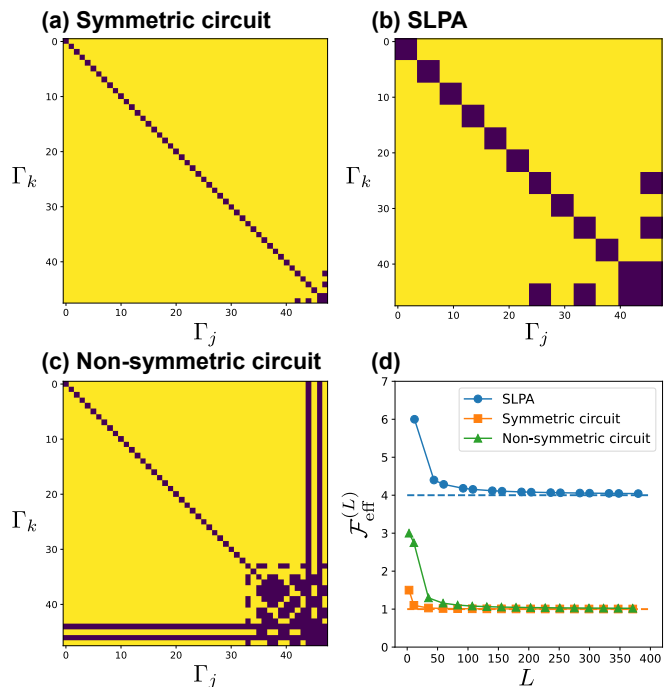


FIG. 6. (a)–(c) Numerical simulations of commutators between two gradient operators $\Gamma_j(\theta)$ and $\Gamma_k(\theta)$ in the SLPA and symmetric and non-symmetric circuits for $n = 4$ qubits and $L = 48$ parameters. The black and yellow regions represent $[\Gamma_j(\theta), \Gamma_k(\theta)] = 0$ and $[\Gamma_j(\theta), \Gamma_k(\theta)] \neq 0$ for random θ , respectively. (d) Changes in gradient measurement efficiency as the number of parameters L is varied. Its value is computed by minimizing the number of simultaneously measurable groups of $\Gamma_j(\theta)$'s for random θ . The blue circles, orange squares, and green triangles are the results of the SLPA and symmetric and non-symmetric circuits, which approach four and one in the limit of $L \rightarrow \infty$, respectively.

faster convergence of training and test losses compared to the other models in terms of the cumulative number of measurement shots. This fast convergence stems from the high gradient measurement efficiency of the SLPA. As discussed above, the SLPA has $\mathcal{F}_{\text{eff}} = 4$ in the deep circuit limit, which is four times greater than the other two models with $\mathcal{F}_{\text{eff}} = 1$. Furthermore, the parameter-shift method used in the symmetric and non-symmetric circuits requires twice the number of circuits for estimating a gradient component than the direct measurement used in the SLPA. Thus, the number of measurement shots per epoch for the SLPA is one-eighth that of the other models in total, leading to a drastic reduction in the quantum measurement resources needed for training.

Besides the high gradient measurement efficiency, the SLPA exhibits a high generalization performance. As shown in Fig. 7 (b), the test loss after training in the SLPA is comparable to that of the symmetric circuit. This is because, as in the symmetric circuit, the symmetry of the unknown function $f(\rho)$ is encoded in the SLPA to improve generalization. In contrast, the non-symmetric circuit sufficiently reduces the training loss

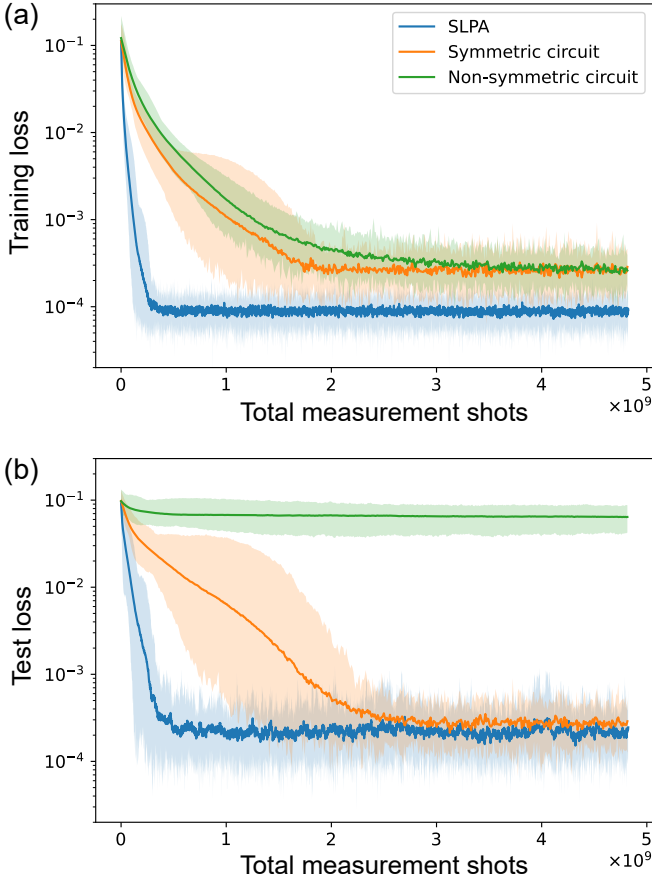


FIG. 7. (a)–(b) Changes in training and test losses during the training process for $n = 4$ qubits and $L = 96$ parameters. We use $N_{\text{shot}} = 1000$ measurement shots per circuit for gradient estimation, and the horizontal axes of the graphs indicate the cumulative number of shots. The solid lines and shaded areas represent the mean, maximum, and minimum of the losses for 20 sets of random initial parameters.

but not the test loss, indicating its low generalization. These results highlight the importance of symmetry encoding in this problem.

In Appendix F, we provide some additional results for fewer N_{shot} . Even in these cases, similar trends to the results in this section can be observed, although the final accuracy after training is worse due to the statistical errors in the gradient estimation.

D. High trainability

High trainability is essential to solve large-scale problems in QNNs. There is a concern that the global operators of the SLPA may lead to low trainability due to a barren plateau [48], namely the exponentially flat landscape of the cost function. This subsection shows that such a concern is unnecessary, i.e., that the global operators do not directly cause a barren plateau in the SLPA. Rather, our model can be less prone to the barren plateau

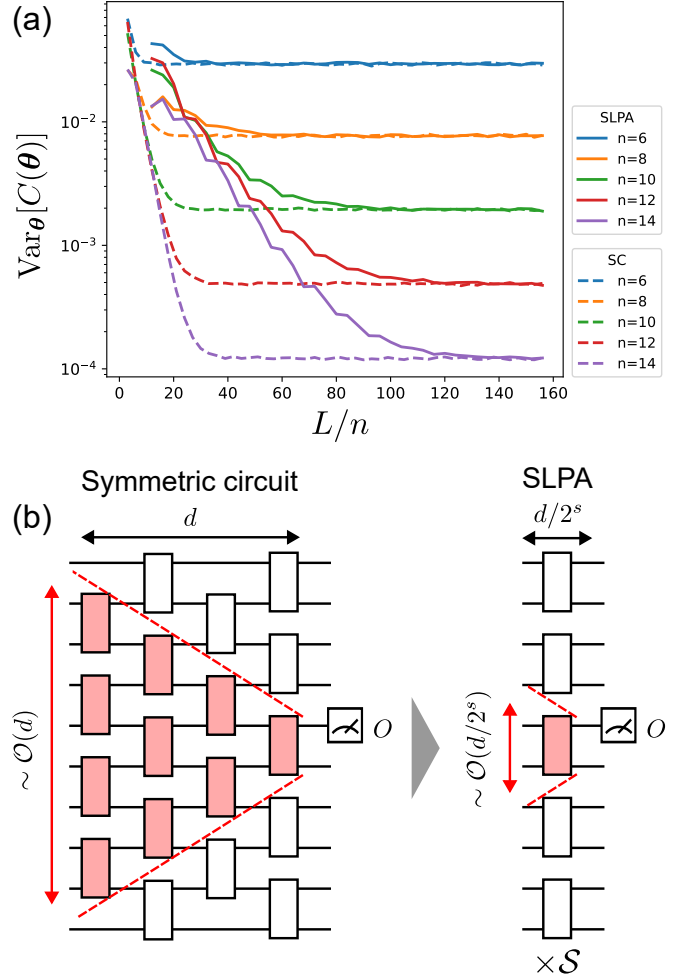


FIG. 8. (a) The variance of the cost function for several numbers of qubits n and numbers of parameters L . The variance is computed by sampling 10000 parameter points from the uniform distribution $\theta \in [-\pi/2, \pi/2]^L$. The solid and dashed lines indicate the results of the SLPA and the symmetric circuit (SC), respectively. (b) Adjoint action of a local unitary circuit on a local observable. In the SLPA, given that the total number of Pauli rotation gates is the same as the symmetric circuit, the circuit depth is effectively reduced by a factor of 2^s , leading to high trainability.

phenomenon than the based symmetric model.

First of all, numerical evidence is presented in Fig. 8 (a), where we investigate the variance of the cost function in the parameter space for the symmetric circuit and the SLPA with varying the number of qubits n and the number of parameters L . In the symmetric circuit, $\text{Var}_{\theta}[C(\theta)]$ decreases as the circuit depth L/n and finally converges to a finite value. The converged value of $\text{Var}_{\theta}[C(\theta)]$ becomes exponentially small as the number of qubits n increases, which indicates that a barren plateau occurs in a deep symmetric circuit. In the SLPA, we observe a similar behavior, where $\text{Var}_{\theta}[C(\theta)]$ decreases as L/n and finally converges to almost the same value as the symmetric circuit. However, the convergence of

$\text{Var}_\theta[C(\boldsymbol{\theta})]$ is slower than that of the symmetric circuit. This result implies the high trainability of our model (in addition, together with Fig. 6 (d), these results also support the compatibility of high gradient measurement efficiency and trainability).

We provide an intuitive mechanism for the slow convergence of the cost function variance in the SLPA. To this end, we follow the argument in Ref. [55]. Let us consider the observable in the Heisenberg picture $\tilde{O}(\boldsymbol{\theta}) = U^\dagger(\boldsymbol{\theta})OU(\boldsymbol{\theta})$, where the cost function is written as the Hilbert–Schmidt inner product of the input state ρ and the observable $\tilde{O}(\boldsymbol{\theta})$: $C(\boldsymbol{\theta}) = \text{Tr}[\rho\tilde{O}(\boldsymbol{\theta})]$. When $\tilde{O}(\boldsymbol{\theta})$ lives in an exponentially large subspace, the inner product $\text{Tr}[\rho\tilde{O}(\boldsymbol{\theta})]$ will be exponentially small due to the curse of dimensionality, which is the fundamental cause of barren plateaus. To quantify this mechanism, let \mathcal{B} be the operator subspace where $\tilde{O}(\boldsymbol{\theta})$ lives. That is, $\tilde{O}(\boldsymbol{\theta})$ can be expanded as $\tilde{O}(\boldsymbol{\theta}) = \sum_{P \in \mathcal{B}} \alpha_P(\boldsymbol{\theta})P$ with Pauli operators P . Then, given that the cost function is the inner product of $\tilde{O}(\boldsymbol{\theta})$ and ρ in the subspace \mathcal{B} , the variance of the cost function decreases inversely proportional to the dimension of \mathcal{B} : $\text{Var}_\theta[C(\boldsymbol{\theta})] \sim 1/\text{poly}(\dim(\mathcal{B}))$. For example, an exponentially large $\dim(\mathcal{B})$ generally results in an exponentially small variance of the cost function. Therefore, $\dim(\mathcal{B})$ gives an insight into barren plateaus.

We investigate $\dim(\mathcal{B})$ of the symmetric circuit and the SLPA to show that our model has smaller $\dim(\mathcal{B})$ when the stabilizers commute with the observable O . Suppose that $\tilde{O}(\boldsymbol{\theta})$ in the symmetric circuit of Eq. (54) is expanded as

$$\tilde{O}_{\text{SC}}(\boldsymbol{\theta}) = \sum_{P \in \mathcal{B}_{\text{SC}}} \alpha_P(\boldsymbol{\theta})P, \quad (62)$$

where P is a Pauli operator and $\alpha_P(\boldsymbol{\theta})$ is a coefficient. In the SLPA of Eq. (57), given that the stabilizers $\mathcal{S} = \{S_1, S_2, \dots\}$ are closed under products (i.e., $S_j S_k \in \mathcal{S}$), we have

$$\tilde{O}_{\text{SL}}(\boldsymbol{\theta}) = \sum_{S \in \mathcal{S}} \sum_{P \in \mathcal{B}_{\text{SC}}} \beta_{P,S}(\boldsymbol{\theta})PS, \quad (63)$$

where $\beta_{P,S}(\boldsymbol{\theta})$ is a coefficient. One can verify Eq. (63) using $[S_j, S_k] = [S_j, L_k] = [S_j, O] = 0$ and $e^{-i\theta Q} P e^{i\theta Q} = (\cos^2 \theta \pm \sin^2 \theta)P - i(\cos \theta \sin \theta \mp \cos \theta \sin \theta)PQ$ iteratively in $\tilde{O}(\boldsymbol{\theta})$ (P, Q are Pauli operators, and \pm corresponds to $[P, Q] = 0$ and $\{P, Q\} = 0$ respectively). Equation (63) leads to the operator subspace of SLPA as $\mathcal{B}_{\text{SL}} = \mathcal{B}_{\text{SC}} \times \mathcal{S}$.

This discussion gives the relationship between the dimensions of the operator subspaces in the symmetric circuit and the SLPA:

$$\dim(\mathcal{B}_{\text{SL}}) \leq 2^s \dim(\mathcal{B}_{\text{SC}}). \quad (64)$$

Therefore, if $s = \mathcal{O}(\text{polylog}(n))$, the SLPA never exponentially spoils the trainability of the symmetric circuit. For example, let us consider a local quantum circuit as Eq. (54). When the observable O is local [56], since $\tilde{O}(\boldsymbol{\theta})$

acts only on $\mathcal{O}(d)$ qubits inside the backward light cone as shown in Fig. 8 (b) (d is the circuit depth), we have

$$\dim(\mathcal{B}_{\text{SC}}) \sim \mathcal{O}(4^d) \quad (65)$$

and thus

$$\dim(\mathcal{B}_{\text{SL}}) \lesssim \mathcal{O}(4^{d+s/2}). \quad (66)$$

If d and s are both $\mathcal{O}(\text{polylog}(n))$, we obtain $\dim(\mathcal{B}_{\text{SL}}) \in \mathcal{O}(\text{poly}(n))$, indicating that the SLPA does not suffer from barren plateaus.

We note that the above discussion does not take into account the differences in the number of rotation gates between U_{SC} and U_{SL} . To fairly compare $\dim(\mathcal{B})$ of the symmetric circuit and the SLPA, we should match the total number of rotation gates for these two models. In the SLPA, replacing d with $d/2^s$ in Eq. (66) to match the total number of gates [see Fig. 8 (b)], we have

$$\dim(\mathcal{B}_{\text{SL}}) \lesssim \mathcal{O}(4^{d/2^s + s/2}). \quad (67)$$

Comparing Eqs. (65) and (67), $\dim(\mathcal{B}_{\text{SL}})$ can be smaller than $\dim(\mathcal{B}_{\text{SC}})$ when $d/2^s + s/2 \lesssim d$, which suggests that the SLPA can have a larger variance of the cost function than the symmetric circuit with the same number of rotation gates. We emphasize that since this result does not rely on the details of the model, except for the localities of U_{SC} and O and some commutation relations, we would observe similar behavior in other SLPAs. Finally, in sufficiently deep circuits, $\text{Var}_\theta[C(\boldsymbol{\theta})]$ converges to the same value in both models because the variance of the cost function in the deep circuit limit is determined by the expressivity [33, 46, 47], $\text{Var}_\theta[C(\boldsymbol{\theta})] \sim 1/\mathcal{X}_{\text{exp}}$, and these two models have the same $\mathcal{X}_{\text{exp}} = 4^n/4 - 4$.

VII. DISCUSSIONS AND CONCLUSIONS

This work has proved the general trade-off relation between gradient measurement efficiency and expressivity in a wide class of deep QNNs. This trade-off reveals the theoretical limitation of QNNs that a more expressive QNN requires a higher measurement cost for gradient estimation. On the other hand, it also opens up new possibilities to increase gradient measurement efficiency by reducing the expressivity to suit a given problem, i.e., by encoding prior knowledge of the problem to the quantum circuit as an inductive bias. Based on this idea, we have proposed a general ansatz of CBC called the SLPA, which can reach the upper limit of the trade-off inequality by leveraging prior knowledge of a problem's symmetry. In other words, the SLPA allows us to measure the gradient with theoretically the fewest types of quantum measurements for a given expressivity. Owing to its symmetric structure, the SLPA is particularly effective in solving symmetry-related problems. In learning an unknown symmetric function, we have demonstrated that our ansatz can significantly reduce the quantum resources required for training while maintaining accuracy

and trainability compared to conventional QNNs based on the parameter-shift method.

Although we have shown the effectiveness of the SLPA in the QML task, it is also applicable to other VQAs [23]. For instance, when computing the ground state of a symmetric Hamiltonian with the variational quantum eigensolver [8], symmetry-preserving quantum circuits are often used to improve the accuracy of the computation [57]. Then, we can alternatively employ the SLPA, which is constructed from the symmetry (stabilizer) of the Hamiltonian, to enhance the gradient measurement efficiency of the symmetry-preserving circuit. Note that our trade-off inequality cannot be exactly applied to such problems because the Hamiltonian is a sum of Pauli operators in general, whereas this work has assumed that the observable O is a Pauli operator. While our results can provide a basis for efficient training even in Hamiltonian problems, exploring exact trade-off relations beyond our theory and establishing efficient models in more general situations are crucial future research directions.

The theoretical limit of gradient measurement efficiency also motivates further investigation of other approaches for training quantum circuits. A promising one is the use of gradient-free optimization algorithms, such as Powell's method [58] and simultaneous perturbation stochastic approximation [59]. Such algorithms use only a few quantum measurements to update the circuit parameters, potentially speeding up the training process. However, it remains unclear how effective the gradient-free algorithms are for large-scale problems. Thorough verification and refinement of these algorithms could overcome the challenge of high computational costs in VQAs. Another promising direction is the coherent manipulation of multiple copies of input data. Since our theory has implicitly assumed that only one copy of input data is available at a time, the existence of more efficient algorithms surpassing our trade-off inequality is not prohibited in multi-copy settings. In fact, there is an efficient algorithm for measuring the gradient in multi-copy settings, where $\mathcal{O}(\text{polylog}(L))$ copies of input data are coherently manipulated to be measured by shadow tomography [24, 28]. However, this algorithm is hard to implement in near-term quantum devices due to the requirements of many qubits and long execution times. Exploring more efficient algorithms in multi-copy settings is an important open issue.

ACKNOWLEDGMENTS

Fruitful discussions with Riki Toshio, Yuichi Kamata, and Shintaro Sato are gratefully acknowledged. S.Y. was supported by FoPM, WINGS Program, the University of Tokyo.

Appendix A: QNNs with non-variational Clifford gates

In the main text, we have considered the quantum circuits of the following form:

$$U(\boldsymbol{\theta}) = \prod_{j=1}^L e^{i\theta_j G_j}. \quad (\text{A1})$$

Here we show that even if the quantum circuit has non-variational Clifford gates (e.g., CZ and CNOT gates), it can be transformed into the form of Eq. (A1).

Let us consider the following quantum model:

$$U(\boldsymbol{\theta}) = W_{L+1} \left(\prod_{j=1}^L e^{i\theta_j G_j} W_j \right), \quad (\text{A2})$$

where W_j is a Clifford gate. By swapping the Clifford and the rotation gates with $e^{i\theta_j G_j} W_j = W_j e^{i\theta_j W_j^\dagger G_j W_j}$, we have

$$U(\boldsymbol{\theta}) = \left(\prod_{j=1}^{L+1} W_j \right) \left(\prod_{j=1}^L e^{i\theta_j G'_j} \right) \equiv W U'(\boldsymbol{\theta}), \quad (\text{A3})$$

where $G'_j = W_1^\dagger \cdots W_j^\dagger G_j W_j \cdots W_1$ is a Clifford transformed Pauli operator. We have defined $W = \prod_{j=1}^{L+1} W_j$ and $U'(\boldsymbol{\theta}) = \prod_{j=1}^L e^{i\theta_j G'_j}$. Then, the cost function is written as

$$\begin{aligned} C(\boldsymbol{\theta}) &= \text{Tr} [U(\boldsymbol{\theta}) \rho U^\dagger(\boldsymbol{\theta}) O] \\ &= \text{Tr} [U'(\boldsymbol{\theta}) \rho U'^\dagger(\boldsymbol{\theta}) O'] \end{aligned} \quad (\text{A4})$$

with a Pauli observable $O' = W^\dagger O W$. In other words, the quantum model of $U(\boldsymbol{\theta})$ with the Pauli observable O is equivalent to that of $U'(\boldsymbol{\theta})$ with the Pauli observable O' . Since $U'(\boldsymbol{\theta})$ has the same form of Eq. (A1), the quantum circuit of Eq. (A2) can be transformed to that of Eq. (A1).

Appendix B: Gradient operator

Here, we derive Eq. (3) in the main text. The derivative of the cost function $C(\boldsymbol{\theta}) = \text{Tr}[\rho U^\dagger(\boldsymbol{\theta}) O U(\boldsymbol{\theta})]$ is

$$\frac{\partial C}{\partial \theta_j} = \text{Tr} \left[\rho \frac{\partial U^\dagger}{\partial \theta_j} O U \right] + \text{Tr} \left[\rho U^\dagger O \frac{\partial U}{\partial \theta_j} \right]. \quad (\text{B1})$$

In this equation, $\partial U / \partial \theta_j$ is written as

$$\frac{\partial U}{\partial \theta_j} = i U_{j-} G_j U_{j+}, \quad (\text{B2})$$

where U_{j+} and U_{j-} are the unitaries before and after the j th rotation gate:

$$U_{j+} = \prod_{k=1}^{j-1} e^{i\theta_k G_k}, \quad (\text{B3})$$

$$U_{j-} = \prod_{k=j}^L e^{i\theta_k G_k}. \quad (\text{B4})$$

By inserting $U_{j+}U_{j+}^\dagger = I$ into Eq. (B2), we have

$$\frac{\partial U}{\partial \theta_j} = iU_{j-}(U_{j+}U_{j+}^\dagger)G_jU_{j+} = iU\tilde{G}_j, \quad (\text{B5})$$

with $\tilde{G}_j = U_{j+}^\dagger G_j U_{j+}$ and $U_{j-}U_{j+} = U$. By taking the Hermitian conjugate of Eq. (B5), we also have

$$\frac{\partial U^\dagger}{\partial \theta_j} = -i\tilde{G}_j^\dagger U^\dagger. \quad (\text{B6})$$

Therefore, Eq. (B1) is

$$\begin{aligned} \frac{\partial C}{\partial \theta_j} &= -i\text{Tr}[\rho\tilde{G}_jU^\dagger OU] + i\text{Tr}[\rho U^\dagger OU\tilde{G}_j] \\ &= -i\text{Tr}[\rho[\tilde{G}_j, \tilde{O}]] \\ &= \text{Tr}[\rho\Gamma_j], \end{aligned} \quad (\text{B7})$$

where we have defined $\Gamma_j = -i[\tilde{G}_j, \tilde{O}]$ with $\tilde{O} = U^\dagger OU$.

Appendix C: Proof of main theorem

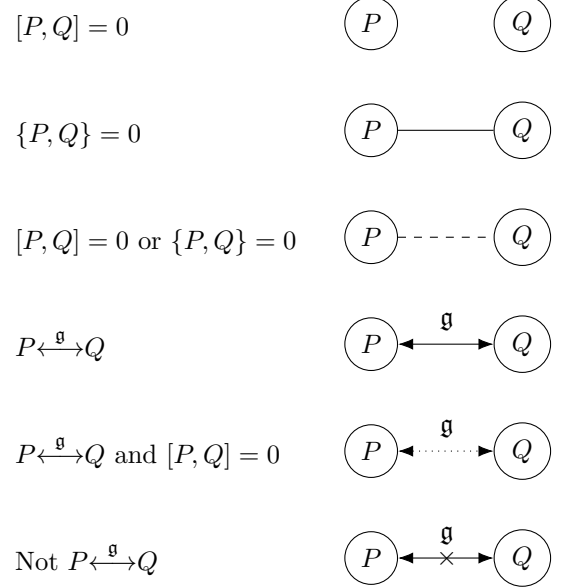
This Appendix proves Theorem 1 in the main text. We first show several properties of the DLA graph and then prove Lemmas 1–5 on the relationship between the simultaneous measurability of gradient components and the DLA structure. Based on these lemmas, we finally prove Theorem 1.

1. Properties of DLA graph

This subsection shows several lemmas on the DLA graph to prove Lemmas 1–5. In the main text, we have introduced the DLA graph to help understand the DLA structure. Each node P of the DLA graph corresponds to a Pauli basis of the DLA \mathcal{G}_{Lie} , and two nodes $P, Q \in \mathcal{G}_{\text{Lie}}$ are connected by an edge if $\{P, Q\} = 0$. We say that $P, Q \in \mathcal{P}_n$ are \mathfrak{g} -connected when there exists a path connecting P and Q on the DLA graph. We also say that a DLA subgraph $\mathcal{G}_{\text{Lie}1} \subset \mathcal{G}_{\text{Lie}}$ is separated when it is not connected with the rest of the DLA graph by edges (see Definitions 5 and 6 for the exact definitions). For the sake of convenience, we additionally define the path and distance on the DLA graph:

Definition 7 (Path and distance). For \mathfrak{g} -connected $P, Q \in \mathcal{P}_n$ ($P \neq Q$), consider $R_1, R_2, \dots, R_{d-1} \in \mathcal{G}_{\text{Lie}}$ such that $\{P, R_1\} = \{R_1, R_2\} = \dots = \{R_{d-1}, Q\} = 0$. Then, we call $P \rightarrow R_1 \rightarrow \dots \rightarrow R_{d-1} \rightarrow Q$ a path between P and Q and define its distance as d .

The graph representations in this work are summarized below:



In what follows, we prove several lemmas on the DLA graph, which are summarized in Fig. 9. From now on, we ignore the coefficients of Pauli operators because only commutation and anti-commutation relations are relevant for the proof.

Lemma 6. *If $P, Q \in \mathcal{P}_n$ ($P \neq Q$) are \mathfrak{g} -connected, the shortest distance between them on the DLA graph is one or two.*

Proof. We prove this lemma by contradiction. Assume that the shortest distance between P and Q on the DLA graph is $d > 2$, and let $R_1, \dots, R_{d-1} \in \mathcal{G}_{\text{Lie}}$ be the nodes on the shortest path. For convenience, we denote P and Q by R_0 and R_d , respectively:



Since this path is the shortest, these nodes are not connected by an edge except for the neighboring nodes:

$$\{R_j, R_k\} = 0 \quad \text{if } |j - k| = 1, \quad (\text{C1})$$

$$\{R_j, R_k\} \neq 0 \quad \text{if } |j - k| \neq 1. \quad (\text{C2})$$

By definition of the DLA, the following nested commutator R is in \mathcal{G}_{Lie} :

$$\begin{aligned} iR &= [iR_{d-1}, [\dots, [iR_3, [iR_2, iR_1]] \dots]] \\ &= (2^{d-2}i^{d-1})R_{d-1} \dots R_1 \in \mathcal{G}_{\text{Lie}}, \end{aligned} \quad (\text{C3})$$

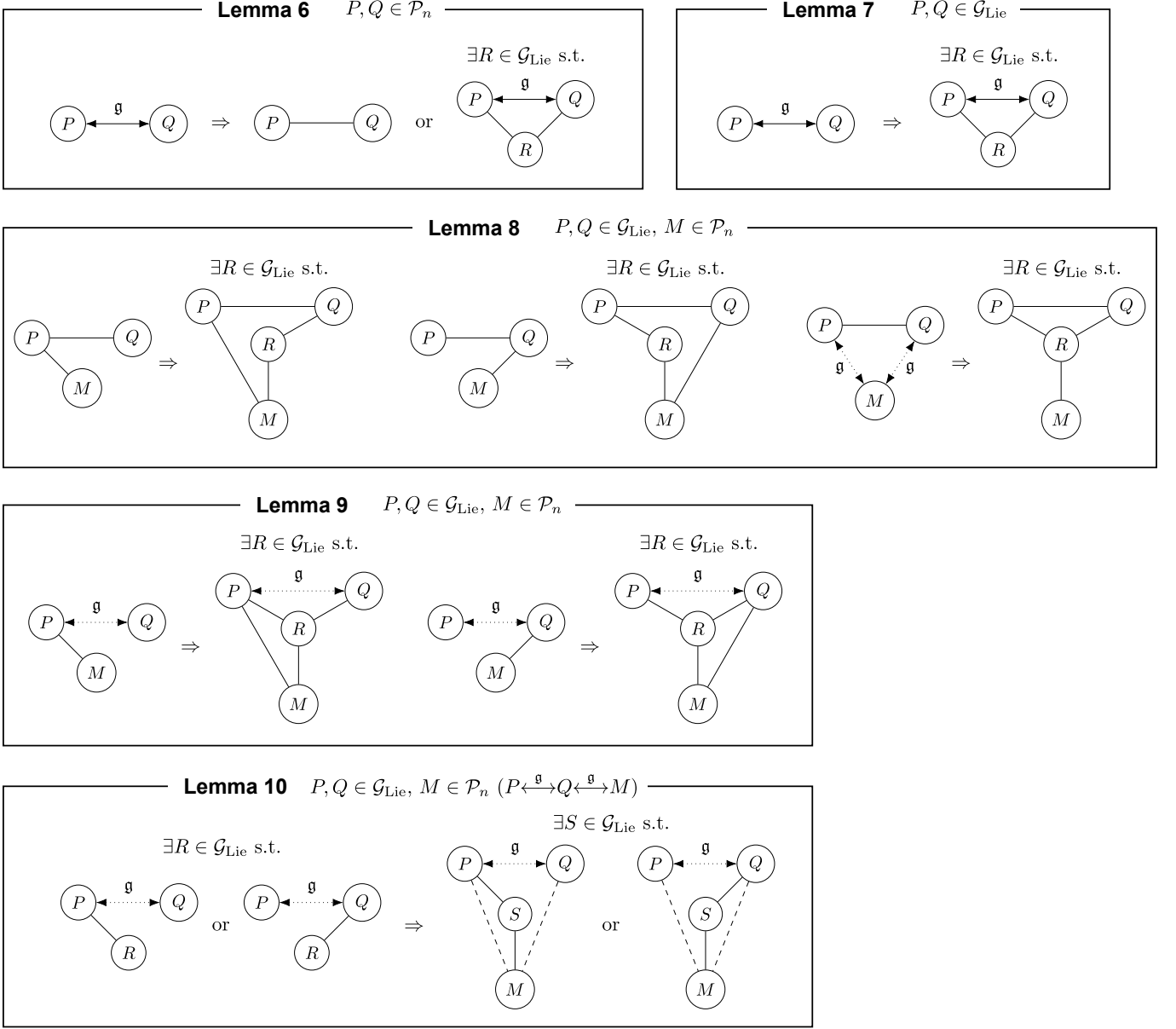


FIG. 9. Summary of Lemmas 6–10.

where we have used Eqs. (C1) and (C2) for the second equation. Then, $P \rightarrow R \rightarrow Q$ is a path of distance two because the Pauli operator $R \in \mathcal{G}_{\text{Lie}}$ anti-commutes with $P = R_0$ and $Q = R_d$. This contradicts the assumption that the shortest distance between P and Q is greater than two. Therefore, the shortest distance is one or two. \square

Lemma 7. *If $P, Q \in \mathcal{G}_{\text{Lie}}$ ($P \neq Q$) are \mathfrak{g} -connected, there exists $R \in \mathcal{G}_{\text{Lie}}$ such that $\{P, R\} = \{Q, R\} = 0$.*

Proof. By Lemma 6, the shortest distance between P and Q on the DLA graph is one or two. If the shortest distance is two, there exists $R \in \mathcal{G}_{\text{Lie}}$ such that $\{P, R\} = \{Q, R\} = 0$ by definition of the distance. If

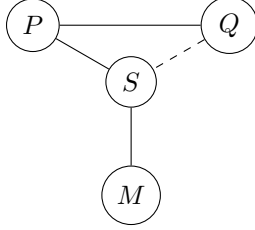
the shortest distance is one (i.e., $\{P, Q\} = 0$), $iR = [iP, iQ] = -2PQ \in \mathcal{G}_{\text{Lie}}$ satisfies $\{P, R\} = \{Q, R\} = 0$, as required. \square

Lemma 8. *For $P, Q \in \mathcal{G}_{\text{Lie}}$ and $M \in \mathcal{P}_n$ satisfying $\{P, Q\} = 0$ and $P \xleftrightarrow{g} Q \xleftrightarrow{g} M$, the following statements hold:*

- (i) *If $\{P, M\} = [Q, M] = 0$, there exists $R \in \mathcal{G}_{\text{Lie}}$ s.t. $[P, R] = \{Q, R\} = \{M, R\} = 0$.*
- (ii) *If $[P, M] = \{Q, M\} = 0$, there exists $R \in \mathcal{G}_{\text{Lie}}$ s.t. $\{P, R\} = [Q, R] = \{M, R\} = 0$.*
- (iii) *If $[P, M] = [Q, M] = 0$, there exists $R \in \mathcal{G}_{\text{Lie}}$ s.t. $\{P, R\} = \{Q, R\} = \{M, R\} = 0$.*

Proof. We prove the three cases separately.

- (i) If $\{P, M\} = [Q, M] = 0$ holds, $R = P \in \mathcal{G}_{\text{Lie}}$ satisfies $[P, R] = \{Q, R\} = \{M, R\} = 0$.
- (ii) If $[P, M] = \{Q, M\} = 0$ holds, $R = Q \in \mathcal{G}_{\text{Lie}}$ satisfies $\{P, R\} = [Q, R] = \{M, R\} = 0$.
- (iii) By Lemma 6, the shortest distance between P and M is two because of $[P, M] = 0$ (note that $P \neq M$ from $\{P, Q\} = [M, Q] = 0$). Thus, there exists $S \in \mathcal{G}_{\text{Lie}}$ such that $\{P, S\} = \{M, S\} = 0$:

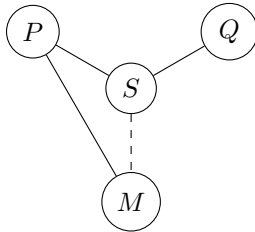


If $\{Q, S\} = 0$, $R = S \in \mathcal{G}_{\text{Lie}}$ satisfies $\{P, R\} = \{Q, R\} = \{M, R\} = 0$. On the other hand, if $[Q, S] = 0$, $iR = [iP, iS] = -2PS \in \mathcal{G}_{\text{Lie}}$ satisfies $\{P, R\} = \{Q, R\} = \{M, R\} = 0$. Therefore, in both cases, there exists $R \in \mathcal{G}_{\text{Lie}}$ such that $\{P, R\} = \{Q, R\} = \{M, R\} = 0$.

□

Lemma 9. For $P, Q \in \mathcal{G}_{\text{Lie}}$ and $M \in \mathcal{P}_n$ satisfying $[P, Q] = 0$ and $P \xleftarrow{\mathfrak{g}} Q \xleftarrow{\mathfrak{g}} M$, if $\{P, M\} = [Q, M] = 0$ or $[P, M] = \{Q, M\} = 0$, there exists $R \in \mathcal{G}_{\text{Lie}}$ such that $\{P, R\} = \{Q, R\} = \{M, R\} = 0$.

Proof. Consider the case of $\{P, M\} = [Q, M] = 0$ (the other case is similarly provable). Given that $P \neq Q$ holds from $\{P, M\} = [Q, M] = 0$, there exists $S \in \mathcal{G}_{\text{Lie}}$ such that $\{P, S\} = \{Q, S\} = 0$ by Lemma 7, where $M \neq S$ because of $[Q, M] = \{Q, S\} = 0$:



Lemma 6 states that the shortest distance between M and S is one or two. If the shortest distance is one, $R = S$ satisfies $\{P, R\} = \{Q, R\} = \{M, R\} = 0$. If the shortest distance is two (i.e., $[M, S] = 0$), $iR = [iS, iP] = -2SP \in \mathcal{G}_{\text{Lie}}$ satisfies $\{P, R\} = \{Q, R\} = \{M, R\} = 0$. Therefore, there always exists $R \in \mathcal{G}_{\text{Lie}}$ such that $\{P, R\} = \{Q, R\} = \{M, R\} = 0$. □

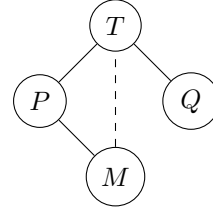
Lemma 10. For $P, Q \in \mathcal{G}_{\text{Lie}}$ and $M \in \mathcal{P}_n$ satisfying $[P, Q] = 0$ and $P \xleftarrow{\mathfrak{g}} Q \xleftarrow{\mathfrak{g}} M$, if there exists $R \in \mathcal{G}_{\text{Lie}}$

such that $\{P, R\} = [Q, R] = 0$ or $[P, R] = \{Q, R\} = 0$, then there exists $S \in \mathcal{G}_{\text{Lie}}$ such that $\{P, S\} = [Q, S] = \{M, S\} = 0$ or $[P, S] = \{Q, S\} = \{M, S\} = 0$.

Proof. Consider the case of $\{P, R\} = [Q, R] = 0$ (the other case is similarly provable). We prove the lemma in two cases, (i) $R = M$ and (ii) $R \neq M$.

- (i) $R = M$

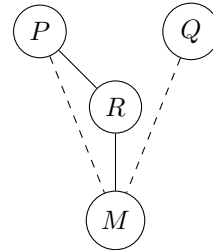
We have $P \neq Q$ from $\{P, M\} = [Q, M] = 0$. Thus, there exists $T \in \mathcal{G}_{\text{Lie}}$ such that $\{P, T\} = \{Q, T\} = 0$ by Lemma 7, where $M \neq T$ because of $[M, Q] = \{T, Q\} = 0$:



If $[T, M] = 0$, $iS = [iM, [iT, iP]] = -4iMPT \in \mathcal{G}_{\text{Lie}}$ satisfies $[P, S] = \{Q, S\} = \{M, S\} = 0$ (note that $R = M$ leads to $M \in \mathcal{G}_{\text{Lie}}$). If $\{T, M\} = 0$, $iS = [iM, iT] = -2MT \in \mathcal{G}_{\text{Lie}}$ satisfies $[P, S] = \{Q, S\} = \{M, S\} = 0$. Therefore, the lemma holds for $R = M$.

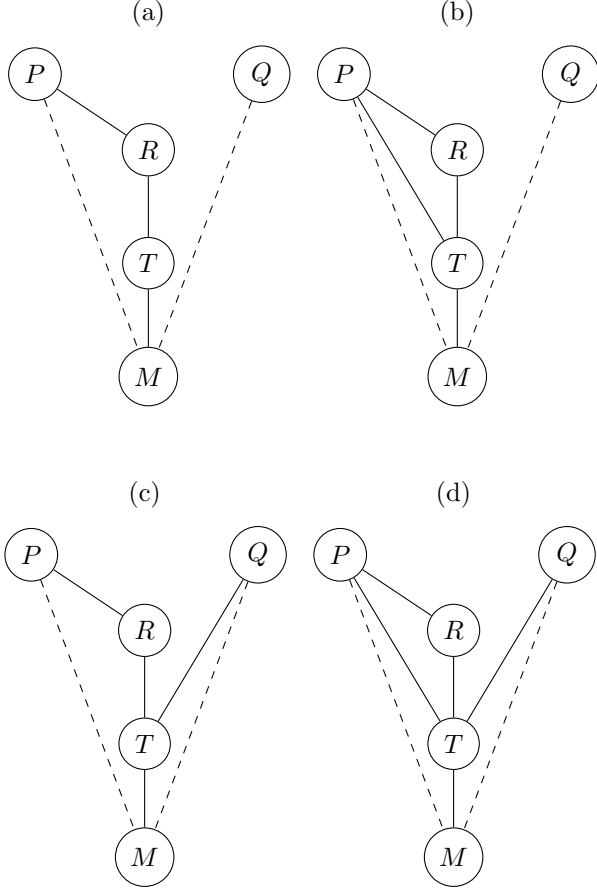
- (ii) $R \neq M$

By Lemma 6, the shortest distance between R and M is one or two. If the shortest distance is one, $S = R \in \mathcal{G}_{\text{Lie}}$ satisfies $\{P, S\} = [Q, S] = \{M, S\} = 0$, i.e., the lemma holds:

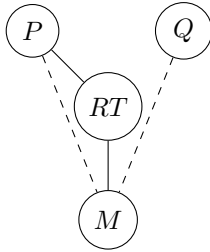


When the shortest distance is two, let $T \in \mathcal{G}_{\text{Lie}}$ be the node connecting R and M . Then, there are four patterns regarding the (anti-)commutation relations between P, Q and T , namely $[P, T] = 0$ or

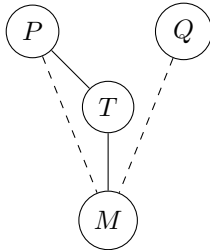
$\{P, T\} = 0$ and $[Q, T] = 0$ or $\{Q, T\} = 0$, as follows:



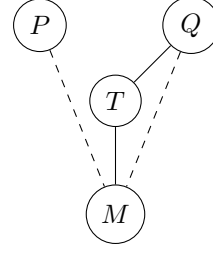
We can concretely construct S satisfying the lemma for these four patterns. (a) If $[P, T] = [Q, T] = 0$, $iS = [iR, iT] = -2RT \in \mathcal{G}_{\text{Lie}}$ satisfies $\{P, S\} = [Q, S] = \{M, S\} = 0$:



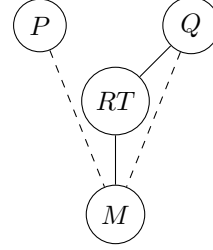
(b) If $\{P, T\} = [Q, T] = 0$, $S = T \in \mathcal{G}_{\text{Lie}}$ satisfies $\{P, S\} = [Q, S] = \{M, S\} = 0$:



(c) If $[P, T] = \{Q, T\} = 0$, $S = T \in \mathcal{G}_{\text{Lie}}$ satisfies $[P, S] = \{Q, S\} = \{M, S\} = 0$:



(d) If $\{P, T\} = \{Q, T\} = 0$, $iS = [iR, iT] = -2RT \in \mathcal{G}_{\text{Lie}}$ satisfies $[P, S] = \{Q, S\} = \{M, S\} = 0$:



Therefore, the lemma holds for $R \neq M$.

These results prove this lemma. \square

2. Simultaneous measurability of gradient components

This subsection proves Lemmas 1–5 in the main text on the relationship between the simultaneous measurability of gradient components and the DLA structure.

As discussed in the main text, two distinct gradient components $\partial_j C(\boldsymbol{\theta})$ and $\partial_k C(\boldsymbol{\theta})$ can be measured simultaneously if $[\Gamma_j(\boldsymbol{\theta}), \Gamma_k(\boldsymbol{\theta})] = 0$ holds for any $\boldsymbol{\theta}$, where $\Gamma_j(\boldsymbol{\theta}) = -i[\tilde{G}_j(\boldsymbol{\theta}), \tilde{O}(\boldsymbol{\theta})]$ is the gradient operator. Here, $\tilde{G}_j(\boldsymbol{\theta}) = U_{j+}^\dagger(\boldsymbol{\theta})G_jU_{j+}(\boldsymbol{\theta})$ and $\tilde{O}(\boldsymbol{\theta}) = U^\dagger(\boldsymbol{\theta})OU(\boldsymbol{\theta})$ are the Heisenberg representations of the generator G_j and the observable O , respectively ($U_{j+}(\boldsymbol{\theta}) = \prod_{k=1}^{j-1} e^{i\theta_k G_k}$ is the unitary circuit before the j th gate). In the DLA graph, the gradient operator $\Gamma_j(\boldsymbol{\theta})$ corresponds to a node of the graph G_j . Below, we show that whether $[\Gamma_j(\boldsymbol{\theta}), \Gamma_k(\boldsymbol{\theta})] = 0$ for any $\boldsymbol{\theta}$ is determined by the structural relationship between G_j, G_k , and O on the DLA graph.

Lemma 1. *If $G_j, G_k \in \mathcal{G}$ are not \mathfrak{g} -connected, $\partial_j C$ and $\partial_k C$ can be simultaneously measured:*

$$\begin{array}{c} \textcircled{G_j} \xleftrightarrow{\mathfrak{g}} \textcircled{G_k} \\ \times \end{array} \Rightarrow [\Gamma_j, \Gamma_k] = 0 \quad \forall \boldsymbol{\theta}.$$

Proof. When G_j and G_k are not \mathfrak{g} -connected, the DLA graph \mathcal{G}_{Lie} is separable into two subgraphs $\mathcal{G}_{\text{Lie}1}$ and $\mathcal{G}_{\text{Lie}2}$

(i.e., $[\mathcal{G}_{\text{Lie1}}, \mathcal{G}_{\text{Lie2}}] = 0$). This is because if the DLA graph is not separable, then any two nodes are \mathfrak{g} -connected. Therefore, we can decompose the DLA \mathfrak{g} into two subalgebras $\mathfrak{g}_1 = \text{span}(\mathcal{G}_{\text{Lie1}})$ and $\mathfrak{g}_2 = \text{span}(\mathcal{G}_{\text{Lie2}})$ that commute with each other:

$$\mathfrak{g} = \mathfrak{g}_1 \oplus \mathfrak{g}_2, \quad [\mathfrak{g}_1, \mathfrak{g}_2] = 0, \quad (\text{C4})$$

where $G_j \in \mathfrak{g}_1$ and $G_k \in \mathfrak{g}_2$. Then, the unitaries of the quantum circuit are decomposed as $U = VW$, $U_{j+} = V_{j+}W_{j+}$, and $U_{k+} = V_{k+}W_{k+}$ with $V, V_{j+}, V_{k+} \in e^{\mathfrak{g}_1}$ and $W, W_{j+}, W_{k+} \in e^{\mathfrak{g}_2}$ (U_{j+} and U_{k+} are the unitary circuits before the j th and k th gates, respectively).

Now, we prove $[\Gamma_j, \Gamma_k] = 0$ using these decompositions. A straightforward calculation shows that the commutator of gradient operators $\Gamma_j = -i[\tilde{G}_j, \tilde{O}]$ and $\Gamma_k = -i[\tilde{G}_k, \tilde{O}]$ is written as

$$\begin{aligned} [\Gamma_j, \Gamma_k] &= -[\tilde{G}_j, \tilde{O}\tilde{G}_k\tilde{O}] - [\tilde{O}\tilde{G}_j\tilde{O}, \tilde{G}_k] \\ &\quad + [\tilde{G}_j, \tilde{G}_k] + \tilde{O}[\tilde{G}_j, \tilde{G}_k]\tilde{O}. \end{aligned} \quad (\text{C5})$$

Below, we show that each term in the above commutator vanishes. Let us first prove $[\tilde{G}_j, \tilde{G}_k] = 0$. From the decomposition of $U_{j+} = V_{j+}W_{j+}$, we have

$$\begin{aligned} \tilde{G}_j &= U_{j+}^\dagger G_j U_{j+} \\ &= W_{j+}^\dagger V_{j+}^\dagger G_j V_{j+} W_{j+} \\ &= V_{j+}^\dagger G_j V_{j+} \in \mathfrak{g}_1, \end{aligned} \quad (\text{C6})$$

where we have used $[V_{j+}, W_{j+}] = [G_j, W_{j+}] = 0$. In the same manner, we have

$$\tilde{G}_k = W_{k+}^\dagger G_k W_{k+} \in \mathfrak{g}_2. \quad (\text{C7})$$

Thereby, $[\tilde{G}_j, \tilde{G}_k] = 0$ is proved from $[\mathfrak{g}_1, \mathfrak{g}_2] = 0$, indicating that the third and fourth terms vanish in Eq. (C5). Next, we prove $[\tilde{G}_j, \tilde{O}\tilde{G}_k\tilde{O}] = 0$. Since $\tilde{O} = U^\dagger O U$ and $\tilde{G}_k = W_{k+}^\dagger G_k W_{k+}$ [see Eq. (C7)], $\tilde{O}\tilde{G}_k\tilde{O}$ is written as

$$\begin{aligned} \tilde{O}\tilde{G}_k\tilde{O} &= (W^\dagger V^\dagger O V W)(W_{k+}^\dagger G_k W_{k+})(W^\dagger V^\dagger O V W) \\ &= W^\dagger V^\dagger O V A V^\dagger O V W \\ &= W^\dagger V^\dagger O A O V W \end{aligned} \quad (\text{C8})$$

where we have defined $A = W W_{k+}^\dagger G_k W_{k+} W^\dagger \in \mathfrak{g}_2$ and used $[V, A] = 0$. Here, for any $w = \sum_i c_i g_i \in \mathfrak{g}_2$, $O w O = \sum_i (-1)^{\sigma_i} c_i g_i$ is also included in \mathfrak{g}_2 , where g_i is the Pauli basis of \mathfrak{g}_2 , c_i is an expansion coefficient, and σ_i is defined as $O g_i O = (-1)^{\sigma_i} g_i$. Therefore, $A' = O A O$ is included in \mathfrak{g}_2 because of $A \in \mathfrak{g}_2$, leading to

$$\begin{aligned} \tilde{O}\tilde{G}_k\tilde{O} &= W^\dagger V^\dagger A' V W \\ &= W^\dagger A' W \in \mathfrak{g}_2, \end{aligned} \quad (\text{C9})$$

where we have used $[A', V] = 0$. Thus, $[\tilde{G}_j, \tilde{O}\tilde{G}_k\tilde{O}] = 0$ holds from Eqs.(C6), (C9), and $[\mathfrak{g}_1, \mathfrak{g}_2] = 0$. Similarly, $[\tilde{O}\tilde{G}_j\tilde{O}, \tilde{G}_k] = 0$ can also be proved. Therefore, the first

and second terms vanish in Eq. (C5). These results prove that $[\Gamma_j, \Gamma_k] = 0$ holds for any θ , i.e., $\partial_j C$ and $\partial_k C$ are simultaneously measurable. \square

Lemma 1 states that $\partial_j C$ and $\partial_k C$ can be simultaneously measured if G_j and G_k are not \mathfrak{g} -connected. Thus, we focus on the case that $G_j, G_k \in \mathcal{G}$ are \mathfrak{g} -connected below. To simplify the proof, we divide the quantum circuit into two parts, $U = U_{\text{fin}} U_{\text{ini}}$, where we have defined $U_{\text{ini}} = \prod_{j=1}^{L_{\text{ini}}} e^{i\theta_j G_j}$ and $U_{\text{fin}} = \prod_{j=L_{\text{ini}}+1}^L e^{i\theta_j G_j}$. The depth of the final part, $L_{\text{fin}} = L - L_{\text{ini}}$, is set as a sufficiently large but constant value such that U_{fin} can express $e^{i\phi_1 Q_1} e^{i\phi_2 Q_2}$ for any $Q_1, Q_2 \in \mathcal{G}_{\text{Lie}}$ and $\phi_1, \phi_2 \in \mathbb{R}$. Note that there exists such L_{fin} due to Condition 3. We emphasize that whether the gradient components for U_{fin} can be simultaneously measured does not affect the gradient measurement efficiency for the full circuit, \mathcal{F}_{eff} , because the contribution from the constant depth circuit to \mathcal{F}_{eff} is negligible in the deep circuit limit (see Definition 3). Therefore, we will use U_{fin} as a buffer circuit for the proof and investigate whether $\partial_j C$ and $\partial_k C$ are simultaneously measurable for the parameters of U_{ini} (i.e., $j, k \leq L_{\text{ini}}$). Then, the gradient operators are given by

$$\begin{aligned} \Gamma_j &= -i[\tilde{G}_j, \tilde{O}] = -i \left[\left(U_{\text{ini}}^\dagger G_j U_{\text{ini}} \right), \left(U_{\text{ini}}^\dagger U_{\text{fin}}^\dagger O U_{\text{fin}} U_{\text{ini}} \right) \right], \\ \Gamma_k &= -i[\tilde{G}_k, \tilde{O}] = -i \left[\left(U_{\text{ini}}^\dagger G_k U_{\text{ini}} \right), \left(U_{\text{ini}}^\dagger U_{\text{fin}}^\dagger O U_{\text{fin}} U_{\text{ini}} \right) \right]. \end{aligned} \quad (\text{C10})$$

According to Definition 1, $\partial_j C$ and $\partial_k C$ are simultaneously measurable if $[\Gamma_j(\theta), \Gamma_k(\theta)] = 0$ for any θ . Therefore, when proving that $\partial_j C$ and $\partial_k C$ cannot be measured simultaneously, it suffices to show that $[\Gamma_j(\theta), \Gamma_k(\theta)] \neq 0$ for a certain θ . In the following proofs, we find θ such that $[\Gamma_j(\theta), \Gamma_k(\theta)] \neq 0$ to prove lemmas.

Lemma 2. For $j, k \leq L_{\text{ini}}$, if $G_j, G_k \in \mathcal{G}$ anti-commute, $\partial_j C$ and $\partial_k C$ cannot be simultaneously measured:

$$\begin{array}{c} \textcircled{G_j} \text{---} \textcircled{G_k} \end{array} \Rightarrow \exists \theta \text{ s.t. } [\Gamma_j, \Gamma_k] \neq 0.$$

Proof. We prove this lemma in two cases: (i) $\{G_j, O\} = \{G_k, O\} = 0$ and (ii) otherwise.

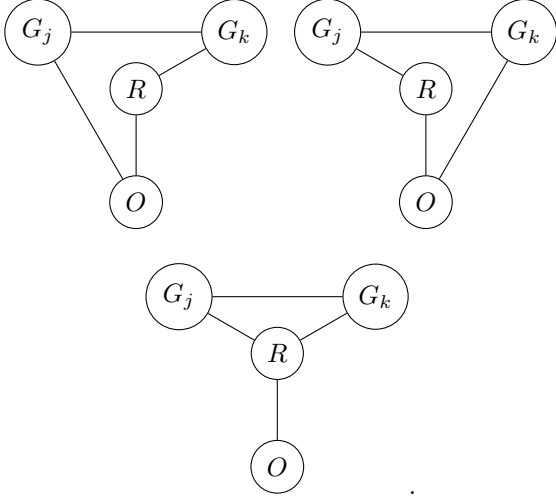
- (i) In this case, $[\Gamma_j(\theta), \Gamma_k(\theta)] \neq 0$ holds for $\theta = 0$. In fact, when $\theta = 0$ (i.e., $U_{\text{ini}} = U_{\text{fin}} = I$), we have $\tilde{G}_j = G_j, \tilde{G}_k = G_k, \tilde{O} = O$, and thus

$$\Gamma_j = -i[\tilde{G}_j, \tilde{O}] = -2iG_j O, \quad (\text{C11})$$

$$\Gamma_k = -i[\tilde{G}_k, \tilde{O}] = -2iG_k O. \quad (\text{C12})$$

Therefore, we obtain $[\Gamma_j, \Gamma_k] = 4[G_j, G_k] \neq 0$ from $\{G_j, O\} = \{G_k, O\} = 0$, showing that $\partial_j C$ and $\partial_k C$ cannot be simultaneously measured.

(ii) By Lemma 8, there exists $R \in \mathcal{G}_{\text{Lie}}$ satisfying one of the following commutation relations:



By setting θ such that $U_{\text{ini}} = I$ and $U_{\text{fin}} = e^{-i\pi R/4}$ in Eq. (C10), we have $\tilde{G}_j = G_j, \tilde{G}_k = G_k, \tilde{O} = e^{i\pi R/4} O e^{-i\pi R/4} = iRO$, and thus

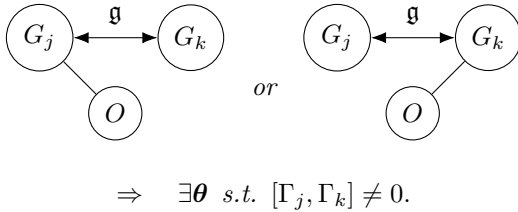
$$\Gamma_j = -i[\tilde{G}_j, \tilde{O}] = 2G_jRO, \quad (\text{C13})$$

$$\Gamma_k = -i[\tilde{G}_k, \tilde{O}] = 2G_kRO. \quad (\text{C14})$$

Therefore, we obtain $[\Gamma_j, \Gamma_k] = 4[G_k, G_j] \neq 0$ from $\{G_j, iRO\} = \{G_k, iRO\} = 0$, showing that $\partial_j C$ and $\partial_k C$ cannot be simultaneously measured.

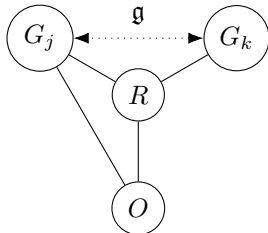
These results prove that $\partial_j C$ and $\partial_k C$ cannot be simultaneously measured for anti-commuting G_j and G_k . \square

Lemma 3. Consider \mathfrak{g} -connected $G_j, G_k \in \mathcal{G}$ for $j, k \leq L_{\text{ini}}$. If $\{G_j, O\} = [G_k, O] = 0$ or $[G_j, O] = \{G_k, O\} = 0$, $\partial_j C$ and $\partial_k C$ cannot be simultaneously measured:



Proof. It suffices to consider only the case of $[G_j, G_k] = 0$ by Lemma 2.

Here, we consider the case of $\{G_j, O\} = [G_k, O] = 0$ (the other case is similarly provable). Then, there exists $R \in \mathcal{G}_{\text{Lie}}$ such that $\{G_j, R\} = \{G_k, R\} = \{O, R\} = 0$ by Lemma 9:



By setting θ such that $U_{\text{ini}} = I$ and $U_{\text{fin}} = e^{i\phi R}$, we have $\tilde{G}_j = G_j, \tilde{G}_k = G_k, \tilde{O} = e^{-i\phi R} O e^{i\phi R} = \cos(2\phi)O + i\sin(2\phi)OR$, and thus

$$\begin{aligned} \Gamma_j &= -i[\tilde{G}_j, \tilde{O}] \\ &= -i\cos(2\phi)[G_j, O] + \sin(2\phi)[G_j, OR] \\ &= -2i\cos(2\phi)G_jO \end{aligned}$$

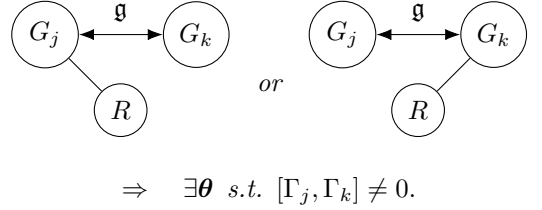
$$\begin{aligned} \Gamma_k &= -i[\tilde{G}_k, \tilde{O}] \\ &= -i\cos(2\phi)[G_k, O] + \sin(2\phi)[G_k, OR] \\ &= 2\sin(2\phi)G_kOR. \end{aligned}$$

Therefore, we have

$$[\Gamma_j, \Gamma_k] = -4i\cos(2\phi)\sin(2\phi)[G_jO, G_kOR]. \quad (\text{C15})$$

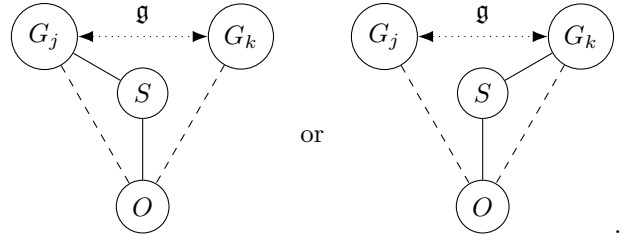
From the commutation relations between G_j, G_k, R and O , we have $[G_jO, G_kOR] \neq 0$, showing that there exists θ such that $[\Gamma_j, \Gamma_k] \neq 0$. Therefore, $\partial_j C$ and $\partial_k C$ cannot be simultaneously measured if $\{G_j, O\} = [G_k, O] = 0$ or $[G_j, O] = \{G_k, O\} = 0$. \square

Lemma 4. Consider \mathfrak{g} -connected $G_j, G_k \in \mathcal{G}$ for $j, k \leq L_{\text{ini}}$. If there exists $R \in \mathcal{G}_{\text{Lie}}$ such that $\{G_j, R\} = [G_k, R] = 0$ or $[G_j, R] = \{G_k, R\} = 0$, $\partial_j C$ and $\partial_k C$ cannot be simultaneously measured:

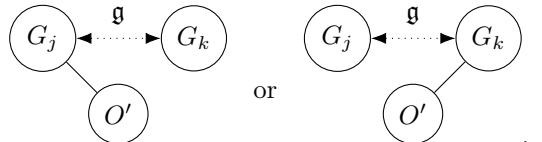


Proof. It suffices to consider only the case of $[G_j, G_k] = 0$ and $[G_j, O] = [G_k, O] = 0$ or $\{G_j, O\} = \{G_k, O\} = 0$ by Lemmas 2 and 3.

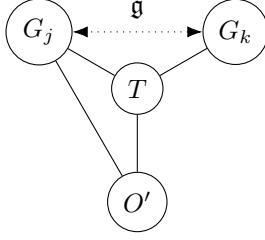
When $\{G_j, R\} = [G_k, R] = 0$ or $[G_j, R] = \{G_k, R\} = 0$, there necessarily exists $S \in \mathcal{G}_{\text{Lie}}$ satisfying $\{G_j, S\} = [G_k, S] = \{O, S\} = 0$ or $[G_j, S] = \{G_k, S\} = \{O, S\} = 0$ by Lemma 10:



Assume $\{G_j, S\} = [G_k, S] = \{O, S\} = 0$ (the other case is similarly provable). Then, we consider $O' = iSO \in \mathcal{P}_n$, which satisfies $\{G_j, O'\} = [G_k, O'] = 0$ or $[G_j, O'] = \{G_k, O'\} = 0$ ($\because [G_j, O] = [G_k, O] = 0$ or $\{G_j, O\} = \{G_k, O\} = 0$):



We assume $\{G_j, O'\} = [G_k, O'] = 0$ (the other case is similarly provable). By Lemma 9, there exists $T \in \mathcal{G}_{\text{Lie}}$ satisfying $\{G_j, T\} = \{G_k, T\} = \{O', T\} = 0$:



By setting θ such that $U_{\text{ini}} = I$ and $U_{\text{fin}} = e^{-i\pi S/4} e^{i\phi T}$ in Eq. (C10), we have $\tilde{G}_j = G_j$, $\tilde{G}_k = G_k$, $\tilde{O} = e^{-i\phi T} e^{i\pi S/4} O e^{-i\pi S/4} e^{i\phi T} = \cos(2\phi)O' + i\sin(2\phi)O'T$, and thus

$$\begin{aligned} \Gamma_j &= -i[\tilde{G}_j, \tilde{O}] \\ &= -i\cos(2\phi)[G_j, O'] + \sin(2\phi)[G_j, O'T] \quad (\text{C16}) \\ &= -2i\cos(2\phi)G_jO' \end{aligned}$$

$$\begin{aligned} \Gamma_k &= -i[\tilde{G}_k, \tilde{O}] \\ &= -i\cos(2\phi)[G_k, O'] + \sin(2\phi)[G_k, O'T] \quad (\text{C17}) \\ &= 2\sin(2\phi)G_kO'T. \end{aligned}$$

Therefore, we have

$$[\Gamma_j, \Gamma_k] = -4i\cos(2\phi)\sin(2\phi)[G_jO', G_kO'T]. \quad (\text{C18})$$

From the commutation relations between G_j, G_k, O' and T , we have $[G_jO', G_kO'T] \neq 0$, showing that there exists θ such that $[\Gamma_j, \Gamma_k] \neq 0$. Therefore, $\partial_j C$ and $\partial_k C$ cannot be simultaneously measured if there exists $R \in \mathcal{G}_{\text{Lie}}$ such that $\{G_j, R\} = [G_k, R] = 0$ or $[G_j, R] = \{G_k, R\} = 0$. \square

Lemma 5. For $j < k \leq L_{\text{ini}}$, if $G_j = G_k$, $\partial_j C$ and $\partial_k C$ cannot be simultaneously measured:

$$\textcircled{G_j} = \textcircled{G_k} \Rightarrow \exists \theta \text{ s.t. } [\Gamma_j, \Gamma_k] \neq 0.$$

Proof. By Condition 1, there exists ℓ ($j < \ell < k$) such that $\{G_j, G_\ell\} = 0$. Then we consider $G'_k = iG_\ell G_k = i[G_\ell, G_k]/2 \in \mathcal{G}_{\text{Lie}}$, which satisfies $\{G_j, G'_k\} = 0$. We prove this lemma in two cases: (i) $\{G_j, O\} = \{G'_k, O\} = 0$ and (ii) otherwise.

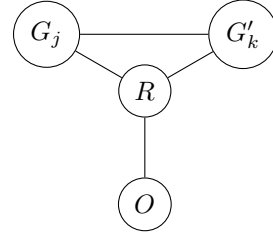
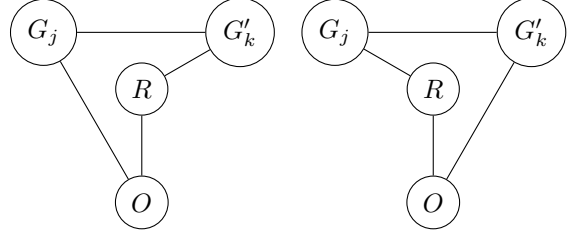
(i) We set θ such that $U_{j+} = I$, $U_{k+} = e^{-i\pi G_\ell/4}$, and $U = I$ (i.e., $U_{\text{ini}} = e^{-i\pi G_\ell/4}$ and $U_{\text{fin}} = e^{+i\pi G_\ell/4}$). Then we have $\tilde{G}_j = G_j$, $\tilde{G}_k = e^{i\pi G_\ell/4} G_k e^{-i\pi G_\ell/4} = G'_k$, $\tilde{O} = O$, and thus

$$\Gamma_j = -i[\tilde{G}_j, \tilde{O}] = -2iG_jO, \quad (\text{C19})$$

$$\Gamma_k = -i[\tilde{G}_k, \tilde{O}] = -2iG'_kO. \quad (\text{C20})$$

Therefore, we obtain $[\Gamma_j, \Gamma_k] = 4[G_j, G'_k] \neq 0$ from $\{G_j, O\} = \{G'_k, O\} = 0$, showing that $\partial_j C$ and $\partial_k C$ cannot be simultaneously measured.

(ii) By Lemma 8, there exists $R \in \mathcal{G}_{\text{Lie}}$ satisfying one of the following commutation relations:



By setting θ such that $U_{j+} = I$, $U_{k+} = e^{-i\pi G_\ell/4}$, and $U = e^{-i\pi R/4}$ (i.e., $U_{\text{ini}} = e^{-i\pi G_\ell/4}$, and $U_{\text{fin}} = e^{-i\pi R/4} e^{+i\pi G_\ell/4}$), we have $\tilde{G}_j = G_j$, $\tilde{G}_k = G'_k$, $\tilde{O} = e^{i\pi R/4} O e^{-i\pi R/4} = iRO$, and thus

$$\Gamma_j = -i[\tilde{G}_j, \tilde{O}] = 2G_jRO, \quad (\text{C21})$$

$$\Gamma_k = -i[\tilde{G}_k, \tilde{O}] = 2G'_kRO. \quad (\text{C22})$$

Therefore, we obtain $[\Gamma_j, \Gamma_k] = 4[G_j, G'_k] \neq 0$ from $\{G_j, iRO\} = \{G'_k, iRO\} = 0$, showing that $\partial_j C$ and $\partial_k C$ cannot be simultaneously measured.

These results prove that $\partial_j C$ and $\partial_k C$ cannot be simultaneously measured if $G_j = G_k$. \square

3. Proof of trade-off inequality

The main text leaves the derivations of Eqs. (35) and (36) in the proof of Theorem 1. Here, we show these equations.

a. Preliminaries

We first show several lemmas for preliminaries.

Lemma 11. Consider a set of commuting Pauli operators $\mathcal{S} = \{S_1, S_2, \dots\}$, where $[S_j, S_k] = 0 \forall S_j, S_k \in \mathcal{S}$. Define a subset of Pauli operators, $\mathcal{P}_{\mathcal{S}} \subset \mathcal{P}_n$, stabilized by \mathcal{S} as

$$\mathcal{P}_{\mathcal{S}} = \{P \in \mathcal{P}_n \mid [P, S_j] = 0 \forall S_j \in \mathcal{S}\}. \quad (\text{C23})$$

Then, letting s be the number of independent Pauli operators in \mathcal{S} , the following equality and inequalities hold:

$$|\mathcal{P}_{\mathcal{S}}| = \frac{4^n}{2^s} \leq \frac{4^n}{|\mathcal{S}|}, \quad |\mathcal{S}| \leq 2^n. \quad (\text{C24})$$

Proof. Let $g_1, \dots, g_s \in \mathcal{S}$ be independent Pauli operators in \mathcal{S} . According to Proposition 10.4 in Ref. [60], there is $h_j \in \mathcal{P}_n$ such that $\{g_j, h_j\} = 0$ and $[g_k, h_j] = 0$ for all $k \neq j$. We consider

$$\begin{aligned} \mathcal{H}(\mathbf{x}) &\equiv h_1^{x_1} \cdots h_s^{x_s} \mathcal{P}_S \\ &= \{h_1^{x_1} \cdots h_s^{x_s} P \mid P \in \mathcal{P}_S\} \subset \mathcal{P}_n, \end{aligned} \quad (\text{C25})$$

where $\mathbf{x} = (x_1, \dots, x_s)$ is a binary vector ($x_j = 0, 1$). The set $\mathcal{H}(\mathbf{x})$ has the following properties:

1. $\mathcal{H}(\mathbf{x}) \cap \mathcal{H}(\mathbf{x}') = \emptyset$ for $\mathbf{x} \neq \mathbf{x}'$.
2. $|\mathcal{H}(\mathbf{x})| = |\mathcal{P}_S|$ for any \mathbf{x}
3. $\bigsqcup_{\mathbf{x}} \mathcal{H}(\mathbf{x}) = \mathcal{P}_n$

Let us prove the first property. By construction, we have $Pg_j - (-1)^{x_j} g_j P = 0$ for any $P \in \mathcal{H}(\mathbf{x})$. This means that, for $\mathbf{x} \neq \mathbf{x}'$, $\mathcal{H}(\mathbf{x})$ and $\mathcal{H}(\mathbf{x}')$ have different (anti-)commutation relations with g_1, \dots, g_s , leading to $\mathcal{H}(\mathbf{x}) \cap \mathcal{H}(\mathbf{x}') = \emptyset$. The second property also holds because $h_1^{x_1} \cdots h_s^{x_s} P \neq h_1^{x'_1} \cdots h_s^{x'_s} P'$ for $P \neq P'$. The third property is proved by contradiction. Let us assume that there exists $P \in \mathcal{P}_n$ satisfying $P \notin \bigsqcup_{\mathbf{x}} \mathcal{H}(\mathbf{x})$. Then, a binary vector \mathbf{y} is defined such that $Pg_j - (-1)^{y_j} g_j P = 0$. Because $P' = h_1^{y_1} \cdots h_s^{y_s} P$ satisfies $[P', g_j] = 0$ for any g_j , P' belongs to \mathcal{P}_S by definition. Hence, we have $P = h_1^{y_1} \cdots h_s^{y_s} P' \in \mathcal{H}(\mathbf{y})$. This contradicts the assumption of $P \notin \bigsqcup_{\mathbf{x}} \mathcal{H}(\mathbf{x})$. Therefore, we have $\bigsqcup_{\mathbf{x}} \mathcal{H}(\mathbf{x}) = \mathcal{P}_n$.

These properties lead to $4^n = |\mathcal{P}_n| = |\bigsqcup_{\mathbf{x}} \mathcal{H}(\mathbf{x})| = \sum_{\mathbf{x}} |\mathcal{H}(\mathbf{x})| = 2^s |\mathcal{P}_S|$, proving $|\mathcal{P}_S| = 4^n / 2^s$. Besides, given that s independent Pauli operators can generate only 2^s Pauli operators by multiplying them, we have $|\mathcal{S}| \leq 2^s$, which readily shows $|\mathcal{P}_S| = 4^n / 2^s \leq 4^n / |\mathcal{S}|$. Also, combining $|\mathcal{P}_S| \leq 4^n / |\mathcal{S}|$ and $|\mathcal{S}| \leq |\mathcal{P}_S|$ (the latter is derived from the fact that $\forall S_j \in \mathcal{S}$ is included in \mathcal{P}_S), we obtain $|\mathcal{S}| \leq 2^n$. \square

Lemma 12. *Let c be a real constant. For real variables $a_1, \dots, a_q \geq c$ and a real constant $A \geq c^q$, the following inequality holds under a constraint $\prod_{j=1}^q a_j \leq A$:*

$$\sum_{j=1}^q a_j \leq \frac{A}{c^{q-1}} + c(q-1). \quad (\text{C26})$$

Proof. We first prove this lemma for $c = 1$ by mathematical induction.

- (i) For $q = 1$, $a_1 \leq A$ holds trivially by the constraint.
- (ii) We assume that this lemma holds for $q = m$. That is, under the constraint $\prod_{j=1}^m a_j \leq A$, $\sum_{j=1}^m a_j \leq A + m - 1$ holds for any $A \geq 1$.

Now, we consider the case of $q = m + 1$, where the constraint is given by $\prod_{j=1}^{m+1} a_j \leq A$. Let us fix a_{m+1} in the range of $1 \leq a_{m+1} \leq A$ (if $a_{m+1} > A$, the condition $a_1, \dots, a_m \geq 1$ cannot be satisfied). Then, the constraint for a_1, \dots, a_m is written as

$\prod_{j=1}^m a_j \leq A/a_{m+1} = \tilde{A}$. Under this constraint, we have $\sum_{j=1}^m a_j \leq \tilde{A} + m - 1 = A/a_{m+1} + m - 1$ from the assumption for $q = m$. Therefore, we have $\sum_{j=1}^{m+1} a_j = a_{m+1} + (\sum_{j=1}^m a_j) \leq a_{m+1} + A/a_{m+1} + m - 1$. For $1 \leq x \leq A$, $f(x) = x + A/x$ has a maximum value $f(1) = f(A) = A + 1$. Thus, we finally obtain $\sum_{j=1}^{m+1} a_j \leq A + m$, indicating that the lemma holds even for $q = m + 1$.

These discussions prove the lemma for $c = 1$ by mathematical induction. Then, we rescale a_j by a factor of c as $a_j \rightarrow a'_j = ca_j$, where the constraint is also rescaled as $\prod_{j=1}^q a'_j = c^q \prod_{j=1}^q a_j \leq c^q A = A'$. Therefore, we obtain

$$\sum_{j=1}^q a'_j = c \sum_{j=1}^q a_j \leq cA + c(q-1) = \frac{A'}{c^{q-1}} + c(q-1),$$

where we have used the lemma for $c = 1$ in the inequality. This proves the lemma for any $c > 0$. \square

b. Overview of Sec. IV C

For convenience, we briefly summarize Sec. IV C to prove Theorem 1. In this proof, we decompose the DLA graph into several subgraphs that consist of (potentially) simultaneously measurable nodes, deriving the upper limit of the gradient measurement efficiency. We first decompose the DLA graph into separated subgraphs as

$$\mathcal{G}_{\text{Lie}} = (\mathcal{A}_1 \sqcup \cdots \sqcup \mathcal{A}_p) \sqcup (\mathcal{B}_1 \sqcup \cdots \sqcup \mathcal{B}_q), \quad (\text{C27})$$

where \mathcal{A}_x 's and \mathcal{B}_x 's have one and multiple nodes, respectively. Since \mathcal{A}_x and \mathcal{B}_x are separated, they satisfy

$$[\mathcal{A}_x, \mathcal{A}_y] = [\mathcal{B}_x, \mathcal{B}_y] = 0 \quad \forall x \neq y, \quad (\text{C28})$$

$$[\mathcal{A}_x, \mathcal{B}_y] = 0 \quad \forall x, y. \quad (\text{C29})$$

By Lemma 1, when G_j and G_k are nodes in different separated subgraphs \mathcal{A}_x or \mathcal{B}_x , $\partial_j C$ and $\partial_k C$ are simultaneously measurable. Next, to examine the simultaneous measurability in each subgraph \mathcal{B}_x , we further decompose it into r_x subgraphs as

$$\mathcal{B}_x = \mathcal{C}_x^1 \sqcup \cdots \sqcup \mathcal{C}_x^{r_x}, \quad (\text{C30})$$

where \mathcal{C}_x^a 's satisfy

$$[\mathcal{C}_x^a, \mathcal{C}_x^b] = 0 \quad \text{or} \quad \{\mathcal{C}_x^a, \mathcal{C}_x^b\} = 0 \quad (\text{C31})$$

and

$\forall a \neq b, \exists c$, s.t.

$$\begin{cases} [\mathcal{C}_x^a, \mathcal{C}_x^c] = 0 \\ [\mathcal{C}_x^b, \mathcal{C}_x^c] = 0 \end{cases} \quad \text{or} \quad \begin{cases} \{\mathcal{C}_x^a, \mathcal{C}_x^c\} = 0 \\ [\mathcal{C}_x^b, \mathcal{C}_x^c] = 0. \end{cases} \quad (\text{C32})$$

Equation (C31) implies that all nodes in each subgraph share the same commutation relations for every node in

the DLA graph $R \in \mathcal{G}_{\text{Lie}}$ as $[P, R] = 0 \forall P \in \mathcal{C}_x^a$ or $\{P, R\} = 0 \forall P \in \mathcal{C}_x^a$. This readily leads to the commutation relations within the same subgraph as $[P, Q] = 0$ for $\forall P, Q \in \mathcal{C}_x^a$. In addition, from Eq. (C32), when the circuit generators $G_j, G_k \in \mathcal{G}$ belong to different \mathcal{C}_x^a 's, there exists $R \in \mathcal{B}_x$ such that $\{G_j, R\} = [G_k, R] = 0$ or $[G_j, R] = \{G_k, R\} = 0$. Then, $\partial_j C$ and $\partial_k C$ are not simultaneously measurable by Lemma 4. Finally, we decompose \mathcal{C}_x^a into the commuting and anti-commuting parts with the observable O :

$$\mathcal{C}_x^a = \mathcal{C}_x^{a+} \sqcup \mathcal{C}_x^{a-}, \quad (\text{C33})$$

where $\mathcal{C}_x^{a\pm}$ commute and anti-commute with the observable O , respectively:

$$[\mathcal{C}_x^{a+}, O] = 0, \quad \{\mathcal{C}_x^{a-}, O\} = 0. \quad (\text{C34})$$

For $G_j \in \mathcal{C}_x^{a+}$ and $G_k \in \mathcal{C}_x^{a-}$, $\partial_j C$ and $\partial_k C$ are not simultaneously measurable by Lemma 3. Therefore, the maximum size of $\mathcal{C}_x^{a\pm}$ bounds the maximum number of simultaneously measurable gradient components in each \mathcal{B}_x . To evaluate gradient measurement efficiency and expressivity, we define

$$v = \max_{\mathcal{C}_x^a} (|\mathcal{C}_x^a|), \quad (\text{C35})$$

$$w = \max_{\mathcal{C}_x^{a\pm}} (|\mathcal{C}_x^{a\pm}|), \quad (\text{C36})$$

$$\mathcal{C}_v = \operatorname{argmax}_{\mathcal{C}_x^a} (|\mathcal{C}_x^a|), \quad (\text{C37})$$

$$\mathcal{C}_w = \operatorname{argmax}_{\mathcal{C}_x^{a\pm}} (|\mathcal{C}_x^{a\pm}|). \quad (\text{C38})$$

By Lemmas 1–5, the gradient measurement efficiency \mathcal{F}_{eff} and the expressivity \mathcal{X}_{exp} (i.e., the total number of nodes) are bounded as

$$\mathcal{F}_{\text{eff}} \leq qw, \quad (\text{C39})$$

$$\mathcal{X}_{\text{exp}} \leq p + v(r_1 + \dots + r_q), \quad (\text{C40})$$

where there are no contributions from \mathcal{A}_x to \mathcal{F}_{eff} in the deep circuit limit.

For this DLA decomposition, we consider stabilizer operators $\mathcal{S} = \{S_1, S_2, \dots\}$, which can lead to high gradient measurement efficiency instead of limiting expressivity. The stabilizers are defined as follows. If $v \geq w + p$, we define

$$\mathcal{S} = \{E_1 E_1, E_1 E_2, \dots, E_1 E_v\} \quad (\text{C41})$$

with $\mathcal{C}_v = \{E_1, \dots, E_v\}$. Otherwise, we define

$$\mathcal{S} = \{F_1 F_1, F_1 F_2, \dots, F_1 F_w\} \sqcup \{A_1, \dots, A_p\} \quad (\text{C42})$$

with $\mathcal{C}_w = \{F_1, \dots, F_w\}$ and $A_x \in \mathcal{A}_x$. Note that the elements of \mathcal{S} are not duplicated [61]. From Eq. (C31), the stabilizers \mathcal{S} commute with themselves and the DLA (i.e., $[\mathcal{S}, \mathcal{S}] = [\mathcal{G}_{\text{Lie}}, \mathcal{S}] = 0$), thus limiting the expressivity of the circuit. Here, let us define a subgroup of Pauli operators, $\mathcal{P}_S \subset \mathcal{P}_n$, stabilized by \mathcal{S} as

$$\mathcal{P}_S = \{P \in \mathcal{P}_n \mid [P, S_j] = 0 \forall S_j \in \mathcal{S}\}. \quad (\text{C43})$$

By Lemma 11, we have $|\mathcal{P}_S| \leq 4^n/|\mathcal{S}|$. In what follows, using the DLA decomposition and the stabilizers, we derive

$$\mathcal{X}_{\text{exp}} \leq \frac{4^n v}{4^{q-1} |\mathcal{S}|^2} + (3q - 4)v + p \quad (\text{C44})$$

and

$$\frac{4^n v}{4^{q-1} |\mathcal{S}|^2} + (3q - 4)v + p \leq \frac{4^n}{qw} - qw. \quad (\text{C45})$$

Combining Eqs. (C39), (C44), and (C45), we finally obtain the trade-off inequality $\mathcal{X}_{\text{exp}} \leq 4^n/\mathcal{F}_{\text{eff}} - \mathcal{F}_{\text{eff}}$.

c. Proof of Eq. (35)

Here, we prove the following inequality:

$$\mathcal{X}_{\text{exp}} \leq \frac{4^n v}{4^{q-1} |\mathcal{S}|^2} + (3q - 4)v + p. \quad (\text{C46})$$

Let us first show the following lemma:

Lemma 13. $r_x \geq 3$.

Proof. If $r_x = 1$, all the elements of $\mathcal{B}_x = \mathcal{C}_x^1$ commute with each other by Eq. (C31), which contradicts the fact that \mathcal{B}_x is a connected graph, thus $r_x \geq 2$. If $r_x = 2$, Eq. (C31) leads to $\{\mathcal{C}_x^1, \mathcal{C}_x^2\} = 0$ because \mathcal{B}_x is connected. Then, for $P \in \mathcal{C}_x^1$ and $Q \in \mathcal{C}_x^2$, $iR = [iP, iQ] = -2PQ$ satisfies $\{P, R\} = \{Q, R\} = 0$. This indicates that R is included in \mathcal{B}_x but not in both \mathcal{C}_x^1 and \mathcal{C}_x^2 , thus showing the existence of \mathcal{C}_x^3 . Therefore $r_x \geq 3$. \square

Now, we prove Eq. (35). Let $C_{x,a} \in \mathcal{C}_x^a$ be a representative element of \mathcal{C}_x^a and define $\mathcal{D}_x = \{I, C_{x,1}, \dots, C_{x,r_x}\}$. Also, let $S_a \in \mathcal{S}$ and $D_{x,a} \in \mathcal{D}_x$ be the a th elements of \mathcal{S} and \mathcal{D}_x , respectively. Then we consider the following Pauli operator:

$$M_{\mathbf{a}} = S_{a_0} D_{1,a_1} \dots D_{q,a_q}, \quad (\text{C47})$$

where $\mathbf{a} = (a_0, \dots, a_q)$ is a vector with $a_0 \in \{1, \dots, |\mathcal{S}|\}$ and $a_x (\neq 0) \in \{1, \dots, r_x + 1\}$. The operator $M_{\mathbf{a}}$ has the following properties:

- (i) $M_{\mathbf{a}} \in \mathcal{P}_S$,
- (ii) $M_{\mathbf{a}} \neq M_{\mathbf{b}}$ for $\mathbf{a} \neq \mathbf{b}$.

The first property is readily proved by noticing $[M_{\mathbf{a}}, \mathcal{S}] = 0$, which is derived from $[\mathcal{S}, \mathcal{S}] = [D_x, \mathcal{S}] = 0$. We prove the second property below. If $a_x \neq b_x$ ($x \geq 1$), according to Eq. (C32), there exists $R \in \mathcal{B}_x$ such that $[D_{x,a_x}, R] = \{D_{x,b_x}, R\} = 0$ (or $\{D_{x,a_x}, R\} = [D_{x,b_x}, R] = 0$) and $[\mathcal{S}, R] = [D_{y(\neq x)}, R] = 0$. These commutation relations lead to $[M_{\mathbf{a}}, R] \neq [M_{\mathbf{b}}, R]$, showing $M_{\mathbf{a}} \neq M_{\mathbf{b}}$. If $a_0 \neq b_0$ and $a_x = b_x$ for all $x \geq 1$, $M_{\mathbf{a}} = M_{\mathbf{b}}$ leads to $S_{a_0} = S_{b_0}$, which contradicts the fact that the elements of \mathcal{S} are not duplicated, showing $M_{\mathbf{a}} \neq M_{\mathbf{b}}$. Therefore, $M_{\mathbf{a}} \neq M_{\mathbf{b}}$ for $\mathbf{a} \neq \mathbf{b}$.

Given that $M_{\mathbf{a}} \in \mathcal{P}_{\mathcal{S}}$ and $M_{\mathbf{a}} \neq M_{\mathbf{b}}$ for $\mathbf{a} \neq \mathbf{b}$, the following inequality holds:

$$|\mathcal{S}|(r_1 + 1) \cdots (r_q + 1) \leq |\mathcal{P}_{\mathcal{S}}|, \quad (\text{C48})$$

where the left-hand side corresponds to the number of $M_{\mathbf{a}}$. Since $|\mathcal{P}_{\mathcal{S}}| \leq 4^n/|\mathcal{S}|$, we have

$$\prod_{x=1}^q (r_x + 1) \leq \frac{4^n}{|\mathcal{S}|^2}. \quad (\text{C49})$$

This constraint gives a new upper bound of the expressivity $\mathcal{X}_{\text{exp}} \leq p + v \sum_{x=1}^q r_x$ in Eq. (C40). By minimizing $\sum_{x=1}^q r_x$ in \mathcal{X}_{exp} under the constraint $\prod_{x=1}^q (r_x + 1) \leq 4^n/|\mathcal{S}|^2$, we obtain

$$\begin{aligned} \mathcal{X}_{\text{exp}} &\leq p + v \sum_{x=1}^q r_x \\ &\leq v \sum_{x=1}^q (r_x + 1) - qw + p \\ &\leq v \left[\frac{4^n}{4^{q-1}|\mathcal{S}|^2} + 4(q-1) \right] - qw + p \\ &= \frac{4^n v}{4^{q-1}|\mathcal{S}|^2} + (3q-4)v + p, \end{aligned} \quad (\text{C50})$$

where we have used Lemma 12 with $r_x + 1 \geq 4$ in the derivation of the third line. This is Eq. (35), as required.

For later use, we derive another inequality. Combining Eq. (C49) and $r_x + 1 \geq 4$, we have

$$\frac{4^n}{|\mathcal{S}|^2} \geq 4^q. \quad (\text{C51})$$

This inequality will be used in the proof of Eq. (36).

d. Proof of Eq. (36)

Here, we prove the following inequality:

$$\frac{4^n v}{4^{q-1}|\mathcal{S}|^2} + (3q-4)v + p \leq \frac{4^n}{qw} - qw. \quad (\text{C52})$$

By considering the difference between the both sides, we have

$$\begin{aligned} &(\text{RHS}) - (\text{LHS}) \\ &= \frac{4^n}{4^{q-1}qw|\mathcal{S}|^2} (4^{q-1}|\mathcal{S}|^2 - qvw) - qw - (3q-4)v - p. \end{aligned}$$

This is written as

$$\begin{aligned} &(\text{RHS}) - (\text{LHS}) \\ &\geq \frac{4^q|\mathcal{S}|^2 - 4qvw}{qw} - qw - (3q-4)v - p. \\ &= \frac{4^q|\mathcal{S}|^2 - 3q^2vw - q^2w^2 - pqw}{qw} \\ &\geq \frac{4q^2|\mathcal{S}|^2 - 3q^2|\mathcal{S}|w - q^2w^2 - pq^2w}{qw} \\ &= \frac{q(4|\mathcal{S}|^2 - 3|\mathcal{S}|w - w^2 - pw)}{w} \\ &= \frac{q[(4|\mathcal{S}| + w)(|\mathcal{S}| - w) - pw]}{w} \\ &\geq \frac{q[(4|\mathcal{S}| + w)p - pw]}{w} \\ &= \frac{4pq|\mathcal{S}|}{w} \\ &\geq 0. \end{aligned}$$

Here, we have used Eq. (C51) with $4^{q-1}|\mathcal{S}|^2 - qvw \geq 0$ in the second line, $4^q \geq 4q^2$, $q^2 \geq q$, and $|\mathcal{S}| = \max(v, w + p) \geq v$ in the fourth line, and $|\mathcal{S}| = \max(v, w + p) \geq w + p$ in the seventh line. This result proves Eq. (36).

Appendix D: Gradient measurement in commuting block circuits

Here, we briefly review how to measure gradients in the CBC according to Ref. [26]. In the CBC of Eq. (37), for an input state $|\phi\rangle$ and an Pauli observable O , the cost function $C(\boldsymbol{\theta}) = \langle \phi | U^\dagger(\boldsymbol{\theta}) O U(\boldsymbol{\theta}) | \phi \rangle$ is written as

$$C(\boldsymbol{\theta}) = \langle \phi_a | W_a^\dagger O W_a | \phi_a \rangle, \quad (\text{D1})$$

where we have defined the quantum state at the a th block and the quantum circuit after the a th block as

$$|\phi_a\rangle = U_a(\boldsymbol{\theta}_a) \cdots U_1(\boldsymbol{\theta}_1) |\phi\rangle, \quad (\text{D2})$$

$$W_a = U_B(\boldsymbol{\theta}_B) \cdots U_{a+1}(\boldsymbol{\theta}_{a+1}). \quad (\text{D3})$$

Using $\partial |\phi_a\rangle / \partial \theta_j^a = iG_j^a |\phi_a\rangle$, we have the derivative of the cost function by the j th parameter of the a th block:

$$\frac{\partial C}{\partial \theta_j^a} = \langle \phi_a | (iW_a^\dagger O W_a G_j^a - iG_j^a W_a^\dagger O W_a) | \phi_a \rangle. \quad (\text{D4})$$

Then, since all generators in the block share the same commutation relations with other blocks, we can define \tilde{W}_a such that $W_a G_j^a = G_j^a \tilde{W}_a$. This \tilde{W}_a is easily obtained by using $e^{i\theta P} G_j^a = G_j^a e^{\pm i\theta P}$ (P is a Pauli operator), where \pm correspond to the cases of $[G_j^a, P] = 0$ and $\{G_j^a, P\} = 0$, respectively. Thereby, we have

$$\frac{\partial C}{\partial \theta_j^a} = \langle \phi_a | \left(W_a^\dagger (-1)^{g_j^a} iG_j^a O \tilde{W}_a - \tilde{W}_a^\dagger iG_j^a O W_a \right) | \phi_a \rangle, \quad (\text{D5})$$

where $g_j^a = 0$ if $[G_j^a, O] = 0$ and $g_j^a = 1$ if $\{G_j^a, O\} = 0$. By introducing a Pauli operator $O_j^a = i^{g_j^a} G_j^a O$ and a unitary operator $W'_a = i^{g_j^a + 1} W_a$, the derivative is written as

$$\begin{aligned} & \frac{\partial C}{\partial \theta_j^a} \\ &= \langle \phi_a | \left((W'_a)^\dagger O_j^a \tilde{W}_a + \tilde{W}_a^\dagger O_j^a (W'_a) \right) | \phi_a \rangle \\ &= \frac{1}{2} \left[\langle \phi_a | \left(\tilde{W}_a^\dagger + (W'_a)^\dagger \right) O_j^a \left(\tilde{W}_a + W'_a \right) | \phi_a \rangle \right. \\ & \quad \left. - \langle \phi_a | \left(\tilde{W}_a^\dagger - (W'_a)^\dagger \right) O_j^a \left(\tilde{W}_a - W'_a \right) | \phi_a \rangle \right] \\ &= \frac{1}{2} \left[\langle \phi_a | (L_{W'_a}^+)^\dagger O_j^a L_{W'_a}^+ | \phi_a \rangle - \langle \phi_a | (L_{W'_a}^-)^\dagger O_j^a L_{W'_a}^- | \phi_a \rangle \right], \end{aligned} \quad (\text{D6})$$

where we have defined the linear combinations of unitaries $L_{W'_a}^\pm = \tilde{W}_a \pm W'_a$.

These $L_{W'_a}^\pm$ can be implemented using an ancilla qubit as shown in Fig. 10. For the quantum state $|\phi_a\rangle$ and the ancilla qubit $H|0\rangle$ (H is a Hadamard gate), we apply a W' gate controlled on the ancilla qubit being in $|1\rangle$, followed by a \tilde{W} gate controlled on the ancilla qubit being in $|0\rangle$. After these controlled gates, we finally apply a H gate on the ancilla qubit and then have

$$|\psi_a\rangle = \frac{1}{2} (|0\rangle L_{W'_a}^+ |\phi_a\rangle + |1\rangle L_{W'_a}^- |\phi_a\rangle). \quad (\text{D7})$$

For this quantum state, we can estimate the derivative by measuring an observable $\tilde{O}_j^a = 2(Z \otimes O_j^a)$ as

$$\begin{aligned} & \langle \psi_a | \tilde{O}_j^a | \psi_a \rangle \\ &= \frac{1}{2} \left[\langle \phi_a | (L_{W'_a}^+)^\dagger O_j^a L_{W'_a}^+ | \phi_a \rangle - \langle \phi_a | (L_{W'_a}^-)^\dagger O_j^a L_{W'_a}^- | \phi_a \rangle \right] \\ &= \frac{\partial C}{\partial \theta_j^a}. \end{aligned} \quad (\text{D8})$$

In this method, we can simultaneously measure multiple derivatives in the same block if their generators share the same commutation relations with the observable O (i.e., the same g_j^a). This is because the measured observables \tilde{O}_j^a are commutative, $[\tilde{O}_j^a, \tilde{O}_k^a] = 0$, when $g_j^a = g_k^a$. Therefore, given that the generators of the final block commuting with O do not contribute to the gradient, we can estimate the full gradient with only $2B - 1$ types of quantum circuits.

Appendix E: Dynamical Lie algebra in numerical experiment

Lemma 14. Consider a set of generators

$$\mathcal{G} = \{X_j X_{j+1}, Y_j Y_{j+1}, Z_j Z_{j+1}\}_{j=1}^n \quad (\text{E1})$$

with even n . Then, the Lie closure of \mathcal{G} is given by

$$\mathcal{G}_{\text{Lie}} = \mathcal{Q}_S, \quad (\text{E2})$$

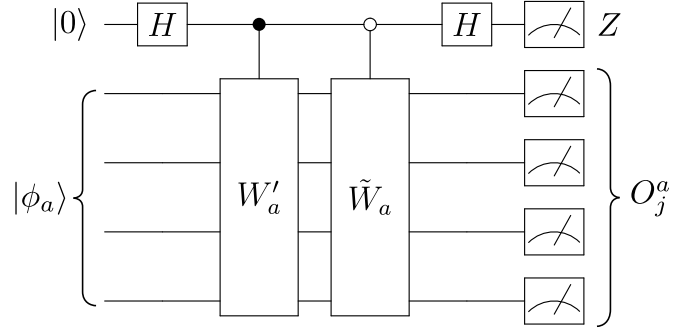


FIG. 10. Gradient measurement in commuting block circuits.

where we have defined $\mathcal{Q}_S = \mathcal{P}_S \setminus \mathcal{S}$ with

$$\mathcal{S} = \{I, \prod_{j=1}^n X_j, \prod_{j=1}^n Y_j, \prod_{j=1}^n Z_j\}, \quad (\text{E3})$$

$$\mathcal{P}_S = \{P \in \mathcal{P}_n \mid [P, S_j] = 0 \forall S_j \in \mathcal{S}\}. \quad (\text{E4})$$

This readily leads to $\dim(\mathfrak{g}) = |\mathcal{G}_{\text{Lie}}| = 4^n/4 - 4$ by Lemma 11.

Proof. We prove this lemma by showing $\mathcal{G}_{\text{Lie}} \subseteq \mathcal{Q}_S$ and $\mathcal{Q}_S \subseteq \mathcal{G}_{\text{Lie}}$.

We first show $\mathcal{G}_{\text{Lie}} \subseteq \mathcal{Q}_S$. One can easily verify $\mathcal{G}_{\text{Lie}} \subseteq \mathcal{P}_S$ because all the generators in \mathcal{G} commute with \mathcal{S} . Thus, it suffices to show $\mathcal{G}_{\text{Lie}} \cap \mathcal{S} = \emptyset$. We prove this by contradiction. Assume $S_j \in \mathcal{S}$ is contained in \mathcal{G}_{Lie} . Then, because $S_j \notin \mathcal{G}$, there exist anti-commuting Pauli operators $P, Q \in \mathcal{G}_{\text{Lie}}$ such that $S_j \propto [P, Q] = 2PQ$. Then, we have $[S_j, P] = [2PQ, P] \neq 0$, which contradicts the fact that S_j commutes with all the operators in \mathcal{P}_S and thus \mathcal{G}_{Lie} . Therefore, \mathcal{G}_{Lie} does not contain \mathcal{S} , proving $\mathcal{G}_{\text{Lie}} \subseteq \mathcal{Q}_S$.

We then show $\mathcal{Q}_S \subseteq \mathcal{G}_{\text{Lie}}$. For convenience, we call the number of X, Y , and Z operators in a Pauli string P as the weight of P . Below, we prove $\mathcal{Q}_S \subseteq \mathcal{G}_{\text{Lie}}$ by mathematical induction with respect to the weight of Pauli strings. To this end, let us introduce the subset of \mathcal{Q}_S with weight- w :

$$\mathcal{Q}_S^w = \{P \in \mathcal{Q}_S \mid \text{the weight of } P \text{ is } w\}. \quad (\text{E5})$$

The sum of \mathcal{Q}_S^w gives $\bigsqcup_{w=0}^n \mathcal{Q}_S^w = \mathcal{Q}_S$. For example, we have

$$\mathcal{Q}_S^0 = \emptyset, \quad (\text{E6})$$

$$\mathcal{Q}_S^1 = \emptyset, \quad (\text{E7})$$

$$\mathcal{Q}_S^2 = \{X_j X_k, Y_j Y_k, Z_j Z_k\}_{j,k=1}^n, \quad (\text{E8})$$

\vdots

where we have used $[\mathcal{Q}_S^w, \mathcal{S}] = 0$ and $I \notin \mathcal{Q}_S$. We also define the numbers of X, Y , and Z operators in $P \in \mathcal{P}_n$ as $w_X(P), w_Y(P)$, and $w_Z(P)$, respectively. By definition, $w_X(P) + w_Y(P) + w_Z(P) = w$ holds for $\forall P \in \mathcal{Q}_S^w$.

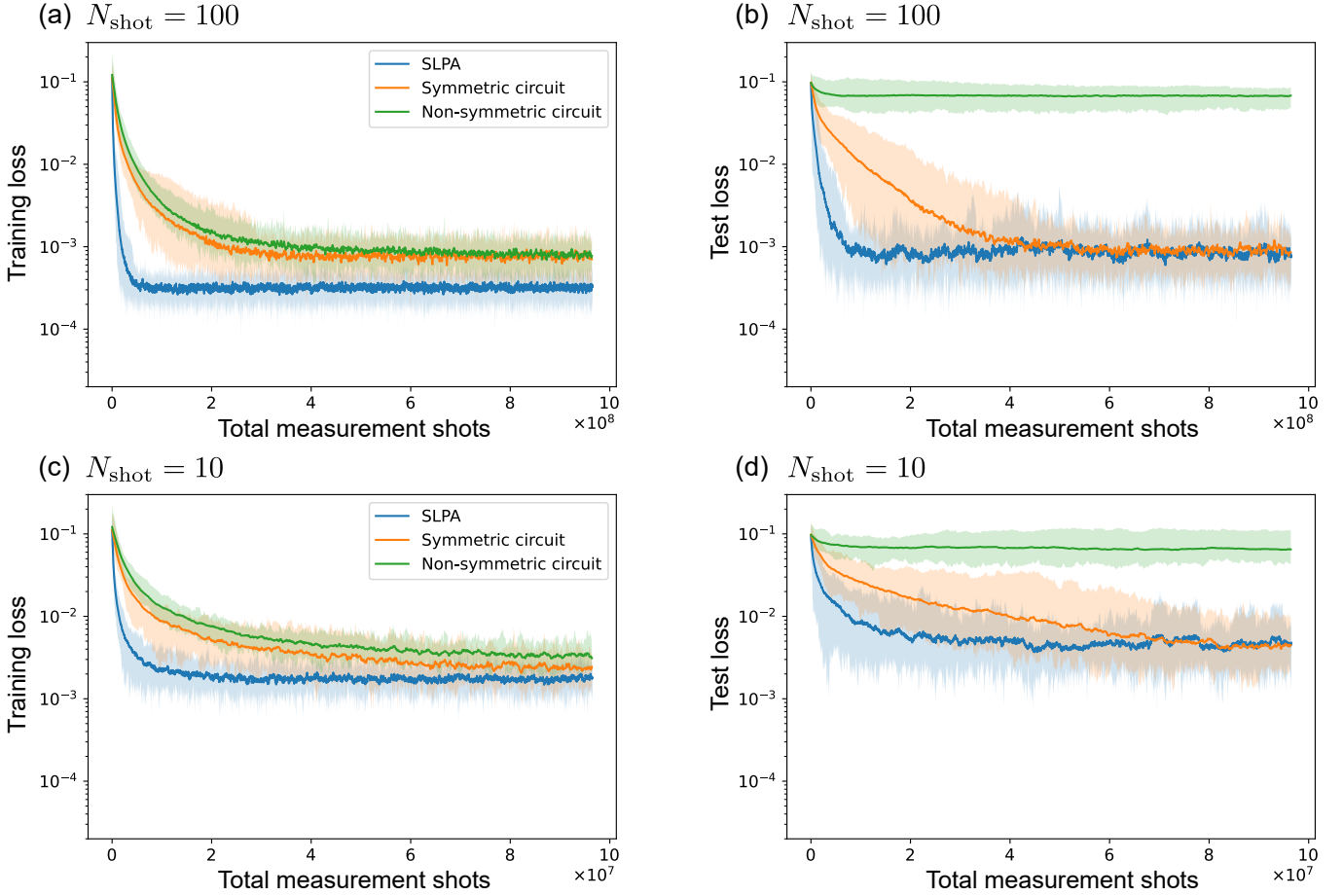


FIG. 11. (a)–(d) Changes in training and test losses during the training process for (a), (b) $N_{\text{shot}} = 100$ and (c), (d) $N_{\text{shot}} = 10$. The horizontal axes of the graphs indicate the cumulative number of measurement shots. The solid lines and shaded areas represent the mean, maximum, and minimum of the losses for 20 sets of random initial parameters. The numbers of qubits and parameters are $n = 4$ and $L = 96$, respectively.

Let us prove $\mathcal{Q}_S^w \subset \mathcal{G}_{\text{Lie}}$ by mathematical induction for w . Since $\mathcal{Q}_S^0 = \mathcal{Q}_S^1 = \emptyset$, it suffices to consider $w \geq 2$. We first show that $\mathcal{Q}_S^2 \subset \mathcal{G}_{\text{Lie}}$, i.e., $X_j X_k$, $Y_j Y_k$, and $Z_j Z_k$ for $j < k$ are contained in \mathcal{G}_{Lie} . For example, let us consider $X_j X_k$. Because of $X_j X_{j+1} \in \mathcal{G}$, we trivially have $X_j X_{j+1} \in \mathcal{G}_{\text{Lie}}$. Then, since $Y_{j+1} Y_{j+2}, Z_{j+1} Z_{j+2} \in \mathcal{G}_{\text{Lie}}$, a nested commutator $[[X_j X_{j+1}, Y_{j+1} Y_{j+2}], Z_{j+1} Z_{j+2}] = X_j X_{j+2}$ is also contained in \mathcal{G}_{Lie} . Similarly, we have $[[X_j X_{j+2}, Y_{j+2} Y_{j+3}], Z_{j+2} Z_{j+3}] = X_j X_{j+3} \in \mathcal{G}_{\text{Lie}}$. Repeating this procedure, we can easily show that $X_j X_k \in \mathcal{G}_{\text{Lie}}$ for any $j < k$. In the same way, we can show $Y_j Y_k, Z_j Z_k \in \mathcal{G}_{\text{Lie}}$ for any $j < k$, proving $\mathcal{Q}_S^2 \subset \mathcal{G}_{\text{Lie}}$.

Next, we prove $\mathcal{Q}_S^w \subset \mathcal{G}_{\text{Lie}}$ for $3 \leq w \leq n-1$ by mathematical induction (we prove the case of $w = n$ later). Assume $\mathcal{Q}_S^w \subset \mathcal{G}_{\text{Lie}}$ for $2 \leq w \leq n-2$. Then, we show that $\forall P \in \mathcal{Q}_S^{w+1}$ is contained in \mathcal{G}_{Lie} in two cases: (i) two or more of $w_X(P), w_Y(P), w_Z(P)$ are greater than one, and (ii) otherwise.

(i) The weight- $(w+1)$ Pauli string is written as $P =$

$\sigma_{\gamma_1}^{\mu_1} \cdots \sigma_{\gamma_{w+1}}^{\mu_{w+1}}$, where we have defined

$$\sigma_j^\mu = \begin{cases} X_j & \mu = 1 \\ Y_j & \mu = 2 \\ Z_j & \mu = 3 \end{cases} \quad (\text{E9})$$

and the qubit indices $\gamma_1 < \cdots < \gamma_{w+1}$. Given that two or more of $w_X(P), w_Y(P), w_Z(P)$ are greater than one, there necessarily exist $1 \leq j < k \leq w+1$ such that $\mu_j \neq \mu_k$. Then, we define $Q = iPR$ using a weight-2 Pauli string $R = \sigma_{\gamma_j}^{\mu_k} \sigma_{\gamma_k}^{\mu_j} \in \mathcal{Q}_S^2$. One can easily show that Q is a weight- w Pauli string and is contained in \mathcal{Q}_S^w because of $P \in \mathcal{Q}_S^{w+1}$ and $R \in \mathcal{Q}_S^2$. Therefore, we have $Q \in \mathcal{G}_{\text{Lie}}$ by assumption. We can construct P by taking the commutator $P \propto [R, Q]$, proving $P \in \mathcal{G}_{\text{Lie}}$ for the case (i).

(ii) When P contains only one of $X, Y,$ and Z operators, we can construct P using another qubit γ' that is different from $\gamma_1, \dots, \gamma_{w+1}$. For example, let us consider a Pauli string that has only X operators: $P = X_{\gamma_1} \cdots X_{\gamma_{w+1}} \in \mathcal{Q}_S^{w+1}$ (then $w+1$

is even because of $[P, \prod_j Y_j] = 0$). Given that any weight- $(w+1)$ Pauli string with two or more of X, Y , and Z operators is contained in \mathcal{G}_{Lie} according to the proof of the case (i), $S = X_{\gamma_1} \cdots X_{\gamma_{w-1}} Y_{\gamma_w} Y_{\gamma_{w+1}} \in \mathcal{Q}_{\mathcal{S}}^{w+1}$ is also contained in \mathcal{G}_{Lie} . Then, we can construct P from $S, Z_{\gamma_w} Z_{\gamma'}, Z_{\gamma_{w+1}} Z_{\gamma'} \in \mathcal{G}_{\text{Lie}}$ as $P \propto [[S, Z_{\gamma_w} Z_{\gamma'}], Z_{\gamma_{w+1}} Z_{\gamma'}]$, showing that $P \in \mathcal{G}_{\text{Lie}}$. Similarly, Pauli strings that have only Y or Z operators are also contained in \mathcal{G}_{Lie} . Therefore, $P \subset \mathcal{G}_{\text{Lie}}$ holds for the case (ii).

These results prove that $\mathcal{Q}_{\mathcal{S}}^w \subset \mathcal{G}_{\text{Lie}}$ for $2 \leq w \leq n-1$ by mathematical induction. Finally, we prove $\mathcal{Q}_{\mathcal{S}}^n \subset \mathcal{G}_{\text{Lie}}$. Because $\forall P \in \mathcal{Q}_{\mathcal{S}}^n$ has at least two of X, Y , and Z operators (note that $\mathcal{Q}_{\mathcal{S}}$ does not contain \mathcal{S}), we can construct P from weight- $(n-1)$ and weight-2 Pauli strings Q and R in a similar way to the above discussion on the case (i).

In summary, we show $\mathcal{Q}_{\mathcal{S}}^w \subset \mathcal{G}_{\text{Lie}}$ for any w , proving $\mathcal{Q}_{\mathcal{S}} = \bigsqcup_{w=0}^n \mathcal{Q}_{\mathcal{S}}^w \subseteq \mathcal{G}_{\text{Lie}}$. Therefore, together with $\mathcal{G}_{\text{Lie}} \subseteq \mathcal{Q}_{\mathcal{S}}$, we have proved this lemma. \square

Appendix F: Numerical results for fewer measurement shots

This Appendix provides additional results in the numerical demonstration of learning the unknown symmetric function. Here, numerical experiments are performed with the same settings as in the main text, except for the number of measurement shots per circuit, N_{shot} . While the main text assumes $N_{\text{shot}} = 1000$, this Appendix uses $N_{\text{shot}} = 100$ and 10.

In Fig. 11, we can observe similar behaviors to the case of $N_{\text{shot}} = 1000$ for both $N_{\text{shot}} = 100$ and 10. The SLPA can significantly reduce the total number of measurement shots required for training while maintaining high generalization. Meanwhile, the final accuracy after training becomes worse as N_{shot} decreases for all the models. This indicates that fewer measurement shots result in larger statistical errors in gradient estimation and, thus, worse accuracy. Therefore, within these numerical experiments, the minimum N_{shot} required for training is determined by the acceptable accuracy of the problem, which is independent of the choice of models.

-
- [1] G. E. Hinton, S. Osindero, and Y. W. Teh, A fast learning algorithm for deep belief nets, *Neural Computation* **18**, 1527 (2006).
 - [2] A. Krizhevsky, I. Sutskever, and G. E. Hinton, ImageNet classification with deep convolutional neural networks, *Commun. ACM* **60**, 84 (2012).
 - [3] A. Vaswani, N. Shazeer, N. Parmar, J. Uszkoreit, L. Jones, A. N. Gomez, L. Kaiser, and I. Polosukhin, Attention is all you need, in *Proceedings of the 31st International Conference on Neural Information Processing Systems*, NIPS'17 (Curran Associates Inc., Red Hook, NY, USA, 2017) p. 6000–6010.
 - [4] J. M. Jumper, R. Evans, A. Pritzel, T. Green, M. Figurnov, O. Ronneberger, K. Tunyasuvunakool, R. Bates, A. Zidek, A. Potapenko, A. Bridgland, C. Meyer, S. A. A. Kohl, A. Ballard, A. Cowie, B. Romera-Paredes, S. Nikolov, R. Jain, J. Adler, T. Back, S. Petersen, D. Reiman, E. Clancy, M. Zielinski, M. Steinegger, M. Pacholska, T. Berghammer, S. Bodenstein, D. Silver, O. Vinyals, A. W. Senior, K. Kavukcuoglu, P. Kohli, and D. Hassabis, Highly accurate protein structure prediction with alphafold, *Nature* **596**, 583 (2021).
 - [5] G. Carleo and M. Troyer, Solving the quantum many-body problem with artificial neural networks, *Science* **355**, 602 (2017).
 - [6] D. E. Rumelhart, G. E. Hinton, and R. J. Williams, Learning representations by back-propagating errors, *Nature* **323**, 533 (1986).
 - [7] A. G. Baydin, B. A. Pearlmutter, A. A. Radul, and J. M. Siskind, Automatic Differentiation in Machine Learning: a Survey, *Journal of Machine Learning Research* **18**, 1 (2018).
 - [8] A. Peruzzo, J. McClean, P. Shadbolt, M.-H. Yung, X.-Q. Zhou, P. J. Love, A. Aspuru-Guzik, and J. L. O'Brien, A variational eigenvalue solver on a photonic quantum processor, *Nat. Commun.* **5**, 4213 (2014).
 - [9] E. Farhi, J. Goldstone, and S. Gutmann, A quantum approximate optimization algorithm, [arXiv:1411.4028 \[quant-ph\]](https://arxiv.org/abs/1411.4028) (2014).
 - [10] E. Farhi and H. Neven, Classification with quantum neural networks on near term processors, [arXiv:1802.06002 \[quant-ph\]](https://arxiv.org/abs/1802.06002) (2018).
 - [11] J.-G. Liu and L. Wang, Differentiable learning of quantum circuit Born machines, *Phys. Rev. A* **98**, 062324 (2018).
 - [12] K. Mitarai, M. Negoro, M. Kitagawa, and K. Fujii, Quantum circuit learning, *Phys. Rev. A* **98**, 032309 (2018).
 - [13] M. Benedetti, E. Lloyd, S. Sack, and M. Fiorentini, Parameterized quantum circuits as machine learning models, *Quantum Sci. Technol.* **4**, 043001 (2019).
 - [14] M. Schuld, A. Bocharov, K. M. Svore, and N. Wiebe, Circuit-centric quantum classifiers, *Phys. Rev. A* **101**, 032308 (2020).
 - [15] C. Bravo-Prieto, R. LaRose, M. Cerezo, Y. Subasi, L. Cincio, and P. J. Coles, Variational Quantum Linear Solver, *Quantum* **7**, 1188 (2023), 1909.05820v4.
 - [16] E. Anschuetz, J. Olson, A. Aspuru-Guzik, and Y. Cao, Variational Quantum Factoring, in *Quantum Technology and Optimization Problems*, Lecture notes in computer science (Springer International Publishing, Cham, 2019) pp. 74–85.
 - [17] S. Khatri, R. LaRose, A. Poremba, L. Cincio, A. T. Sornborger, and P. J. Coles, Quantum-assisted quantum compiling, *Quantum* **3**, 140 (2019), 1807.00800v5.
 - [18] P. D. Johnson, J. Romero, J. Olson, Y. Cao, and A. Aspuru-Guzik, QVECTOR: an algorithm for device-tailored quantum error correction, [arXiv:1711.02249 \[quant-ph\]](https://arxiv.org/abs/1711.02249) (2017).
 - [19] N. Wiebe, A. Kapoor, and K. M. Svore, Quantum Deep Learning, [arXiv:1412.3489 \[quant-ph\]](https://arxiv.org/abs/1412.3489) (2014).

- [20] M. Schuld, I. Sinayskiy, and F. Petruccione, An introduction to quantum machine learning, *Contemp. Phys.* **56**, 172 (2015).
- [21] J. Biamonte, P. Wittek, N. Pancotti, P. Rebentrost, N. Wiebe, and S. Lloyd, Quantum machine learning, *Nature* **549**, 195 (2017).
- [22] V. Dunjko and H. J. Briegel, Machine learning & artificial intelligence in the quantum domain: a review of recent progress, *Rep. Prog. Phys.* **81**, 074001 (2018).
- [23] M. Cerezo, A. Arrasmith, R. Babbush, S. C. Benjamin, S. Endo, K. Fujii, J. R. McClean, K. Mitarai, X. Yuan, L. Cincio, and P. J. Coles, Variational quantum algorithms, *Nat. Rev. Phys.* **3**, 625 (2021).
- [24] A. Abbas, R. King, H.-Y. Huang, W. J. Huggins, R. Movassagh, D. Gilboa, and J. R. McClean, On quantum backpropagation, information reuse, and cheating measurement collapse, [arXiv:2305.13362 \[quant-ph\]](https://arxiv.org/abs/2305.13362) (2023).
- [25] M. Schuld, V. Bergholm, C. Gogolin, J. Izaac, and N. Killoran, Evaluating analytic gradients on quantum hardware, *Phys. Rev. A* **99**, 032331 (2019).
- [26] J. Bowles, D. Wierichs, and C.-Y. Park, Backpropagation scaling in parameterised quantum circuits, [arXiv:2306.14962 \[quant-ph\]](https://arxiv.org/abs/2306.14962) (2023).
- [27] B. Coyle, E. A. Cherrat, N. Jain, N. Mathur, S. Raj, S. Kazdaghi, and I. Kerenidis, Training-efficient density quantum machine learning, [arXiv:2405.20237 \[quant-ph\]](https://arxiv.org/abs/2405.20237) (2024).
- [28] S. Aaronson, Shadow tomography of quantum states, [arXiv:1711.01053 \[quant-ph\]](https://arxiv.org/abs/1711.01053) (2017).
- [29] F. Albertini and D. D'Alessandro, Notions of controllability for quantum mechanical systems, in *Proceedings of the 40th IEEE Conference on Decision and Control (Cat. No. 01CH37228)*, Vol. 2 (2001) pp. 1589–1594 vol.2.
- [30] R. Zeier and T. Schulte-Herbrüggen, Symmetry principles in quantum systems theory, *Journal of Mathematical Physics* **52**, 113510 (2011).
- [31] D. D'Alessandro, *Introduction to Quantum Control and Dynamics*, Chapman & Hall/CRC Applied Mathematics & Nonlinear Science (Taylor & Francis, 2007).
- [32] M. Larocca, N. Ju, D. García-Martín, P. J. Coles, and M. Cerezo, Theory of overparametrization in quantum neural networks, *Nat. Comput. Sci.* **3**, 542 (2023).
- [33] M. Larocca, P. Czarnik, K. Sharma, G. Muraleedharan, P. J. Coles, and M. Cerezo, Diagnosing barren plateaus with tools from quantum optimal control, *Quantum* **6**, 824 (2022), [2105.14377v3](https://arxiv.org/abs/2105.14377v3).
- [34] J. M. Kübler, S. Buchholz, and B. Schölkopf, The inductive bias of quantum kernels, [arXiv:2106.03747 \[quant-ph\]](https://arxiv.org/abs/2106.03747) (2021).
- [35] M. M. Bronstein, J. Bruna, T. Cohen, and P. Veličković, Geometric deep learning: Grids, groups, graphs, geodesics, and gauges, [arXiv:2104.13478 \[cs.LG\]](https://arxiv.org/abs/2104.13478) (2021).
- [36] G. Verdon, T. McCourt, E. Luzhnica, V. Singh, S. Leichenauer, and J. Hidar, Quantum Graph Neural Networks, [arXiv:1909.12264 \[quant-ph\]](https://arxiv.org/abs/1909.12264) (2019).
- [37] H. Zheng, Z. Li, J. Liu, S. Strelchuk, and R. Kondor, Speeding up learning quantum states through group equivariant convolutional quantum ansätze, *PRX quantum* **4**, 020327 (2023).
- [38] M. Larocca, F. Sauvage, F. M. Sباهي, G. Verdon, P. J. Coles, and M. Cerezo, Group-invariant quantum machine learning, *PRX quantum* **3**, 030341 (2022).
- [39] J. J. Meyer, M. Mularski, E. Gil-Fuster, A. A. Mele, F. Arzani, A. Wilms, and J. Eisert, Exploiting symmetry in variational quantum machine learning, *PRX quantum* **4**, 010328 (2023).
- [40] A. Skolik, M. Cattelan, S. Yarkoni, T. Bäck, and V. Dunjko, Equivariant quantum circuits for learning on weighted graphs, [arXiv:2205.06109 \[quant-ph\]](https://arxiv.org/abs/2205.06109) (2022).
- [41] M. Ragone, P. Braccia, Q. T. Nguyen, L. Schatzki, P. J. Coles, F. Sauvage, M. Larocca, and M. Cerezo, Representation theory for Geometric Quantum Machine Learning, [arXiv:2210.07980 \[quant-ph\]](https://arxiv.org/abs/2210.07980) (2022).
- [42] Q. T. Nguyen, L. Schatzki, P. Braccia, M. Ragone, P. J. Coles, F. Sauvage, M. Larocca, and M. Cerezo, Theory for Equivariant Quantum Neural Networks, [arXiv:2210.08566 \[quant-ph\]](https://arxiv.org/abs/2210.08566) (2022).
- [43] L. Schatzki, M. Larocca, Q. T. Nguyen, F. Sauvage, and M. Cerezo, Theoretical guarantees for permutation-equivariant quantum neural networks, [arXiv:2210.09974 \[quant-ph\]](https://arxiv.org/abs/2210.09974) (2022).
- [44] F. Sauvage, M. Larocca, P. J. Coles, and M. Cerezo, Building spatial symmetries into parameterized quantum circuits for faster training, *Quantum Sci. Technol.* **9**, 015029 (2024).
- [45] K. Chinzei, Q. H. Tran, K. Maruyama, H. Oshima, and S. Sato, Splitting and parallelizing of quantum convolutional neural networks for learning translationally symmetric data, *Phys. Rev. Res.* **6**, 023042 (2024).
- [46] M. Ragone, B. N. Bakalov, F. Sauvage, A. F. Kemper, C. O. Marrero, M. Larocca, and M. Cerezo, A unified theory of barren plateaus for deep parametrized quantum circuits, [arXiv:2309.09342 \[quant-ph\]](https://arxiv.org/abs/2309.09342) (2023).
- [47] E. Fontana, D. Herman, S. Chakrabarti, N. Kumar, R. Yalovetzky, J. Heredge, S. H. Sureshbabu, and M. Pistotoia, The adjoint is all you need: Characterizing Barren Plateaus in quantum ansätze, [arXiv:2309.07902 \[quant-ph\]](https://arxiv.org/abs/2309.07902) (2023).
- [48] J. R. McClean, S. Boixo, V. N. Smelyanskiy, R. Babbush, and H. Neven, Barren plateaus in quantum neural network training landscapes, *Nat. Commun.* **9**, 4812 (2018).
- [49] For $j \neq k$, $A_j \neq A_k$ and $A_1 A_j \neq A_1 A_k$ trivially hold. For any j and k , $A_j \neq A_1 A_k$ also holds because of $\{A_j, O\} = [A_1 A_k, O] = 0$.
- [50] J. Preskill, Quantum computing in the NISQ era and beyond, *Quantum* **2**, 79 (2018).
- [51] D. Litinski, A game of surface codes: Large-scale quantum computing with lattice surgery, *Quantum* **3**, 128 (2019).
- [52] Y. Akahoshi, K. Maruyama, H. Oshima, S. Sato, and K. Fujii, Partially Fault-Tolerant Quantum Computing Architecture with Error-Corrected Clifford Gates and Space-Time Efficient Analog Rotations, *PRX Quantum* **5**, 010337 (2024).
- [53] D. P. Kingma and J. Ba, Adam: A method for stochastic optimization, in *3rd International Conference on Learning Representations, ICLR 2015, San Diego, CA, USA, May 7-9, 2015, Conference Track Proceedings*, edited by Y. Bengio and Y. LeCun (2015).
- [54] H. Robbins and S. Monro, A Stochastic Approximation Method, *Ann. Math. Stat.* **22**, 400 (1951).
- [55] M. Cerezo, M. Larocca, D. García-Martín, N. L. Diaz, P. Braccia, E. Fontana, M. S. Rudolph, P. Bermejo, A. Ijaz, S. Thanasilp, E. R. Anschuetz, and Z. Holmes, Does provable absence of barren plateaus imply classical simulability? Or, why we need to rethink variational quantum computing, [arXiv:2312.09121 \[quant-ph\]](https://arxiv.org/abs/2312.09121)

- (2023).
- [56] M. Cerezo, A. Sone, T. Volkoff, L. Cincio, and P. J. Coles, Cost function dependent barren plateaus in shallow parametrized quantum circuits, *Nat. Commun.* **12**, 1791 (2021).
- [57] B. T. Gard, L. Zhu, G. S. Barron, N. J. Mayhall, S. E. Economou, and E. Barnes, Efficient symmetry-preserving state preparation circuits for the variational quantum eigensolver algorithm, *Npj Quantum Inf.* **6**, 1 (2020).
- [58] M. J. D. Powell, An efficient method for finding the minimum of a function of several variables without calculating derivatives, *Comput. J.* **7**, 155 (1964).
- [59] J. C. Spall, Multivariate stochastic approximation using a simultaneous perturbation gradient approximation, *IEEE Transactions on Automatic Control* **37**, 332 (1992).
- [60] M. A. Nielsen and I. L. Chuang, *Quantum Computation and Quantum Information* (Cambridge University Press, 2010).
- [61] If $v \geq w + p$, $E_1 E_j \neq E_1 E_k (\Leftrightarrow E_j \neq E_k)$ trivially holds for $j \neq k$. If $v < w + p$, $F_1 F_j \neq F_1 F_k (\Leftrightarrow F_j \neq F_k)$ and $A_j \neq A_k$ hold for $j \neq k$. We also have $F_1 F_j \neq A_k$ because of $[F_1 F_j, O] = \{A_k, O\} = 0$. Therefore, the elements of \mathcal{S} are not duplicated.